Mechanisms of fate determination in the nervous system: the roles of the Rbp-j and Olig3 transcription factors

Inaugural-Dissertation
to obtain the academic degree
Doctor rerum naturalium (Dr. rer. nat.)

submitted to the Department of Biology, Chemistry and Pharmacy
of Freie Universität Berlin

by

Justyna Cholewa-Waclaw
from Miechow, Poland

March, 2009

The work described in this thesis was supervised by Prof. Dr. Carmen Birchmeier and performed at Max-Delbrück Center for Molecular Medicine in Berlin from November 2005 to November 2008.

1st Reviewer: Prof. Dr. Carmen Birchmeier

2nd Reviewer: Prof. Dr. Fritz Rathjen

Date of defense: 07.07.09

Acknowledgments

I would like to thank Prof. Dr. Carmen Birchmeier for giving me the opportunity to work in her research group, for the constructive supervision and support. I thank Prof. Dr. Fritz Rathjen for being my thesis advisor.

I thank all my colleagues for the collaboration and warm atmosphere during all these years. In particular, I would like to thank Dr. Thomas Müller for valuable advice and discussion as well as for his patient help with the microarray analysis, the generation of the mutant mice and for revising the thesis. I am grateful to Dr. Hendrik Wildner for his precious supervision at the beginning of my thesis work. I also thank Dr. Dominique Bröhl for his help during the last months of my thesis work and his help in editing the thesis. I thank Dr. Robert Storm for introducing me to the hindbrain analysis and Claudia Päseler and Petra Stallerow for excellent technical assistance. I would like to thank Dr. Katja Reuter for sharing unpublished data.

I thankfully acknowledge Jane Johnson and Raymond MacDonald for fruitful discussions and sharing unpublished data.

This work could not be finished without constant support of my husband Bartek. In particular, I am grateful to him for developing program for counting cell nuclei.

TABLE OF CONTENTS

1 . Introduction

The human nervous system represents a network of more than 100 billion neurons, which are interconnected in a complex circuit. It provides the cellular basis for the perception of the external world, and for intricate processes like memory or cognition. The enormous complexity of this system makes it difficult to investigate how the neural network works and how it governs our behavior. One possible approach to understand the nervous system is to take a step back and to analyze the development that creates the complex mature nervous system. This approach defines how neuronal diversity is established and how neurons organize into networks.

Development of the nervous system is characterized by a spatially and temporarily controlled appearance of neurons and neuronal connections. These steps proceed in an invariant manner in different individuals of one species. Neurogenesis and axonal pathfinding depend on the expression of particular genes. Analyses of the effects of mutations of such genes in model animals like the mouse define gene functions and can provide insight into the genetic basis of mammalian nervous system function and dysfunction.

1.1 . Patterning of the central nervous system

The process assigning positional identity is called patterning. From an early stage of the neural tube development, the process of anterior-posterior regionalization takes place, in which the central nervous system becomes to be divided into domains. In addition to anterior-posterior patterning, the neural tube is also organized along its dorsal-ventral axis. In the following chapters, I will introduce some of the molecular mechanisms responsible for anterior-posterior and dorsal-ventral patterning.

1.1.1 . Anterior-posterior patterning

The early central nervous system is divided into distinct developmental units. The rostral portion of neural tube displays three major swellings called vesicles. The most

rostral one is called the prosencephalon, or forebrain, which will later be further divided into two vesicles, the telencephalon and diencephalon. Posterior to the forebrain develops the mesencephalic vesicle, also called midbrain. The rhombencephalon, or hindbrain, represents the most caudal vesicle, and can be further subdivided into seven rhombomeres. The anterior rhombomere, the metencephalon, gives rise to the cerebellum and the pons, and posterior rhombomeres form the myelencephalon. The myelencephalon will form the medulla oblongata. The caudal region of the central nervous system forms the spinal cord, extending from the hindbrain to the tip of the tail (Joyner, 2002; Sadler, 2005). These domains are characterized by the expression of various marker genes. The marker genes routinely used are: *Otx2* for forebrain and midbrain, *En2* for the midbrain/hindbrain boundary, *Krox20, Kreisler* and numerous *Hox* genes like *Hoxa2* for the hindbrain, and posterior *Hox* genes such as *Hoxb8* and *Hoxb9* for the spinal cord (Maden, 2006).

The activation/transformation model of the neural development proposed by Nieuwkoop (Nieuwkoop, 1952) is based on studies of amphibian embryos, and divides neural induction into two steps. In the first step, signals from the node initiate neural development by inducing neural tissue of an anterior type (forebrain). In a second, the transformation step, the mesoderm underlying the neural tube produces signals, which convert neural tissue with anterior features into more posterior midbrain, hindbrain and spinal cord tissues. There are three factors produced by mesoderm that are involved in the transformation step: Wnts, retinoic acid and fibroblast growth factors (FGFs). Each of these molecules can induce gene expression characteristic for posterior neural tissue and can suppress genes expressed in neural tissue of anterior type (Maden, 2006). For example, Wnts are responsible for the specification of caudal forebrain, midbrain and anterior hindbrain by downregulating anterior and upregulating posterior genes (Kiecker and Niehrs, 2001; Nordstrom *et al.*, 2002). Retinoic acid induces Krox20 and Hoxb8 expression and suppresses Otx2 (Muhr *et al.*, 1999). Retinoic acid is thought to control the specification of posterior hindbrain and cervical spinal cord in a concentration-dependent manner. FGFs work also in a concentration-dependent manner and induce *Krox20* and *Hoxb9* genes (Lamb and Harland, 1995). FGFs are implicated in the patterning of different levels of spinal cord by control of *Hoxc* genes expression (Liu *et al.*, 2001).

1.1.2 . Dorsal-ventral patterning of the spinal cord

Anterior-posterior patterning is a process, in which multiple mechanisms, distinct in particular regions of the central nervous system, are involved. In opposite, molecular mechanisms of the dorsal-ventral patterning are similar in the entire neural tube. Initially, signals derived from adjacent, non-neural tissues initiate the dorsal-ventral patterning process. For instance, dorsal specification is induced by the ectoderm, and ventral specification by the axial mesoderm. Later on, appropriate signals are transferred from non-neural tissue to certain groups of cells within the neural tube, called roof and floor plate in the dorsal and ventral neural tube (located caudally to the telencephalon), respectively (Figure 1.1). Dorsal-ventral patterning is best described in the spinal cord. The main indication of dorsal-ventral patterning is the presence of progenitor cells organized into domains or stripes that express distinct genes (Joyner, 2002).

The ventral neuroepithelium of the spinal cord gives rise to five major populations of neurons generated by distinct progenitor domains distinguished by a specific expression code of transcription factors. Patterning of the ventral neural tube is regulated by the floor plate, which expresses the secreted protein Sonic hedgehog (Shh) (Figure 1.1). Shh is known to regulate the specification of neuronal subtype identity in a concentration-dependent manner (Lupo *et al.*, 2006). Shh signaling regulates the activity of the Gli family of transcription factors. A “temporal adaptation” model for the spatial and temporal specification of ventral progenitor cells during exposure to Shh secreted from a ventral source relies on a progressive decrease in the sensitivity of receiving cells to ongoing Shh signaling. The adaptation of cells to ongoing Shh signaling results in different concentrations of Shh, producing distinct profiles of Gli activity. Thus, temporal adaptation transforms different concentrations of Shh, producing increased Gli activity, into a corresponding induction of each progenitor domain (Dessaud *et al.*, 2008). Some lines of evidence showed that other factors could play a role in the specification of ventral neuron types. For instance, retinoic acid can specify the most dorsal progenitor domains of the ventral spinal cord (Figure 1.1) (Lupo *et al.*, 2006). Recent studies demonstrated that the canonical Wnt pathway interacts with the Shh pathway by inducing *Gli3* expression. In turn, Gli3, by acting as a transcriptional repressor, restricts graded, ventral Shh/Gli activity to properly determine

ventral spinal cord cell fates (Alvarez-Medina *et al.*, 2008; Yu *et al.*, 2008).

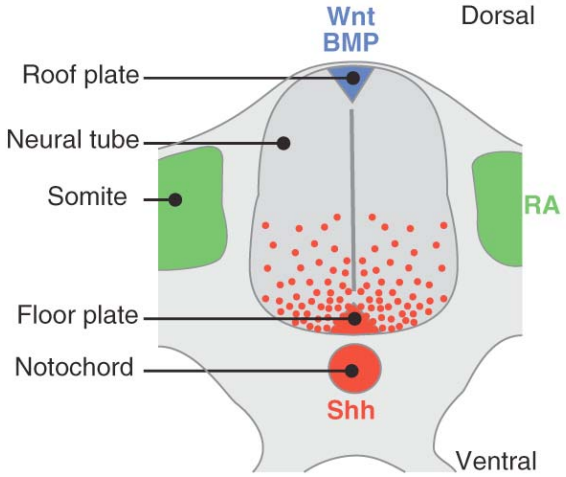

***Figure 1.1* Key regulators of dorsal-ventral patterning of the neural tube.** Schematic illustration represents transverse section of neural tube with indication of roof plate and floor plate. Dorsal portion of neural tube is patterned by BMP and Wnt signals coming from roof plate (blue). Ventral portion is patterned by a gradient of Shh produced by floor plate and notochord (red). Retinoic acid is produced by somites and patterns the intermediate portion of the neural tube (green). Adapted from (Dessaud *et al.*, 2008).

The signaling center for proper organization of the dorsal portion of spinal cord is the roof plate (Figure 1.1). Roof plate ablation using mice expressing diphtheria toxin under the control of the *Gdf7* gene leads to the loss of the three most dorsal types of neurons and to the appearance of an increased number of more ventral neuronal subtypes (Lee *et al.*, 2000; Muller *et al.*, 2002). Further supporting evidence of roof plate functions comes from analysis of the spontaneous mouse mutant *dreher*. In these mice, mutation of the LIM-homeodomain transcription factor *Lmx1a* causes failure of roof plate formation and this in turn causes a decrease in number of dorsal neurons (Millen *et al.*, 2004; Millonig *et al.*, 2000). In chick experiments, the roof plate is able to induce the most dorsal populations of neurons when transplanted into naïve caudal neural plate (Chizhikov and Millen, 2005). Thus, the roof plate is essential for the patterning of the three most dorsal progenitor domains and types of neurons. Several members of the BMP family are expressed in the roof plate. GDF7, BMP4, BMP6 and BMP7 can also induce dorsal neurons in naïve chick caudal neural plate, similarly to the roof plate (Liem *et al.*, 1997). Moreover, chick electroporation data showed that overexpression of either BMP4/7 or constitutively active BMP receptors resulted in increased production of the most dorsal type of neurons (Chizhikov and Millen, 2004; Timmer *et al.*, 2002). In opposite, electroporation of noggin, a common BMP inhibitor, and siRNA for

SMAD4, a component of the BMP signal transduction pathway, leads to the loss of roof plate (Chesnutt *et al.*, 2004). Some experiments indicate that BMPs can act in a concentration-dependent fashion (Timmer *et al.*, 2002). Results obtained from mouse experiments further support the role of BMPs as mediators of roof plate organizer activity. For instance, mutations of both Bmpr1a and Bmpr1b receptors result again in the absence of the most dorsal type of neurons (Wine-Lee *et al.*, 2004). Taken together, these results establish BMPs as crucial factors in the patterning of the dorsal spinal cord via the roof plate.

The Wnt family is also implicated in the dorsal patterning process. For instance, Wnt1 and Wnt3a are expressed in the dorsal midline region of the developing spinal cord. The mutation of both *Wnt1* and *Wnt3a* genes causes a reduction in number of the three most dorsal neuronal subtypes with a complementary increase in the number of more ventral neurons and at the same time shows no effect on the roof plate (Muroyama *et al.*, 2002). Furthermore, the canonical Wnt signaling controls the specification of dorsal neurons by regulating the expression of Olig3 transcription factor in progenitor cells (Zechner *et al.*, 2007). This indicates that Wnts are important components of roof plate signaling.

1.2 . Neuronal subtypes of the dorsal spinal cord and hindbrain

Everywhere in the developing neural tube a similar overall organization is apparent. Undifferentiated progenitor cells are situated around a ventricle, in a domain called the ventricular zone. The ventricular zone of the dorsal spinal cord expresses Pax3 and Pax7 in a graded manner (Figure 1.2 A). These progenitor cells have the capacity to either self renew or to produce differentiated cells of the central nervous system, neurons and glia. The newly born neurons do not divide any longer and migrate laterally into the adjacent domain, the mantle zone. In the alar plates of the spinal cord and rhombomere 7 two phases of neurogenesis can be distinguished: an early (E10-E12) and a late (E12.5-E14). Most of the neuronal types born in the dorsal spinal cord and hindbrain during both waves of neurogenesis integrate and relay somatosensory or viscerosensory information.

1.2.1 . Early-born neurons of the dorsal spinal cord and hindbrain

In the early phase of neurogenesis of the spinal cord, six subtypes of neurons, denoted as dI1-dI6 and defined by the specific expression pattern of distinct homeodomain transcription factors, are born. They are generated from particular domains of the ventricular zone (dP1-dP6) marked by the expression of basic helix-loop-helix (bHLH) transcription factors (Figure 1.2 A). Three neuronal types (dI1-dI3), produced in the most dorsal part of alar plate, are classified as class A neurons, and their specification is dependent on roof plate signals (Lee *et al.*, 2000; Muller *et al.*, 2002). All of these neurons are generated from a progenitor domain expressing the Olig3 transcription factor (Muller *et al.*, 2005). The three dorsal subtypes (dI4-dI6), which arise more ventrally, express Lbx1. Lbx1+ neurons are generated in the absence of the roof plate and they are referred to as class B neurons (Gross *et al.*, 2002; Muller *et al.*, 2002). These neuron types and the progenitor domains, from which they derive, express particular transcription factors, which help to identify them experimentally (Figure 1.2 A).

The fate and function of these neurons were investigated using mutant mice. For instance, analysis of *Math1* mutant mice showed that dI1 neurons give rise to a subset of proprioceptive neurons and the spinocerebellar and cuneocerebellar tracts (Bermingham *et al.*, 2001). Multiple studies revealed neurotransmitter identities of early-born neurons. Class A and dI5 neurons express glutamatergic markers like vesicular glutamate transporter type 2 (VGlut2) and therefore they are classified as excitatory neurons. In opposite, dI4 and dI6 neurons are characterized by expression of GABAergic markers like glutamate decarboxylase 1 (Gad1), an enzyme essential for GABA synthesis and therefore they are classified as inhibitory neurons (Cheng *et al.*, 2004; Glasgow *et al.*, 2005). Unfortunately, fate and function of particular dorsal early-born neuronal subtypes are still not completely understood. This requires further investigation using for instance genetic fate mapping, in particular inducible one, which allows controlling recombination in a time-dependent manner.

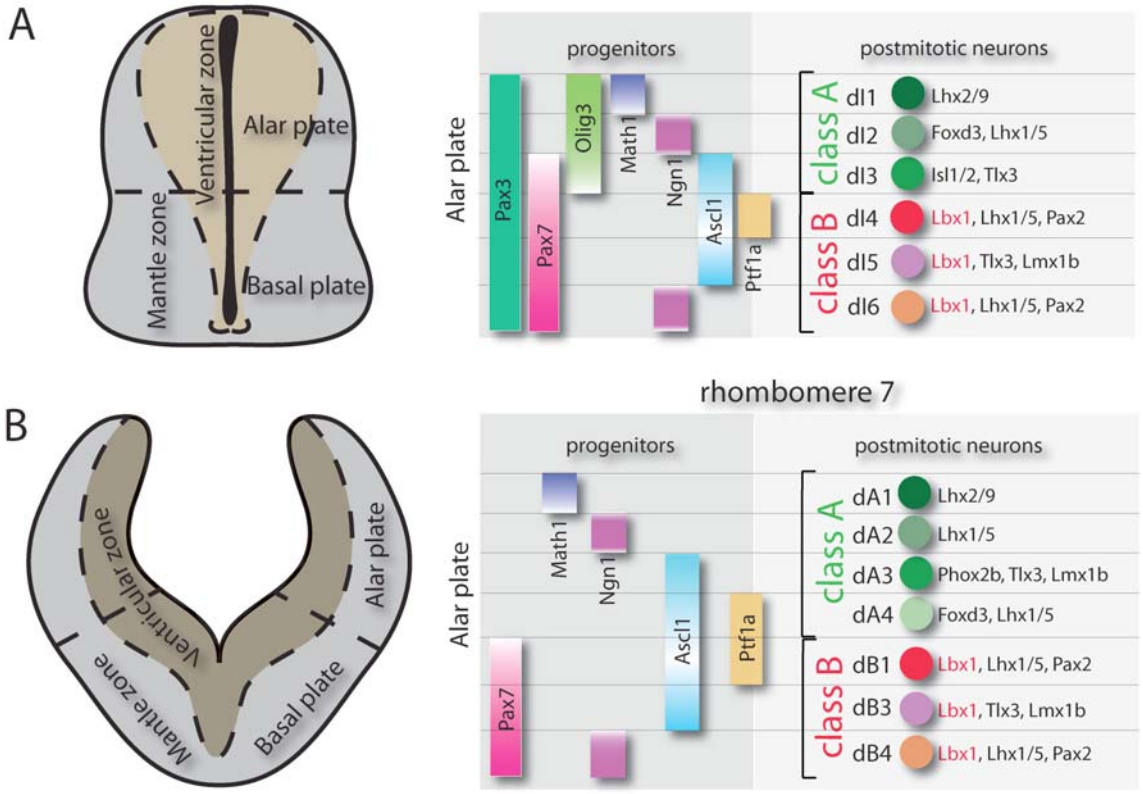

***Figure 1.2* Schematic representation of progenitor and neuron populations defined in the dorsal spinal cord and hindbrain at the early wave of neurogenesis.** Data are compiled from multiple reports (Helms and Johnson, 1998; Gowan *et al.*, 2001; Gross *et al.*, 2002; Muller *et al.*, 2002; Helms and Johnson, 2003; Glasgow *et al.*, 2005; Muller *et al.*, 2005; Qian *et al.*, 2002; Liu *et al.*, 2007; Sieber *et al.*, 2007). (A) Structure of the neural tube at E10.5 including principle domains and diagram showing the organization of the dorsal progenitor domain and dorsal neuron subtypes in the alar plate of the spinal cord. Progenitor populations are defined by expression of bHLH factors. Neuronal populations are defined by expression of homeodomain factors. (B) Structure of rhombomere 7 at E11.5 and diagram showing the organization of the dorsal progenitor domain and dorsal neuron subtypes in the alar plate of the hindbrain.

In the rhombencephalon neuronal subtypes arise that are similar to those of the spinal cord. Moreover, they are generated from progenitor domains expressing bHLH transcription factors similar to the dorsal spinal cord (Figure 1.2 B). Despite similarities between dorsal neurons generated in the spinal cord and hindbrain, particular neuronal types are characterized by distinct marker genes. The most pronounced differences are observed in class A subtypes. For instance, dA3 neurons, which are equivalent of dI3 neurons, express Phox2b and additionally Lmx1b, instead of Isl1/2. An additional subtype dA2 appears in rhombomere 7, which is generated by a progenitor domain expressing Ngn1 similarly to spinal cord dI2 neurons. However, dA2 neurons do not express Foxd3 unlike dI2 neurons do. Instead, dA4 neurons express Foxd3 and they are

generated from a progenitor domain expressing Ptf1a and this is unique for rhombomere 7. Class B neurons of the dorsal hindbrain are molecularly very similar to class B neurons of the dorsal spinal cord. However, in rhombomeres 2-6, an additional dB2 neuronal type appears, which is characterized by co-expression of Phox2b and Lbx1. Moreover, differences also exist between distinct rhombomeres. For instance, seven types of neurons are generated in rhombomeres 4-7 and only six types in rhombomeres 2-3 (Sieber *et al.*, 2007).

Some functions and the fate of dorsal neuronal subtypes are known in the hindbrain. For instance, dA1 neurons give rise to mossy fiber neurons of the lateral reticular and external cuneate nucleus and additional derivatives in the pons and in the cerebellum (Bermingham *et al.*, 2001; Li *et al.*, 2004; Landsberg *et al.*, 2005; Machold and Fishell, 2005; Wang *et al.*, 2005). dA3 neurons contribute to viscerosensory relay neurons of the nucleus of the solitary tract and to neurons in the area postrema (Pattyn *et al.*, 2000; Qian *et al.*, 2001). dA4 neurons give rise to climbing fiber neurons of the inferior olivary nucleus in rhombomere 7 (Yamada *et al.*, 2007). Finally, class B neurons contribute to somatosensory relay neurons of the spinal trigeminal nucleus and contribute to inhibitory neurons of the nucleus of the solitary tract (Sieber *et al.*, 2007). dB2 neurons, which are characterized by co-expression of Lbx1 and Phox2b, are apparently involved in respiratory control by generating the retrotrapezoid nucleus as well as other neurons (Pagliardini *et al.*, 2008).

1.2.2 . Late-born neurons of the dorsal spinal cord and hindbrain

The second phase of neurogenesis in the alar plate lasts from E12 until E14 in the dorsal spinal cord and E13 to E15 in the hindbrain. During the late wave, the majority of the dorsal progenitors of the spinal cord produces two neuronal subtypes, dILA and dILB neurons, which arise in a salt-and-pepper pattern (Figure 1.3 A) (Gross *et al.*, 2002; Muller *et al.*, 2002). Both populations arise from a broad progenitor domain expressing Ascl1 and Ptf1a. One of those, dILA neurons, is generated exclusively by asymmetric cell division, whereas dILB neurons are produced by either symmetric or asymmetric cell division (Wildner *et al.*, 2006). dIL neurons settle in superficial layers of the dorsal horn and receive information from sensory neurons of the periphery

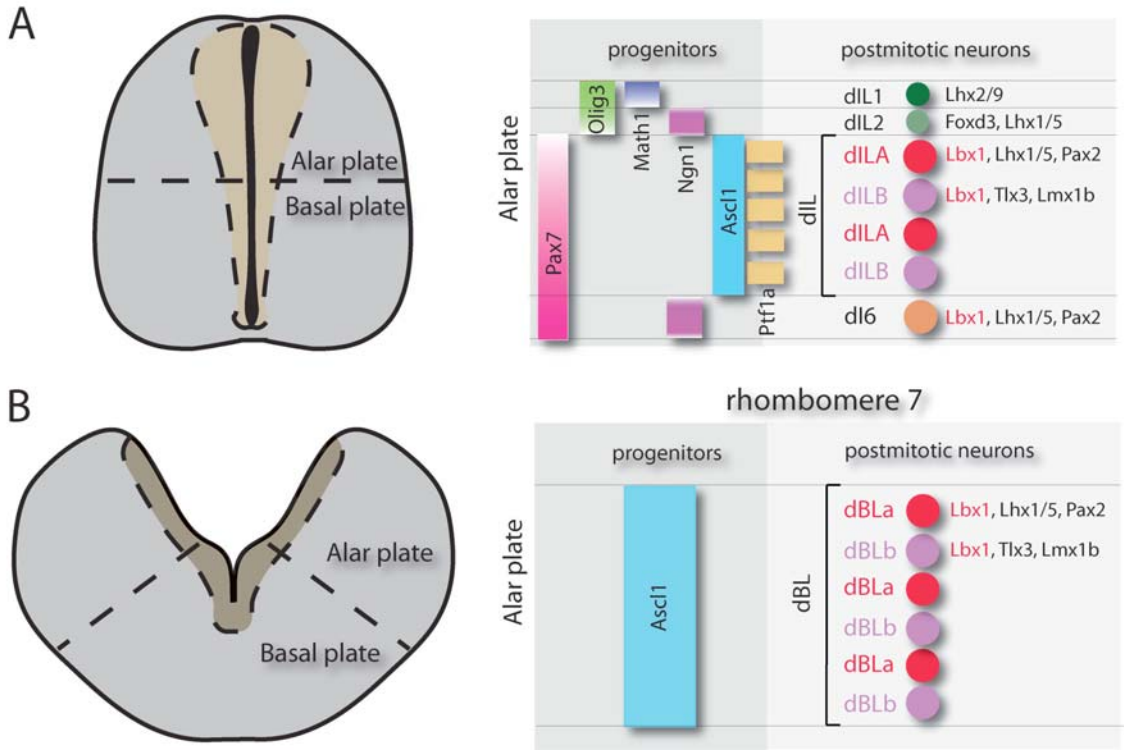

***Figure 1.3* Schematic representation of progenitor and neuron populations defined in the dorsal spinal cord and hindbrain at the second wave of neurogenesis.** Data are compiled from multiple reports (Helms and Johnson, 2003; Mizuguchi *et al.*, 2006; Wildner *et al.*, 2006; Sieber *et al.*, 2007). (A) Structure of the neural tube at E12.5 and diagram showing the organization of the dorsal progenitor domain and dorsal neuron subtypes in the alar plate of the spinal cord. Progenitor populations are defined by expression of bHLH factors. Neuronal populations are defined by expression of homeodomain factors. (B) Structure of rhombomere 7 at E13.5 and diagram showing the organization of the dorsal progenitor domain and dorsal neuron subtypes in the alar plate of the hindbrain.

(Gross *et al.*, 2002; Muller *et al.*, 2002). The neurotransmitter identity of dIL neurons is known: Pax2-positive dILA neurons and Tlx3-positive dILB neurons give rise to GABAergic and glutamatergic neurons, respectively (Cheng *et al.*, 2004; Glasgow *et al.*, 2005). Neurons of the inhibitory (GABAergic) and excitatory (glutamatergic) fates further diversify during subsequent development and express specific neuropeptides. Most of these are expressed exclusively in inhibitory or excitatory neurons of the dorsal horn. In particular, genes encoding prepronociceptin, preproenkephalin, galanin, prodynorphin and neuropeptide Y are expressed by inhibitory neurons, whereas cholecystokinin, gastrin-releasing peptide, tachykinin 1 and adenylate cyclase activating polypeptide 1 are produced by excitatory neurons (Brohl *et al.*, 2008; Huang *et al.*, 2008; Xu *et al.*, 2008).

In principle, the late neurogenic wave in the alar plate of rhombomere 7 proceeds in a similar way as in the dorsal spinal cord. The broad progenitor domain expressing Ascl1 gives rise to two subtypes of neurons denoted as dBLa and dBLb (Figure 1.3 B). Similarly to the dorsal spinal cord, these neurons arise in a salt-and-pepper pattern. dBL neurons contribute to somatosensory neurons of the spinal trigeminal nucleus (Sieber *et al.*, 2007).

1.3 . The role of bHLH transcription factors in the specification of neurons

One important class of genes that regulates cellular diversity in the nervous system encodes basic helix-loop-helix (bHLH) transcription factors. These transcription factors form a heterodimer with ubiquitously expressed bHLH factors, for instance E47, and activate gene expression by binding to the E-box. Some of bHLH factors act as proneural factors that function within the Notch pathway to single out neuronal progenitors and promote their differentiation. These factors play additional important roles in the determination of neuronal fates (Kageyama *et al.*, 2005).

1.3.1 . The Olig3 bHLH transcription factor

Olig genes encode a repressor-type subfamily of bHLH transcription factors. A characteristic feature of this family is the substitution of a conserved phenylalanine or leucine residue by methionine in the basic helix-loop-helix domain and the presence of a particular amino acid cluster in their N- and C-terminal region (Takebayashi *et al.*, 2000). The function of two family members, Olig1 and Olig2, in the development of motoneurons and oligodendrocytes has been extensively investigated (Mizuguchi *et al.*, 2001; Novitch *et al.*, 2001; Zhou *et al.*, 2001; Lu *et al.*, 2002; Takebayashi *et al.*, 2002a; Zhou and Anderson, 2002; Arnett *et al.*, 2004). The third member, Olig3, shares 79% identity with Olig1 and 95% identity with Olig2 within the bHLH domain (Takebayashi *et al.*, 2000). Around E9.25 expression of Olig3 is found in the neural tube and is restricted to a dorsal domain that extends from the midbrain/hindbrain boundary caudally into the spinal cord. Additionally, Olig3 is expressed in three groups of post-

mitotic neurons in the ventral spinal cord (Takebayashi *et al.*, 2002b). Olig3 marks dorsal progenitors that generate class A neurons in the spinal cord. In *Olig3* mutant mice, dI1 neurons are produced in reduced number, dI2 and dI3 neurons are not formed, and at their expense ectopic dI4 neurons appear. Thus, Olig3 is crucial for the correct specification of class A neurons and suppresses class B neuronal fates. These functions are fulfilled via mutual inhibition between Olig3 and Lbx1. Ectopic expression experiments in the chick demonstrate that Olig3 cooperates with Ascl1 and that the two factors together are able to specify dI3 neurons. Therefore, Olig3 provides permissive functions that are exerted by repressing Lbx1, and in addition Olig3 plays a role as an instructive factor for the specification of dI3 neurons (Muller *et al.*, 2005). Furthermore, recent work demonstrated that Olig3 expression in the spinal cord is controlled by dorsal patterning signals. Using *β-catenin* gain-of-function and compound *β-catenin* gain-of-function/*Olig3* loss-of-function mutation in mice, it was shown that the canonical Wnt pathway controls the specification of dI2 and dI3 neurons by regulating the expression of Olig3 in progenitor cells. Moreover, the BMP pathway acts upstream of Wnt signals in the control of Olig3 expression (Zechner *et al.*, 2007).

1.3.2 . Ptf1a function in the nervous system

The *Ptf1a/p48* gene (pancreatic transcription factor 1 a) encodes a bHLH transcription factor related to the Twist subclass of bHLH genes, and it is one of three subunits of the pancreatic exocrine tissue specific transcription factor complex, PTF1. Mutation of the human *PTF1A* gene causes a permanent neonatal diabetes mellitus and cerebellar hypoplasia, whereas a null mutation of *Ptf1a/p48* in the mouse leads to pancreatic and cerebellar agenesis and neonatal lethality (Sellick *et al.*, 2004). The *Ptf1a/p48* gene is expressed in the cerebellar primordia, dorsal hindbrain and spinal cord at early stages of development, and in the pancreas. Ptf1a expression in the dorsal neural tube is dynamic and changes with time between E10.5 and E12.5. In *Ptf1a* mutant mice, dI4 and dILA neurons are not formed during the early and late phase of neurogenesis, respectively. In opposite, numbers of dI5 and dILB neurons are increased. The function of Ptf1a in the generation of dILA neurons is achieved by a suppression of Tlx3, which allows the formation of GABAergic neurons while suppressing the formation of glutamatergic neurons (Glasgow *et al.*, 2005). Similarly, Ptf1a is present in the mouse cerebellum and

in the retina of the frog and mice, where it is essential for the formation of GABAergic neurons (Hoshino *et al.*, 2005; Dullin *et al.*, 2007; Nakhai *et al.*, 2007).

Ptf1a is also expressed in the alar plate of the caudal hindbrain. Recently, it has been shown that Ptf1a positive cells of rhombomere 7 give rise to GABAergic neurons of the spinal trigeminal nucleus and the nucleus of the solitary tract and to glutamatergic climbing fiber neurons that generate the inferior olivary nucleus and that Ptf1a is required for the determination of the fate of climbing fiber neurons. These findings demonstrate that Ptf1a function is not only exclusively restricted to the specification of GABAergic neurons, but is also essential for the development of non-GABAergic cell types (Yamada *et al.*, 2007).

Ptf1a is a component of the unusual heterotrimeric transcription factor PTF1, which is composed of two further subunits. Analyses of PTF1 in pancreas, which were published during my doctoral work, revealed that it is a heterotrimeric factor consisting of (in addition to Ptf1a) a member of the class A bHLH factors like E12, E47 and Tcf12, and Rbp-l, a paralogue of Rbp-j, or Rbp-j itself (Figure 1.4) (Beres *et al.*, 2006). A single amino acid change in Ptf1a (W298A) that eliminates its ability to bind Rbp-j (but does not affect its binding to Rbp-l) results in deficits of pancreatic development (Masui *et al.*, 2007). When I started my thesis, it was not known whether Ptf1a and Rbp-j interact during the development of the nervous system.

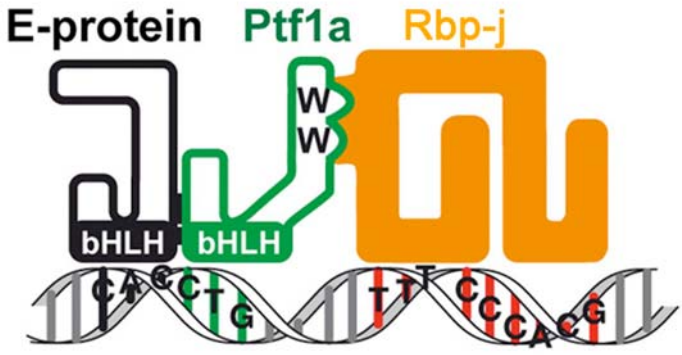

***Figure 1.4* Diagram of the PTF1 trimer.** The PTF1 complex is composed of the bHLH factor Ptf1a, a class A bHLH factor and Rbp-j and is binding to a DNA sequence containing an E-box and TC-box. Adapted from (Hori *et al.*, 2008).

1.4 . Functions of the Notch pathway in the neural development

The function of the Notch pathway in the development of the central and peripheral nervous system was extensively studied in *Drosophila melanogaster*. Particularly interesting is the role of Notch as a fate determinant in asymmetric cell divisions. In asymmetric cell divisions, the two daughter cells inherit different fate determinants from the mother cell. It is thought that the asymmetric localization of the Numb protein in the mother cell causes its segregation to one of two daughter cells, and that Numb represses Notch signaling in this cell (Rhyu *et al.*, 1994). The second daughter cell does not inherit Numb, and therefore Notch signaling occurs in this cell. Thus, this difference in Notch signaling in the two daughter cells allows them to assume distinct fates (Muskavitch, 1994; Cayouette and Raff, 2002). In the mammalian nervous system, Notch signaling controls the maintenance of neuronal progenitors, the choice between neuronal and glial fates, neuronal migration and axonal branching. Particularly, *Notch1* and *Rbp-j* mutations lead to enhanced neurogenesis and neural progenitor pool depletion (de la Pompa *et al.*, 1997). Regulation of neurogenesis is mediated via the interaction between proneural genes like *Ascl1* or *Ngn2* and the Notch pathway by lateral inhibition (Louvi and Artavanis-Tsakonas, 2006; Kageyama *et al.*, 2008). Also in mammals, some lines of evidence link the Notch receptor with neuronal cell fate choice, similarly to those observed previously in *Drosophila*. For instance, the Notch1 receptor is asymmetrically inherited by daughter cells of mitotically active cortical progenitor cells (Chenn and McConnell, 1995). In the ventral spinal cord, Notch signaling activated by ligand DLL4 is important for the fate choice between V2a and V2b ventral neuronal populations generated from apparently identical progenitors (Peng *et al.*, 2007). In the dorsal spinal cord, Notch signaling was implicated in the promotion of dILB fate (Mizuguchi *et al.*, 2006).

1.4.1 . Rbp-j function in the Notch pathway

Recombination signal sequence-binding protein Jκ (Rbp-j, RBP-Jκ, CBF1, CSL, Rbpsuh) is the mammalian homolog of the *Drosophila* gene *suppressor of hairless* and is a highly conserved protein that is ubiquitously expressed at early developmental

stages (Honjo, 1996). Rbp-j plays a central role as a main transcriptional mediator of Notch signaling (Honjo, 1996). A single *Rbp-j* gene is identified in mammals (Tamura *et al.*, 1995; Kadesch, 2000). In addition, a Rbp-j-related gene named *Rbp-l* exists in mammals, which however does not interact with any of the known Notch receptors (Minoguchi *et al.*, 1997). Rbp-j is a transcription factor comprised of N-terminal and C-terminal Rel homology domains and a central atypical β-trefoil DNA binding domain.

Notch signaling occurs when the ligand on one cell interacts with the Notch receptor on the neighboring cell. This interaction triggers two proteolytic cleavages of Notch. The second cleavage results from the action of a γ-secretase and releases the intracellular domain of Notch (NICD) from the membrane. Subsequently, the NICD is translocated to the nucleus and binds to Rbp-j, converting it from a transcriptional repressor to an activator by displacing corepressors. When NICD is bound, the transcriptional coactivator protein Mastermind-like 1 (Maml-1) is also recruited, forming a ternary complex containing Rbp-j, NICD and Maml-1 (Figure 1.5 A) (Tani *et al.*, 2001; Nam *et al.*, 2006; Kovall, 2007). The dominant negative variant of Maml-1 contains the NICD and Rbp-j binding domain (amino acids 13–74 of Maml-1) but lacks its activation domain and it is thought to block Notch signaling (Figure 1.5 B,C). The availability of a mouse strain expressing the dominant negative Maml-1 after Cre-mediated recombination opened new possibilities to investigate the Notch pathway (Tu *et al.*, 2005).

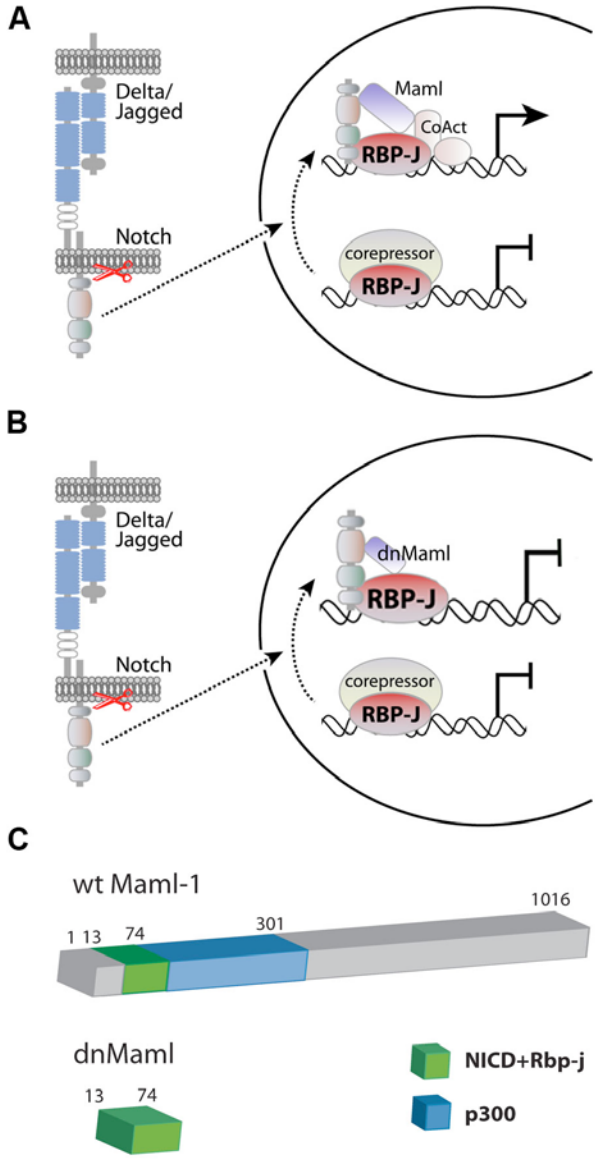

Figure 1.5 **The core of the Notch signaling pathway.** (A) Scheme showing the Notch receptor on the surface of one cell and Delta/Jagged ligands on the surface of an adjacent cell. Interaction of ligand and receptor releases Notch intracellular domain, allowing it to translocate to the nucleus, where it associates with Rbp-j and Maml-1. This complex activates transcription of Notch target genes. Picture kindly provided by Elena Vasyutina. (B) Inhibition of the Notch signaling by a dominant negative variant of Maml-1 (dnMaml). dnMaml is not able to recruit coactivators essential for initiation of transcription. (C) Structure of Maml-1 protein. The domain at the N-terminal end of the protein is responsible for binding Notch intracellular domain (NICD) and RBP-J (green box). dnMaml lacks the domain that recruits coactivators like p300 (blue box).

1.5 . Aims

The aim of my work is to understand processes that underlie a proper development and maturation of the dorsal spinal cord and hindbrain. The determination of neuronal subtypes is controlled by transcription factors. Therefore, the analysis of transcription factor functions can provide insight into the development of the spinal cord and hindbrain.

In the first part of the thesis, I analyze the function of the Rbp-j transcription factor in the dorsal spinal cord development. This revealed one phenotype that was very similar to the one observed in the *Ptf1a* mutant, i.e. a lack of determination of the GABAergic neurons in the dorsal spinal cord, and a second that was similar to the loss of Notch function, i.e. a premature differentiation of neuronal progenitors in the spinal cord. Thus, Rbp-j has two distinct roles, and it functions on one side in neuronal progenitors as a component of the Notch pathway, i.e. in a complex with NICD and Maml-1, and on the other side in neuronal specification, i.e. in a complex with Ptf1a and class A bHLH factors.

The second part is devoted to the Olig3 transcription factor and its function in the dorsal alar plate of the hindbrain. To study the role of Olig3, I used inducible genetic lineage tracing to reveal derivatives of Olig3+ progenitor domain. I demonstrated that they were not formed or appeared in reduced numbers in *Olig3* mutant mice. The analysis of *Olig3/Lbx1* double mutants showed that Olig3 exerts its role in the specification of climbing fiber neurons (dA4) of the inferior olivary nucleus solely by suppressing Lbx1. In opposite, the analysis of *Olig3/Ptf1a* double mutants revealed that Olig3 provides additional instructive information during the determination of noradrenergic neurons (dA3) of the nucleus of the solitary tract.

2 . Materials and Methods

2.1 . Abbreviations

bp	Base pair
BAC	Bacterial artificial chromosome
BCIP	5-Bromo-4-chloro-3-indolyl-phosphate
BrdU	5-Bromo-2-deoxyuridine
BSA	Bovine serum albumin
cDNA	Complementary DNA
DEPC	Diethylpyrocarbonate
DIG	Digoxigenin
DMEM	Dulbecco's Modified Eagle Medium
DMF	Dimethylformamide
DMSO	Dimethylsulfoxide
DNA	Deoxyribonucleic acid
dNTP	Deoxyribonucleotide triphosphate
DTA	Diphtheria toxin A
EDTA	Ethylenediaminetetraacetic acid
ERT	Tamoxifen responsive Estrogen Receptor ligand binding domain
ES cell	Embryonic stem cell
FCS	Fetal calf serum
FRT	Flipase recognition target
G418	Geneticin
GFP	Green fluorescent protein
HEPES	4-(2-Hydroxyethyl)-1-piperazineethane sulfonic acid
HH	Hamburger-Hamilton stage

HS	Horse serum
IRES	Internal ribosome entry site
LB	Luria-Bertani medium or Lysogeny broth
LIF	Leukemia inhibitory factor
mRNA	Messenger ribonucleic acid
NaAc	Sodium acetate
NBT	Nitro blue tetrazolium chloride
NEN	Blocking reagent
neo	Neomycin resistance gene
NH_4Ac	Ammonium acetate
NLS	Nuclear localization signal
NP-40	Nonidet-P40
pA	polyA
PBS	Phosphate buffered saline
PBX	PBS containing 0.1% Triton X-100
PCR	Polymerase chain reaction
PFA	Paraformaldehyde
PGK	Phosphoglycerate kinase
RNA	Ribonucleic acid
RNase	Ribonuclease
SDS	Sodium dodecyl sulfate
SSC	Saline sodium citrate
TAE	Tris-acetate-EDTA
TE	10mM Tris buffer containing 1 mM EDTA
Tris	2-Amino-2-hydroxymethyl-propane-1,3-diol
X-gal	5-Bromo-4-chloro-3-indolyl-beta-D-galactopyranoside

2.2 . Materials

2.2.1 . Chemicals

All chemicals and kits for molecular biology were purchased from following companies: Roth (Karlsruhe), Sigma-Aldrich Chemie (Steinheim), Invitrogen (Karlsruhe), Merck (Darmstadt), Gibco BRL (Karlsruhe), Clontech (Heidelberg), Molecular Probes (Eugene, USA), Macherey-Nagel (Düren), PerkinElmer Life Sciences (Boston, USA), Promega (Mannheim), Stratagene (Amsterdam, Netherlands), Qiagen Sciences (Maryland, USA), Biotez (Berlin), Ambion (Huntingdon, UK). Enzymes and enzymes' buffers were obtained from New England Biolabs (Frankfurt am Main). Oligonucleotides were produced by MWG-Biotech (Ebersberg). Cy2-, Cy3- and Cy5-conjugated secondary antibodies were provided by Dianova (Hamburg).

2.2.2 . Bacterial strains

Escherichia coli XL1-Blue MRF	(Jerpseth, 1992)
Escherichia coli DH10B	Invitrogen
Escherichia coli DY380	(Yu *et al.*, 2000)
Escherichia coli EL350	(Lee *et al.*, 2001)

2.2.3 . Vectors

pBluescript II SK+	(Sorge, 1988)
pGEM-Teasy	Promega
pZERO-Cre-mpA	H. Wende, MDC, Berlin
pKS-DTA	M. Treier, EMBL, Heidelberg
RCASBP B mOlig3	T. Müller, MDC, Berlin

RCASBP B mPtf1a	D. Bröhl, MDC, Berlin

2.2.4 . Antibodies

Immunofluorescence was performed using the following primary antibodies: guinea pig anti-Islet1/2 (1:20,000; Tom Jessell, Columbia University, New York, USA), mouse anti-Lhx1/5 (1:10; 4F2; Developmental Studies Hybridoma Bank, University of Iowa, USA), guinea pig anti-Lmx1b (1:5000; (Muller *et al.*, 2002)), mouse anti-Ascl1 (1:500; BD Biosciences Pharmingen, USA), rabbit anti-Pax2 (1:1000; Zymed, USA), goat anti-β-galactosidase (1:500; Biogenesis, UK), mouse anti-NeuN (1:1000; Chemicon, USA), rat anti-Ki67 (1:50; DakoCytomation, Denmark), mouse anti-TuJ1 (1:1000; Covance, USA), guinea pig anti-Olig3 (1:5000; (Muller *et al.*, 2005)), rabbit anti-Foxd3 (1:2000; Martyn Goulding, Salk Institute, La Jolla, USA), guinea pig anti-Foxd3 (1:10,000; (Zechner *et al.*, 2007)), guinea pig and rabbit anti-Tlx3 (1:10,000; (Muller *et al.*, 2002)), guinea pig and rabbit anti-Lbx1 (1:10,000; (Muller *et al.*, 2002)), chick anti-β-galactosidase (1:500; Abcam, UK), rabbit anti-Phox2b (1:500; Christo Goridis and Jean-Francois Brunet, Ecole Normale Superieure, Paris, France), mouse anti-NF68 (1:4; Sigma, Germany), guinea pig and rabbit anti-Ptf1a (1:10,000) and rabbit anti-Ngn1 (1:1000; Jane Johnson, Southwestern Medical Center, Dallas, USA), mouse anti-Pax7 (1:10; Developmental Studies Hybridoma Bank, University of Iowa, USA), rabbit anti-Lhx2/9 (1:2000) and rabbit anti-Math1 (1:2500; Tom Jessell, Columbia University, New York, USA), rabbit anti-Cre (1:10,000; Novagen, USA), rat anti-BrdU (1:200; Abcam, UK) and sheep anti-GFP (1:1500; Biogenesis, UK). The secondary antibodies coupled with Cy2, Cy3 or Cy5 fluorescent reagent were dissolved in sterile 50% glycerin to a final concentration of 0.5 mg/ml. Dilutions of 1:500 for Cy2, Cy3 and Cy5 were routinely used.

2.2.5 . Riboprobes for *in situ* hybridization

In situ hybridization was performed using a chicken Ptf1a riboprobe (H.Wildner, MDC, Berlin) and a chicken Foxd3 riboprobe (D. Zechner, MDC, Berlin).

2.2.6 . Cell lines

Embryonic stem (ES) cells from the line E14.1, derived from the 129/Ola mouse strain (Hooper *et al.*, 1987; Kuhn *et al.*, 1991) were used to introduce targeted mutations into the mouse.

2.2.7 . Chicken strains

Fertilized chicken eggs (White Leghorn) were provided by Charles River (Sulzfeld).

2.2.8 . Mouse strains

Wild type mice: C57Bl/6J-inbred and CD1-outbred mouse strains were provided by Charles River (Sulzfeld).

Pax3^{cre} (Jonathan A. Epstein, University of Pennsylvania, Philadelphia): *Pax3*^{cre} knock-in mice were generated by homologous recombination in ES cells by inserting a Cre recombinase coding sequence and a *loxP*-flanked PGK-neo cassette into the first exon of the *Pax3* gene. Most of the first *Pax3* exon downstream of the transcription start site including the initiating ATG was replaced. After passing through the male germ line, the *PGK-neo* cassette was removed within the targeted locus (Engleka *et al.*, 2005).

Pax7^{CreERT2} TG4 (Benedetta Martarelli, MDC, Berlin): *Pax7*^{CreERT2} mice were generated as BAC transgenics using pronuclear injection. The 185 kb BAC clone RP23-387L10 (RZPD, Germany) containing the *Pax7* locus was modified by homologous recombination in bacteria using a cassette encoding the entire sequence of *CreERT2* (containing the initiating ATG codon) and *IRES-eGFP-pA* designed to replace the second exon of *Pax7*. Exon 1 was modified to remove possible ATG codons.

Rbp-j$^{flox/flox}$ (Tasaku Honjo, Kyoto University, Kyoto): the *Rbp-j* conditional allele was generated by introduction of *loxP* sites into the *Rbp-j* locus, flanking exon 6 and 7. ES clones containing the *loxP*-flanked (flox) *Rbp-j* locus were used to generate chimeric mice and the mutant mouse line was established through germ-line transmission (Tanigaki *et al.*, 2002).

Rbp-j$^{\Delta/+}$: these mice were generated by crossing *Rbp-j*$^{flox/+}$ mice with a Cre-deleter strain (Schwenk *et al.*, 1995).

DNMAML (Warren Pear, University of Pennsylvania, Philadelphia): this strain was generated by introducing a *loxP*-flanked *PGK-Neo-tpA* cassette followed by a GFP-tagged dominant negative variant of Mastermind-like 1 (dnMaml) into the *ROSA26* locus. Upon Cre expression, the *PGK-Neo-pA* cassette is excised, thereby allowing dnMaml expression and inhibition of Notch signaling (Tu *et al.*, 2005).

ROSA26R (Philippe M. Soriano, Mt. Sinai School of Medicine, New York): this reporter mouse strain for site and time-specific recombinases was generated by inserting a *neo* expression cassette flanked by *loxP* sites, the *lacZ* gene and a polyadenylation sequence (pA) into the ROSA26 locus (Soriano, 1999).

Tau^{nlsLacZ} (Sylvia Arber, University of Basel, Basel): this neuron-specific reporter mouse strain was generated by integrating a *lox-STOP-lox-mGFP-IRES-NLS-LacZ-pA* targeting cassette into exon 2 of the *Tau* locus (Hippenmeyer *et al.*, 2005).

Olig3^{GFP} (Mathias Treier, EMBL, Heidelberg): these mice were generated by homologous recombination in ES cells. *Olig3* coding sequence between the XhoI and FseI restriction sites, which includes the sequences encoding the bHLH domain, was replaced by an *EGFP-IRES-NLS-LacZ* cassette fused in frame to the 5′-coding sequence and a *neo* expression cassette (Muller *et al.*, 2005).

Lbx^{Cre} AF9 (Elena Vasyutina, MDC, Berlin): the *Lbx1*^{Cre} mutant allele was generated by homologous recombination in ES cells. In this allele, a *Cre* cDNA as well as a *neo* expression cassette replaced the first exon of *Lbx1*. Mutant ES cells were used to generate the corresponding mutant mouse strain. The *neo* cassette was removed by crossing mice carrying the *Lbx1*^{CreNeo} allele with *FLPe* deleter mice (Sieber *et al.*, 2007).

2.2.9 . Bacteria culture

Media and agar plates for culture of the *Escherichia coli* strain were prepared according to “Molecular Cloning” (Sambrook, 2001). Bacteria containing plasmid or BAC DNA

were cultured in sterilized LB-medium with an appropriate antibiotic at 37°C overnight. The concentration of ampicillin and kanamycin in agar and medium were 50 μg/ml.

2.2.10 . Cell culture media

Fibroblast Medium:
500 ml DMEM with Glutamax-I, 4500 mg/l Glucose, with Pyridoxine, Sodium pyruvate (Gibco BRL)
60 ml FCS (heat inactivated at 55°C for 30 min, Sigma)
5.7 ml 100x non-essential amino acids (Gibco BRL)
5.7 ml Penicillin/Streptomycin-solution (10000 U/ml Penicillin G/10000μg/ml Streptomycin; Gibco BRL)
1.2 ml 50 mM β-Mercaptoethanol (Gibco BRL)

ES Cell Medium:
500 ml DMEM/Glutamax (see above, Gibco BRL)
90 ml FCS (heat inactivated at 55°C for 30 min, Sigma)
6 ml 100x non-essential amino acids (Gibco BRL)
6 ml Penicillin/Streptomycin-solution (Gibco BRL)
1.2 ml 50 mM β-Mercaptoethanol (Gibco BRL)
60 μl LIF (500-1000 U/ml)

2.3 . Methods

Standard protocols for various procedures like molecular cloning were performed according to "Molecular Cloning" (Sambrook, 2001) or instructions provided by companies. Besides that, detailed descriptions for other specific techniques are provided in following sections.

2.3.1 . Preparation of plasmids and DNA fragments

The Mini-preparations (3 ml culture) of plasmid and BAC DNA were performed by the alkaline lysis method (Birnboim and Doly, 1979). The Maxi-preparations (250 ml culture) of plasmid DNA were performed using the HiPure Plasmid Filter Maxiprep Kit from Invitrogen, according to the manufacturer's protocol. The concentration and purity of the DNA were determined using UV-spectrophotometer.
The purification of DNA fragments from agarose gels and DNA fragments from PCR reactions was performed with the NucleoSpin-Extract II-Kit from Macherey-Nagel. The DNA was eluted with 30 µl TE and stored at -20°C.

2.3.2 . Restriction hydrolysis of DNA, ligation of DNA fragments and transformation into bacteria

The restriction hydrolysis of plasmid and genomic DNA was performed with one or more restriction enzymes according to "Molecular Cloning" (Sambrook, 2001). The ligation of DNA fragments was carried out routinely using 50 ng vector DNA and triple molar surplus of DNA fragment in 20 µl reaction volume. The transformation of competent bacteria cells was performed using heat shock or electrotransformation methods according to (Inoue *et al.*, 1990). The ligation of DNA fragments from PCR reactions was performed using the pGEM-Teasy system according to manufacturer's protocol (Promega).

2.3.3 . Homologous recombination in bacteria

The homologous recombination in bacteria allows the sequence-specific integration of DNA fragments independently from the restriction enzyme system. Homology of 30-50 bp on 5' and 3'ends of a DNA fragment is sufficient to achieve a high sequence recombination rate.

In order to recombine a DNA fragment into a vector, the vector and the DNA fragment were transformed into the DY380 bacteria strain. This strain carries *Red* genes (*exo* and *bet*), which are crucial for recombination and are expressed from the strong λ P_L promoter. The promoter itself is under the control of the temperature-sensitive λ repressor. A permanent expression of *Red* genes is lethal for bacteria. In advance to transformation of the DNA fragment, the recombination machinery was induced by incubation of the culture at 42°C for 15 min and additionally the competency was induced (see also (Lee *et al.*, 2001).

In this doctoral thesis homologous recombination was performed to generate $Olig3^{CrepA}$ and $Olig3^{CreERT2}$ targeting vectors. First, homologous recombination was performed to subclone a long genomic sequence of the *Olig3* gene from a BAC clone into pBluescript carrying a *DTA* cassette (pDTA). In order to do this, the 500 bp long 5' and 3' homologous sequences were obtained by PCR reaction and cloned into pDTA. A second recombination event was performed to introduce DNA fragments containing *CrepA* and *CreERT2* coding sequences followed by a *FRT*-flanked *neo* cassette into the genomic subclone containing the *Olig3* locus.

2.3.4 . DNA sequencing

In order to verify the sequence of DNA fragments cloned or obtained from PCR reactions sequencing was performed.

DNA sequences were determined using the dideoxy-chain-termination reaction protocol (Sanger *et al.*, 1977) modified by Tabor and colleagues (Tabor and Richardson, 1987) and using the non-radioactive 'Thermo Sequenase Fluorescent Labeled Primer Cycle Sequencing'-Kit (Amersham-Pharmacia). Fluorescently labeled primers were obtained from MWG-Biotech. Reaction products were separated on 6% Sequagel XR

polyacrylamide gels (Biozym) in 1xTBE running buffer and analyzed using a Li-Cor-Sequencing device (Model 4000L or 4200, MWG-Biotech).

2.3.5 . Polymerase chain reaction

The polymerase chain reaction (Saiki *et al.*, 1985) was routinely used to genotype mice and embryos, and to amplify DNA fragments for cloning steps. Optimal PCR conditions were established according to general rules (Innis, 1989). Primer sequences were designed using Primer 3 software (http://frodo.wi.mit.edu/). Primers were purchased from MWG-Biotech. Genotyping PCR programs, primer sequences and conditions used in the following experiments are listed below:

1. DNMAML and ROSA26R

Primers: R26R F2: 5' – AAA GTC GCT CTG AGT TGT TAT – 3'
R26R R1295: 5' – GCG AAG AGT TTG TCT TCA ACC – 3'
R26R R3307: 5' – AGC GGG AGA AAT GGA TAT GAA – 3'

Conditions: 2 mM $MgCl_2$; 10 pmol per reaction of each primer, 10% DMSO.

Program:

94°C	4 min	
94°C	1 min	} 35x
60°C	1 min	
72°C	1 min	
72°C	5 min	

2. $Pax7^{CreERT2}$

Primers: P7-cre1: 5' – CTC CCC CAC ACT AAC TGC AT – 3'
P7-cre2: 5' – ATG TTT AGC TGG CCC AAA TG – 3'

Conditions: 2.5 mM $MgCl_2$; 12.5 pmol per reaction of each primer, 6% DMSO.

Program:

94°C	4 min	
94°C	45 sec	} 30x
60°C	45 sec	
72°C	50 sec	
72°C	7 min	

3. $Tau^{nlsLacZ}$ (SAM)

Primers: SAMfwd 3: 5' – GAA CAA AGC AGC CAC TCT C – 3'
SAMrev: 5' – CGA CCT GCA GCC CAA GCT GAT CC – 3'

Conditions: 2 mM $MgCl_2$; 10 pmol per reaction of each primer.

Program:

95°C	4 min	
95°C	45 sec	} 35x
62°C	30 sec	
72°C	1 min	
72°C	5 min	

4. DNeo

Primers: DNeo-fwd: 5' – AGA CAA TCG GCT GCT CTG AT – 3'
DNeo-rev: 5' – ATA CTT TCT CGG CAG GAG CA – 3'

Conditions: 2 mM $MgCl_2$; 10 pmol per reaction of each primer.

Program:

95°C	3 min	
95°C	45 sec	} 35x
60°C	45 sec	
72°C	30 sec	
72°C	5 min	

5. $Olig3^{CrepA}$ and $Olig3^{CreERT2}$

Primers: O3cre2-s: 5' – ATG GCA CGT CAT CTT AAC CAG – 3'
O3cre2-as: 5' – TTC CGG TTA TTC AAC TTG CAC – 3'
O3creER2-as: 5' – CAT GTT TAG CTG GCC CAA AT – 3'

Conditions: 2.5 mM $MgCl_2$; 25 pmol per reaction of each primer, Perpetual Taq.

Program:

95°C	4 min	
95°C	45 sec	} 35x
60°C	30 sec	
72°C	35 sec	
72°C	7 min	

6. Olig3 WT and GFP

Primers: Olig3-wt1: 5' – TTA ATT TCC TGC CTA AAG GCT CCT CAA – 3'
Olig3-wt2: 5' – TCT CCT CCA GGG AGC TGG TGA GCA TG– 3'
Olig3-GFP: 5' – GTG CAG ATG AAC TTC AGG GTC AGC– 3'

Conditions: 2.5 mM $MgCl_2$; 25 pmol per reaction of each primer, Perpetual Taq.

Program:

95°C	5 min	
95°C	45 sec	39x
58°C	35 sec	
72°C	45 sec	
72°C	5 min	

2.3.6 . Isolation of genomic DNA from mouse tissue

To genotype adult mice or embryos by PCR, DNA was isolated from ear holes or brain and tail tissues, respectively. The tissue was lysed for 2-10 h at 55°C in 50 µl of lysis buffer containing proteinase K (1 mg/ml). When the tissue lysis was completed, proteinase K was inactivated by incubation at 95°C for 10 min. Lysates were diluted with distilled water to a final volume of 300 µl or 500 µl and were directly used for PCR.

For Southern blot analysis, a piece of mouse liver was homogenized and incubated in 100 ml of extraction buffer containing RNase A (10 µg/ml) for 1h at 37°C. Afterwards, proteinase K was added in order to lyse the tissue for 3h at 55°C. The DNA was purified by phenol extraction and precipitated from the supernatant with 3M NaAc (pH 5.2) and 2.5 volumes of absolute ethanol. The pellet was washed twice with 70% ethanol and air-dried. The DNA was dissolved in TE buffer.

2.3.7 . Isolation of genomic DNA from ES cells

Genomic DNA was isolated from ES cells that were cultured in gelatinized 96- or 6-well plates. For that, the cells in 96-well plates were washed twice with PBS and then incubated overnight in 50 µl of ES cell lysis buffer (10mM Tris pH 7.5, 10mM EDTA, 10mM NaCl, 0.5% N-lauroylsarcosine, 200 µg/ml proteinase K) per well at 60°C. The

DNA was precipitated with 100µl of ice-cold 100% ethanol mixed with 3M NaAc per well for 30 min at room temperature, washed three times with 70% ethanol and air-dried for 15-20 min. The final restriction hydrolysis of the ES cell DNA was performed with 15 U of the appropriate restriction enzyme per well in a 35µl volume overnight at 37°C. The digested DNA was separated by electrophoresis and used for Southern blot analysis.

The cells in 6-well plates were washed with PBS, 0.5 ml of ES cell lysis buffer was added per well and incubated overnight at 60°C. The DNA was then extracted with 25:24:1 Phenol:Chloroform:Isoamylalcohol (PCI), washed with ethanol and dissolved in an appropriate volume (0.2-1 ml) of TE. Restriction digest for Southern blot analysis was carried out using 5-10 µg of ES genomic DNA per digestion.

2.3.8 . Southern blot

Southern blot analysis was performed to screen ES cell clones for homologous recombination events.

Genomic DNA (10 µg) was digested ON with 20 U of restriction enzyme. Digested DNA was separated on 0.7% agarose gel. The agarose gel was incubated in TAE buffer containing 0.5 µg/ml ethidium bromide in order to visualize DNA. The DNA in the gel was depurinated and denatured. In order to do this, the gel was incubated in 0.2M HCl for 15 min, shortly rinsed in distilled water and denatured by two 25 min long incubations with gentle shaking in a solution of 1.5M NaCl and 0.5M NaOH. The gel was rinsed in 10X SSC and blotted overnight using 20X SSC, in order to transfer the DNA onto a nylon membrane (Hybond N, Amersham-Pharmacia) as described by (Sambrook, 2001; Southern, 1975). Subsequently, the membrane was hybridized with specific radioactive probes. DNA probes (20-50 ng) were radioactively labeled with 50 µCi γ32P-dCTP (Amersham-Pharmacia) using the 'Prime-It RmT Random-Primed Labeling Kit' (Stratagene). The labeled probes were purified from unincorporated nucleotides over Sephadex-G50 spin columns (Probe Quant G50, Amersham-Pharmacia). Prior to the hybridization, probes were denatured by boiling for 5 min. In order to prevent unspecific DNA binding, the membranes were prehybridized in 20-25 ml hybridization solution (6x SSC, 5x Denhardt's solution, 0.5% SDS, 100 µg/ml denatured salmon sperm DNA) at 65°C for at least 2h in the hybridization oven

(Biometra). The denatured probes were then added to the tubes containing the membranes in prehybridization buffer. The hybridization was carried out at 65°C overnight.

In order to remove non-specifically bound probe from the membrane, the following washing steps were performed in a shaking water bath at 70°C: 2x 15 min in 2x SSC, 0.1% SDS; 1x 30 min in 0.1x SSC, 0.1% SDS. The membranes were sealed in plastic bags and exposed to a film (Kodak) for few days at -80°C.

2.3.9 . Fibroblast cell culture

Primary fibroblast cells (feeder cells) were routinely prepared from embryos derived from mouse strains homozygous for a transgene containing a *neo* expression cassette. A confluent plate of embryonic fibroblasts was washed with PBS and incubated for 2 h with 100 µl of mitomycin C stock solution (1 mg/ml in PBS, 5% DMSO, Sigma) in 10 ml of feeder medium. Then the cells were washed twice with PBS, incubated with 3 ml of 1x trypsin/EDTA at 37°C for 5 min, resuspended in feeder medium and centrifuged. The cell pellet was brought to a concentration of 2-3x10^5 cells/ml of feeder medium and plated on gelatinized plates.

Feeder cells as well as ES cells were stored in liquid nitrogen. For thawing, vials with cells were quickly warmed up at 37°C and then the cells were transferred to 10 ml of warm medium. After centrifugation (1100 rpm, 3 min) the cells were resuspended in fresh medium and plated on a cell culture dish.

2.3.10 . ES cell culture, transfection and selection

The ES cells were cultured in the presence of LIF on a layer of growth-arrested feeder cells in order to keep cells in an undifferentiated state. Frozen ES cells were thawed rapidly and the DMSO-containing medium was immediately replaced with warm (37°C) ES medium. ES cells (10^7) were electroporated with 25 µg of linearized targeting vector in 0.8 ml PBS (300 V, 500 µF, BioRad Gene Pulser). Transfected cells were plated on growth-arrested feeder cells at a density of 2.5x10^6 cells per 10 cm dish and cultured in ES cell medium. Selection with 400 µg/ml G418 was performed 48 h later. Fresh selection medium was added daily to ES cells. After additional 5-7 days of

culture with selective medium single, undifferentiated ES cell colonies were picked and cultured for additional 1-2 days in 96-well plates on feeder cells. Then, ES cell colonies were trypsinized and split into two 96-well plates; one plate without feeder cells for screening using Southern Blot analysis (replica plate) and one plate with feeder cells for freezing. To freeze ES cells down, 75µl of ice-cold freezing medium (ES medium containing 13.3% DMSO and 30% of FCS) was added to confluent, trypsinized 96-well plates. The plates were gradually frozen to –80°C in Styrofoam boxes.

To screen the cells for homologous recombination by Southern blot analysis, a replica plate was made of each 96-well plate. The replica plate was coated with 0.1% gelatine (Sigma) before seeding of ES cells. These plates were grown to confluence and used to extract DNA to screen for targeted clones as described above.

2.3.11 . Blastocyst injection

Superovulation and isolation of blastocysts, as well as the injection of embryonic stem cells in blastocysts (Bradley and Robertson, 1986) and the final uterus transfer of the blastocysts were performed by the Transgenic Core Facilities of the Max-Delbrück Center for Molecular Medicine (Berlin).

2.3.12 . *In ovo* electroporation

Fertilized eggs were stored for maximal 10 days at 4°C before the beginning of incubation. The incubation of eggs was performed at 38°C and 60% humidity in an Ehret Brutgerät BSS160 incubator.

Chicken eggs were electroporated at HH16 stage (Hamburger-Hamilton). The stadium of embryos was determined according to Hamburger and Hamilton (Hamilton, 1951). Before electroporation, 5 ml of the albumin was removed via a small hole on the basal pole of the egg and a window was opened on the top of the shell. For plasmid injection, the rhombencephalon of the embryo was exposed by cutting the vitelline membrane with a microscalpel made from a needle. Approximately 0.1–0.2 µl of plasmid solution containing 1.5 µg/µl expression plasmid, 1µg/µl GFP expression plasmid, 0.1% Fast Green in Ringer was injected into the central canal from thoracic spinal cord to rhombencephalon using a micropipette. Micropipettes were made from glass capillary

tubes (GC15OT-10, Clark Electromedical Instruments) by a micropipette processor (Sutter Instrument). A pair of electrodes held by a manipulator was inserted from a window opened on the shell. The electrodes were placed on the vitelline membrane overlying the embryo parallel to the neural tube, and a 25 mV, 50-ms pulse was charged five times with 1 sec interval using an 'Electro Square Porator ECM 830' (BTX Instruments). Electroporated chick embryos were incubated 48h more and then dissected. The efficiency of electroporation was estimated by GFP expression, and only GFP-positive embryos were further analyzed.

Ringer solution:

9.0g NaCl

0.42g KCl

0.24g $CaCl_2$

in 1l of destillated water.

2.3.13 . Preparation of riboprobes for *in situ* hybridization

DIG-labeled antisense RNA probes were transcribed from cDNA templates cloned into a vector (usually pBluescript II SK+ or pGEM-Teasy). To terminate *in vitro* transcription, plasmid DNA was linearized at the 5'-end in respect to the sense direction of cDNA using appropriate restriction enzymes. Routinely 30 µg of cDNA were digested in 30 µl reaction mixture. *In vitro* transcription was initiated from T7, T3 or Sp6 promoters and performed using the 'DIG-RNA Labeling-Kit' (Roche). After the reaction was completed, RNA was purified through the RNA Clean-up Kit from Macherey-Nagel and eluted with 60 µl of RNase-free water. RNA probes were stored in 50% formamide at -70°C.

2.3.14 . Preparation of frozen sections

Immunohistochemical analysis and *in situ* hybridization were performed on frozen sections. Mouse embryos were dissected from the uterus in PBS. Embryonic tails or forebrains were dissected and used to determine the genotype of the embryo by PCR. If prepared embryos were older then E14.0, the tissues surrounding the spinal cord and

hindbrain were removed in order to allow better penetration of fixative solution. Embryo tissue was fixed in freshly prepared 4% PFA in 0.1M phosphate buffer (pH 7.4) at 4°C for 2h. Afterwards, the tissue was washed extensively at 4°C in PBS for several hours and cryo-protected by incubation in 25% sucrose in PBS overnight at 4°C. The next day the tissue was embedded in 'TissueTek' (Sakura, Zoeterwoude, Nederland). 12 µm sections were cut on a cryostat (Microm HM560, Walldorf). Sections were collected onto slides (Histobond, Marienfeld) and dried at 37°C for 40 min. Slides as well as embedded tissues were stored up to 6 months at –70°C.

2.3.15 . Immunohistochemistry

Unspecific binding of antibodies was blocked by incubation usually with 1% inactivated horse serum in PBS containing 0.1% Triton X-100 (HS/PBX) or alternatively with 10% horse serum in PBX containing additionally 0.5% NEN for at least 30 min at room temperature. After the tissue was saturated, slides were incubated with the primary antibodies diluted in 1% HS/PBX overnight at 4°C with rocking. Following the incubation with primary antibodies, sections were washed three times with PBX for 10 min each to remove unbound antibodies, and then Cy2-, Cy3- or Cy5-conjugated secondary antibodies (diluted in 1% HS/PBX) were applied. Sections were incubated with secondary antibodies for 1 h at room temperature. Afterwards, the same washing procedure as above was performed and slides were covered with 'Immu-mount' (Shandon). Special treatment of tissue was performed in case of immunohistochemistry using antibodies against Ki67. Prior to incubation with primary antibodies, sections were incubated in 100% ice-cold methanol containing 1% H_2O_2. Then tissue was washed with PBS and blocked with 1% HS/PBX.

2.3.16 . X-Gal staining

X-Gal staining was modified according to (Lobe *et al.*, 1999). For whole-mount X-Gal staining of embryos and tissues, samples were fixed in 2% PFA in PBS, containing additionally 20 mM $MgCl_2$, for 30-60 min at 4°C with shaking. Following fixation, samples were washed three times for 15 min in PBS and twice for 15 min in a *lacZ*-washing buffer (20 mM $MgCl_2$, 0.01% sodium deoxycholate, 0.02% NP-40 in PBS).

Staining was carried out in the *lacZ*-washing buffer containing 0.5 mg/ml X-gal, 5 mM potassium ferrocyanide and 5 mM potassium ferricyanide at 37°C or room temperature for 30 min up to overnight, with shaking and protection from light. The X-Gal staining on sections prepared either for immunochemistry or from freshly frozen tissue was performed according to the protocol described above, except for a fixation step (fixation for 15 min).

2.3.17 . *In situ* hybridization

The protocol for *in situ* hybridization on frozen sections was adapted from N. Pringle (Richardson lab, London).
Slides with frozen sections were post fixed 15 min with 4% PFA/PBS and treated with acetylation buffer (1.3% Triethylamine (Sigma), 0.06% concentrated HCl, 0.25% acetic anhydride) for 10 min. Afterwards, sections were prehybridized with hybridization buffer for at least 1h at room temperature. DIG-labeled riboprobes were denatured in hybridization buffer for 5 min at 80°C, usually 1 µl RNA solution per slide. Riboprobes were directly applied on sections, cover-slipped and hybridized overnight at 70°C in a sealed container with Whatman filter paper soaked in 5x SSC and 50% formamide.
Hybridization buffer:
50% Formamide (Gibco BRL, Ultrapure)
5x SSC (pH 5.0)
5x Denhardt's (Sigma)
0.15 mg/ml yeast tRNA (Invitrogen)
0.1 mg/ml salmon sperm DNA (PAN Biotech)
H_2O DEPC

After the over-night hybridization, slides were washed with 5x SSC at room temperature to remove the cover-slips, which was followed by washing slides twice 30 min each at 70°C in 0.2x SSC. The slides were then equilibrated in B1 buffer (0.1M Tris pH 7.5, 0.15M NaCl) for 5 min and blocked in B1 solution additionally containing 10% goat serum (blocking solution) for 1 h at room temperature. Anti-DIG antibodies conjugated with alkaline phosphatase were diluted in blocking solution (1:2000), 500 µl

of antibody solution was applied on each slide and incubated overnight in a humidified chamber at 4°C.

The slides were transferred into Coplin jars and washed three times 20 min each in B1 solution, then washed ones for 5 min in staining solution (0.1 M Tris pH 9.0, 0.1 M NaCl, 50 mM $MgCl_2$, 0.1% Tween, 5% polyvinyl alcohol). The color reaction was performed at room temperature in a humidified chamber with staining solution containing 1 µl/ml NBT (Roche) and 1 µl/ml BCIP (Roche). When the signal reached a satisfactory intensity, slides were washed in H_2O several times to stop the reaction and remove excessive NBT/BCIP and covered with 'Immu-Mount' (Shandon).

2.3.18 . Tamoxifen gavaging

A 20 mg/ml stock solution of tamoxifen (Sigma-Aldrich) was prepared in sunflower oil. Tamoxifen was administered by oral gavaging to pregnant females at E9.5 or E10.5. The dose of tamoxifen given was 100 mg/kg. Embryos were dissected 48h, 6 or 8 days after tamoxifen treatment.

2.3.19 . Program for counting cell nuclei

The program, which counts bright, oval-shaped objects in two-dimensional pictures, relies on a method similar to the one described by (Byun *et al.*, 2006), and was developed by Bartlomiej Waclaw. The program is available at http://www.physik.uni-leipzig.de/~waclaw/count/index.html. Gaussian blur is performed for a desired channel (red, green, blue or any combination) and positions of maximal brightness, which are assumed to correspond to nuclei centers of mass, are counted. Neighboring points are counted once if they lie within a radius of a typical cell. This average radius and some other parameters can either be determined automatically or adjusted by the user. Three sections from three different animals each were analyzed. Fluorescence was visualized by laser-scanning microscopy (LSM 5 PASCAL, Carl-Zeiss), using PASCAL software.

3 . Results

The section “Results” is divided in two parts. In the first part, I will focus on the role of the transcription factor Rbp-j in neurogenesis and the determination of neuronal fates of the dorsal spinal cord. In the second part, I will present results concerning the function of the transcription factor Olig3 in the specification of neuronal subtypes of the dorsal hindbrain.

3.1 . Rbp-j function in the dorsal spinal cord

Previous analysis done by Hendrik Wildner showed that one of the neuron types born in the dorsal spinal cord during the late neurogenic phase, the dILA neurons, is generated by asymmetric cell division (Wildner *et al.*, 2006). However, it remained unclear, which molecular mechanisms allow two daughter cells to assume distinct fates. An extensive line of research in *Drosophila melanogaster* demonstrated that the activity of Notch receptors impose asymmetric fates on two daughter cells in the nervous system, making the Notch pathway a probable candidate for the fate choice of dILA neurons. In mammals, four Notch receptors and at least five ligands exist that are expressed in a partially overlapping manner in the nervous system, which may lead to functional redundancy. Therefore, it is difficult to assess the role of the Notch pathway in neural development. However, a simple way to analyze the role of Notch in the dorsal spinal cord is to mutate Rbp-j, the major transcriptional mediator of Notch signaling, of which only one gene exists. However, mice that carry a null-mutation in *Rbp-j* die around day 9 of embryonic development (E9), i.e. at a time when neuronal differentiation begins (de la Pompa *et al.*, 1997). I therefore used conditional mutagenesis, i.e. the *Cre/loxP* technology, to address the role of Rbp-j in the development of neuronal cell types of the dorsal spinal cord. A second approach to interfere with signaling of Notch receptors is a spatially restricted expression of dominant negative variant of Mastermind-like 1 (dnMaml). Overexpression of the dnMaml interferes with the transcriptional activator function of Rbp-j and leads to inhibition of Notch target gene transcription (Tu *et al.*, 2005). To introduce these two mutations into the spinal cord, I employed two different mouse lines that express the Cre recombinase: (i) $Pax3^{Cre}$, which expresses Cre under

the control of the *Pax3* locus; (ii) *Pax7*^{CreERT2}, a BAC transgene that expresses a tamoxifen-inducible variant of the Cre recombinase under the control of the *Pax7* locus. A detailed description of the mouse strains used in these experiments can be found in chapter 2.2.8 .

3.1.1 . Effect of *Rbp-j* mutation on neurogenesis

The *Pax3*^{Cre} line was previously reported to induce efficient recombination in the dorsal neural tube at E9. I verified the extent and onset of recombination induced by *Pax3*^{Cre} using the ROSA26R reporter line that expresses β-galactosidase after Cre-mediated recombination (Soriano, 1999). I observed a very efficient β-galactosidase expression in the whole alar plate at E10.5, in agreement with previous reports and with the known expression of the endogenous *Pax3* gene (Figure 3.1 A).

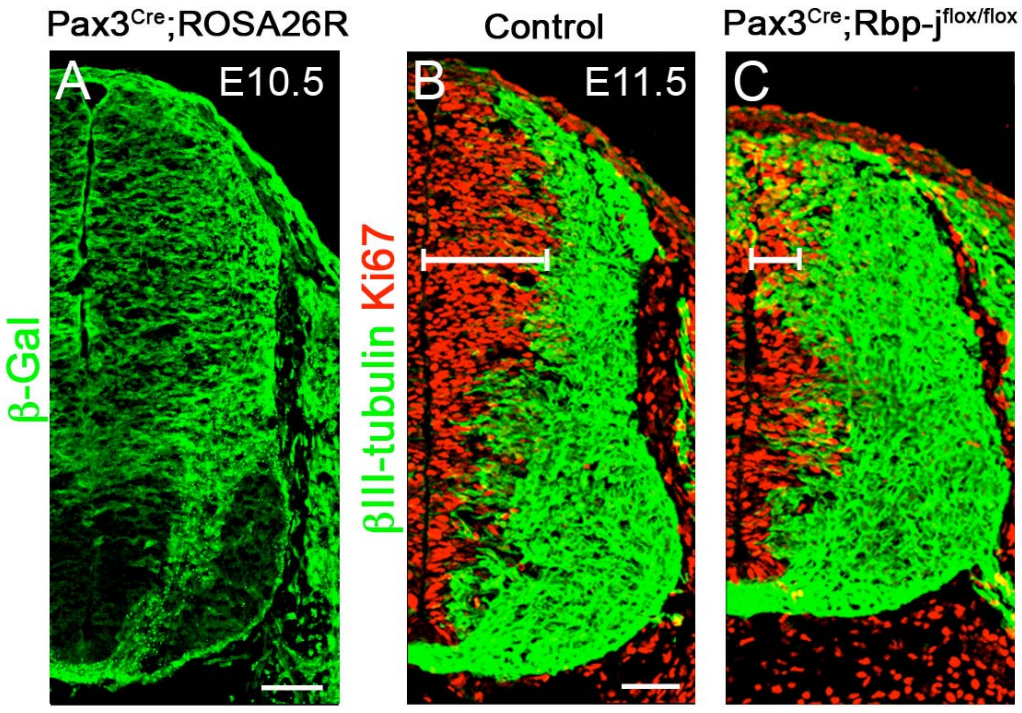

Figure 3.1 **Rbp-j is essential to maintain the progenitor pool in the neural tube.** (A) β-Gal expression in a *Pax3*^{Cre}*;ROSA26R* neural tube at E10.5 demonstrates efficiency and spatial pattern of recombination of the *Pax3*^{Cre} allele. (B, C) Effect of the *Rbp-j* mutation (indicated by the bar) on neurogenesis in the neural tube at E11.5 in *Pax3*^{Cre}*;Rbp-j*$^{flox/flox}$ mutant mice (C) compared with control mice (*Pax3*^{Cre}*;Rbp-j* $^{flox/+}$) (B) visualized with antibodies against Ki67 (red) and βIII-tubulin (green). Bars: 50 μm.

Pax3^{Cre}*;Rbp-j*$^{flox/flox}$ mutant mice were generated and the dorsal spinal cord of these mice was analyzed at E10.5, E11.5 and E12.5, using antibodies against Ki67 that visualize the proliferating progenitor domain, and antibodies against βIII-tubulin to identify differentiated neurons. I observed precocious neuronal differentiation, i.e. an increased number of neurons, and a decreased size of the progenitor domain (Figure 3.1 B,C). This is in accordance with previous reports that demonstrated an important role of Notch signaling in the maintenance of neural progenitors (de la Pompa *et al.*, 1997). The dorsal progenitor domain of *Pax3*^{Cre}*;Rbp-j*$^{flox/flox}$ mice was no longer present at E12.5 (data not shown). Thus, the progenitor pool was depleted before the second wave of neurogenesis commenced, which precluded the functional analysis of Rbp-j in the formation of late neurons using the *Pax3*^{Cre} strain.

Furthermore, I investigated the recombination induced by the *Pax7*^{CreERT2} transgene using the ROSA26R reporter line. After administration of tamoxifen at E10.5, efficient β-galactosidase expression was observed in the ventral part of the alar plate at E12.5 (Figure 3.2 A). I detected a slight decrease in the size of the progenitor domain in *Pax7*^{CreERT2}*;Rbp-j*$^{\Delta/flox}$ mutant mice at E12.5, two days after tamoxifen administration, as visualized by immunohistochemistry using Ki67 and βIII-tubulin antibodies (Figure 3.2 B,C). The reduction in the size of the progenitor domain was pronounced at E13.5 (data not shown). Thus, regardless if I used *Pax3*^{Cre} or *Pax7*^{CreERT2} mouse lines to mutate *Rbp-j*, I observed similar phenotypes, a precocious neuronal differentiation and a depletion of the progenitor pool. However, there was a difference in the strength of the phenotype between the *Pax7*^{CreERT2} transgene and the *Pax3*^{Cre} allele. Using *Pax3*^{Cre}, the mutation of *Rbp-j* caused a very early loss of progenitors, already at E10.5, but when *Pax7*^{CreERT2} was used neurogenesis was only slightly impaired at E12.5. The difference is caused by distinct recombination efficiencies of Cre and tamoxifen-inducible Cre recombinases and the promoters used to control the spatial and temporal expression of Cre. In comparison to the *Pax3*^{Cre} allele, the *Pax7*^{CreERT2} transgene allowed me to introduce the *Rbp-j* mutation at later stages, thus avoiding a premature loss of progenitors. This provided a possibility to investigate the role of Rbp-j in the late wave of neurogenesis.

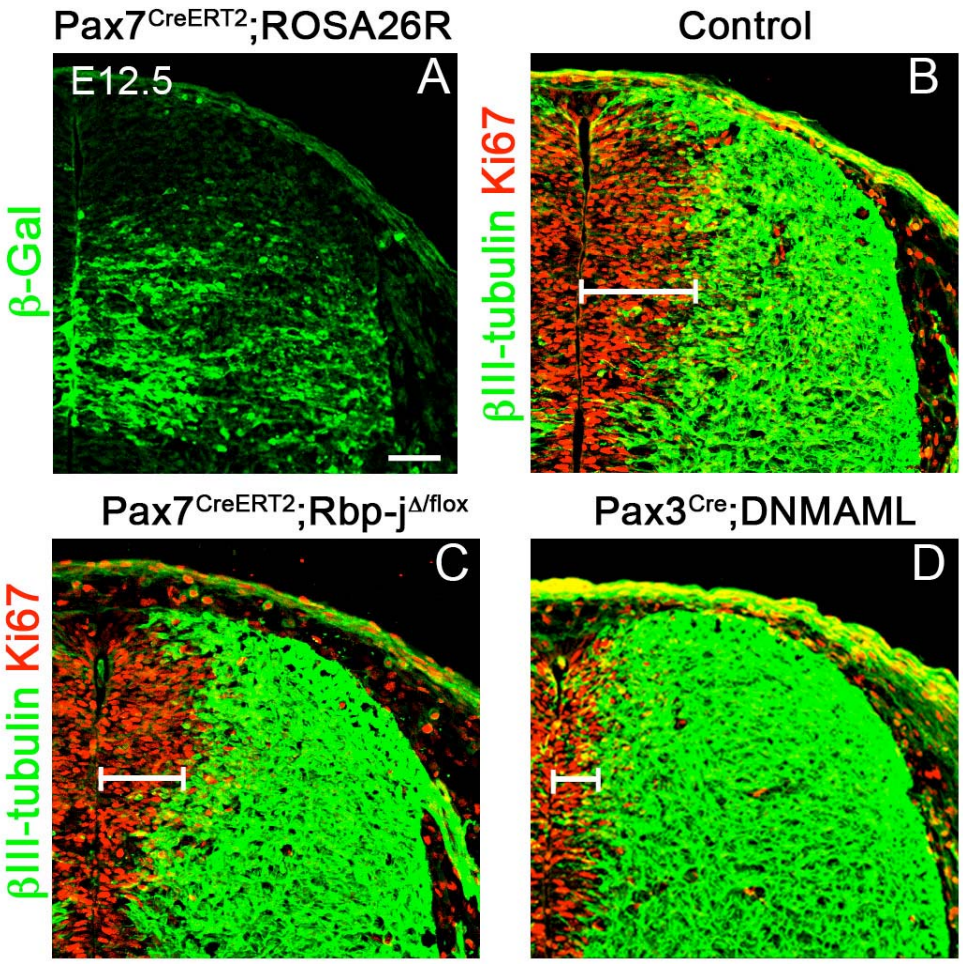

***Figure 3.2* Similar effects of the *Rbp-j* and dnMaml mutations on neurogenesis.** (A) β-Gal expression in a *Pax7^{CreERT2};ROSA26R* alar plate of an E12.5 embryo treated with tamoxifen at E10.5 demonstrates efficiency and spatial pattern of recombination induced by the *Pax7^{CreERT2}* transgene. (B,C) Effect of the *Rbp-j* mutation (indicated by the bar) on neurogenesis in the dorsal spinal cord at E12.5 in a *Pax7^{CreERT2};Rbp-j $^{\Delta/flox}$* embryo treated with tamoxifen at E10.5 (C) compared with control mice (B). (B,D) Effect of the dnMaml mutation (indicated by the bar) on neurogenesis in the dorsal spinal cord at E12.5 in *Pax3^{Cre};DNMAML* mutant mice (C) compared with control mice (B) visualized with antibodies against Ki67 (red) and βIII-tubulin (green). Bar: 50 μm.

In addition, I analyzed neurogenesis in a transgenic strain that expresses a dominant-negative variant of Maml-1 (dnMaml). Comparison of the dorsal spinal cord of control and mutant mice (*Pax3^{Cre};DNMAML*) at E12.5 with antibodies directed against Ki67 and βIII-tubulin demonstrated a reduced size of the progenitor domain in mutant embryos (Figure 3.2 B,D). The observed partial depletion of progenitors is caused likely by inability of dominant negative Maml-1 to fully inhibit Notch signaling.

Thus, regardless of using different mutations (*Rbp-j* and dnMaml) that impair Notch signaling introduced by two different Cre lines ($Pax3^{Cre}$ and $Pax7^{CreERT2}$), I observed qualitatively similar changes in neurogenesis. However, I obtained some quantitative differences, i.e. the observed phenotype was more pronounced in $Pax3^{Cre};Rbp\text{-}j^{flox/flox}$ mice than in $Pax3^{Cre};DNMAML$ mice, which indicates that overexpression of dnMaml is not as efficient as *Rbp-j* mutation. Moreover, quantitative differences were also caused by introducing the *Rbp-j* mutation using distinct Cre lines, i.e. one line expressing constitutively active Cre and the other one expressing tamoxifen-inducible Cre.

3.1.2 . The role of Rbp-j in the specification of early-born neurons

Six populations of neurons can be observed in the dorsal neural tube at E10.5, which are defined by the expression of specific combinations of homeodomain transcription factors and by their appearance at particular positions along the dorsal-ventral axis (Helms and Johnson, 2003). In order to define a Rbp-j function in the generation of early born neurons, I analyzed four of these populations by comparing control and $Pax3^{Cre};Rbp\text{-}j^{flox/flox}$ animals at E10.5. I observed a complete loss of dI4 neurons in the mutant mice, which were identified by their position in the dorsal mantle zone and by their co-expression of Pax2 and Lhx1/5 (Figure 3.3 A,B). This was accompanied by an increase in the number of dI2 (Lhx1/5+), dI3 (Isl1/2+), and dI5 (Lmx1b+/Tlx3+) neurons (Figure 3.3 A,B,C,D; for a quantification see E). The number of dI2 and dI3 neurons was slightly increased in the mutant mice, whereas the increase in the number of dI5 neurons was dramatic. dI2 and dI3 neurons arose at the appropriate positions, whereas the excess of dI5 neurons appeared also at ectopic positions where in normal development dI4 neurons are generated. This indicates that dI4 neurons assumed a dI5 identity in the absence of Rbp-j. In contrast, the comparably small increase in dI2 and dI3 neurons appears to be caused by the general increase in neurogenesis observed in $Pax3^{Cre};Rbp\text{-}j^{flox/flox}$ mutant embryos (summarized in Figure 3.3 F).

In E10.5 neural tubes, dI4 neurons are generated from a progenitor domain (dP4) expressing Ptf1a, whereas dI3, dI4, and dI5 neurons are produced by a broad progenitor domain marked by the expression of Ascl1 (Figure 3.4 A; dP3, dP4, dP5). In the early

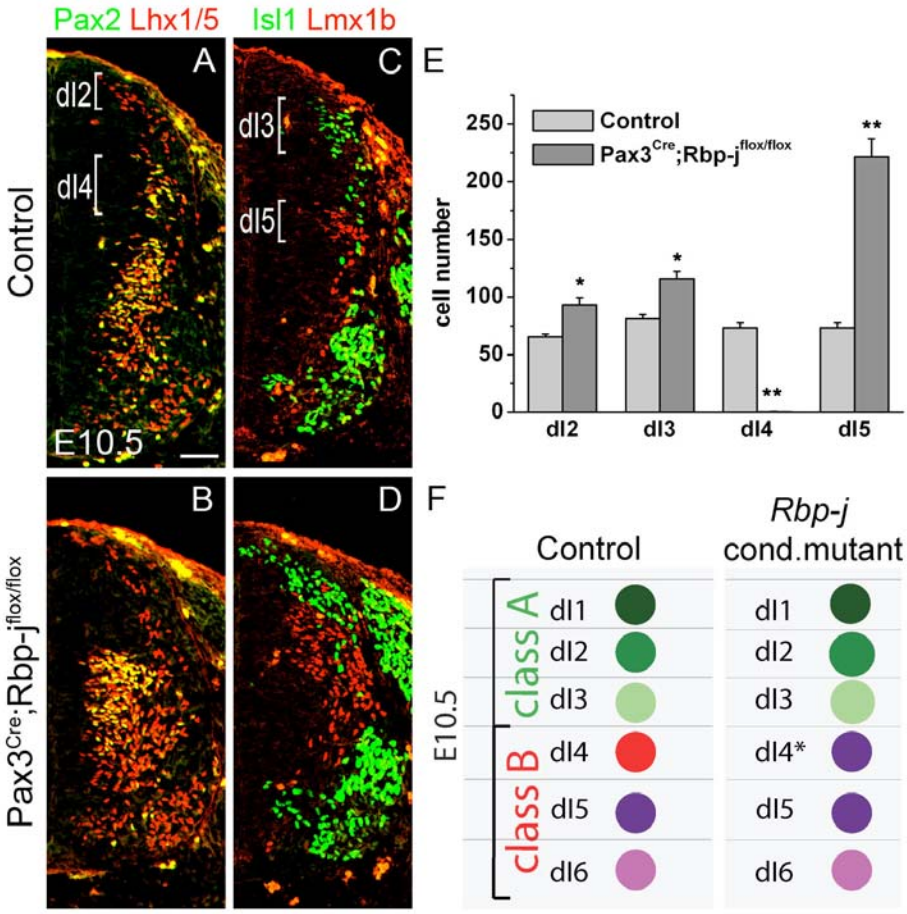

***Figure 3.3* Rbp-j is required to specify dI4 neurons.** Immunohistochemistry on transverse sections of E10.5 neural tubes from control (*Pax3^{Cre};Rbp-j$^{flox/+}$*) (A,C) and mutant *Pax3^{Cre};Rbp-j$^{flox/flox}$* (B,D) embryos. (A,B) dI2 neurons (Lhx1/5+, red) are increased whereas dI4 neurons (Pax2+/Lhx1/5+, yellow) are lost in the *Pax3^{Cre};Rbp-j$^{flox/flox}$* mutant. (C,D) dI3 (Isl1+, green) and dI5 (Lmx1b+, red) neurons are both increased in the *Pax3^{Cre};Rbp-j$^{flox/flox}$* mutant compared with control. These data are quantified in E using sections from the upper limb level of three embryos each. (F) Schematic representation of the *Rbp-j* phenotype observed in spinal cord at E10.5. Error bars represent standard error. (*) $P < 0.05$; (**) $P < 0.001$. Bar: 50 μm.

phase of neurogenesis, Ascl1 expression levels are inversely correlated with Ptf1a expression levels, i.e. Ascl1 expression is generally low in dP4 progenitors, but high in dP3 and dP5 progenitors (Glasgow *et al.*, 2005). Moreover, cells with high levels of Ascl1 expression intermingle with cells, which have low level of Ascl1 expression or with cells, which are negative for Ascl1. The same is observed for Ptf1a (Figure 3.4 A,B,C). In *Pax3^{Cre};Rbp-j$^{flox/flox}$* mutant mice, Ascl1 expression levels were more uniform across the dP3, dP4, and dP5 progenitor domains. Moreover, an increased number of cells expressing Ascl1 were observed in the dP5 progenitor domain (Figure 3.4 A,C,D,F) and that is correlated with an increased number of dI5 neurons observed in

Pax3^{Cre}*;Rbp-j*$^{flox/flox}$ mutant mice. Furthermore, levels of the Ptf1a protein were decreased in *Pax3*^{Cre}*;Rbp-j*$^{flox/flox}$ mutants compared to control animals (Figure 3.4 B,E). Since Ptf1a is known to be essential for the specification of dI4 and dILA neurons, the decreased amount of Ptf1a could cause in turn a decreased number of dI4 neurons. However, in *Pax3*^{Cre}*;Rbp-j*$^{flox/flox}$ mice, dI4 neurons are not specified at all, although Ptf1a is still present in the progenitor domain. Since dILA neurons are correctly specified in *Pax3*^{Cre}*;DNMAML* mutant mice at E12.5, although the amount of Ptf1a is decreased in this mice (see below), I conclude that such a level of Ptf1a suffices to specify dI4 and dILA neurons. Together, my data indicate that Rbp-j is required to determine the fate of dI4 neurons, and that this effect is not mediated by changes in Ptf1a expression.

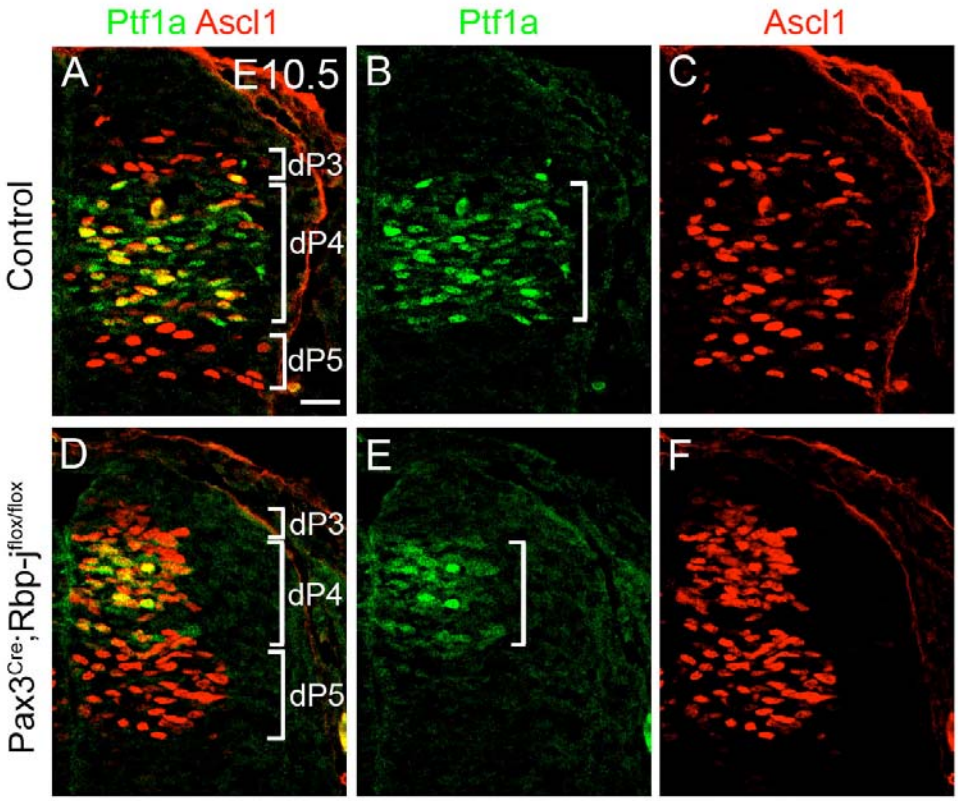

***Figure 3.4* Effect of the *Rbp-j* mutation on expression levels of Ascl1 and Ptf1a proteins.** Immunohistochemistry on neural tube transverse sections of control (*Pax3*^{Cre}*;Rbp-j*$^{flox/+}$) (A-C) and *Pax3*^{Cre}*;Rbp-j*$^{flox/flox}$ mutant embryos at E10.5. (A,D) Expression of Ascl1 (red) and Ptf1a (green) in control and mutant spinal cord. (B,E) Expression of Ptf1a (green) and (C,F) expression of Ascl1 (red) in control and mutant mice. Note that A,B,C and D,E,F show the same sections. Ptf1a expression level appears to be decreased (indicated by the bar) in *Pax3*^{Cre}*;Rbp-j*$^{flox/flox}$ mutant embryos compared with control mice and Ascl1 levels appear more uniform and increased particularly in the domain of dI5 neurons. Bar: 25 μm.

3.1.3 . Analysis of Rbp-j function in the specification of dILA and dILB neurons

dILA and dILB neurons, the major GABAergic and glutamatergic neuronal subtypes of the dorsal spinal cord, arise in a salt-and-pepper pattern from a broad progenitor domain. In order to define the Rbp-j role in the specification of these neuron types and to circumvent the problem of early progenitor depletion in the conditional *Pax3^{Cre};Rbp-j$^{flox/flox}$* mice, I used the *Pax7^{CreERT2}* allele to mutate Rbp-j in a spatially and temporally controlled manner. As mentioned in chapter 3.1.1 after administration of tamoxifen at E10.5, efficient recombination was observed in the ventral part of the alar plate at E12.5 (Figure 3.2 A). Therefore, I restricted my analysis of *Pax7^{CreERT2};Rbp-j$^{\Delta/flox}$* mice to newly born neurons of the ventral alar plate at E12.5 (marked by the white box in Figure 3.5 A,D). I observed a significant reduction in the number of new-born dILA neurons (Pax2+ and Lhx1/5+) in the conditional mutant mice compared to control mice. In contrast, the number of dILB neurons (Lmx1b+ and Tlx3+) was increased (Figure 3.5 A,D; see C,F for quantification). This indicates that dILB neurons were born at the expense of dILA neurons in the *Pax7^{CreERT2};Rbp-j$^{\Delta/flox}$* mutant mice. In addition, I compared the Ptf1a protein levels in the dorsal spinal cord of control and *Pax7^{CreERT2};Rbp-j$^{\Delta/flox}$* mutant animals and observed a minor decrease in the expression level of Ptf1a in the ventral alar plate (Figure 3.5 B,E). Together, my results demonstrate a requirement of Rbp-j in the determination of the GABAergic dI4 and dILA neurons. Furthermore, glutamatergic dI5 and dILB neurons were formed at their expense. In contrast, the *Rbp-j* mutation had no effect on the determination of other dorsal neuron types (dI2 and dI3).

I also assessed the neuron types born in the dorsal spinal cord of *Pax3^{Cre};DNMAML* mice. Since the effect on neurogenesis is not so pronounced in these mutant mice and the progenitor domain is not depleted at E12.5, I could analyze the late phase of neurogenesis using antibodies against Pax2 and Tlx3, which identify dILA and dILB neurons, respectively. Astonishingly, I observed no major loss of dILA (Pax2+) and

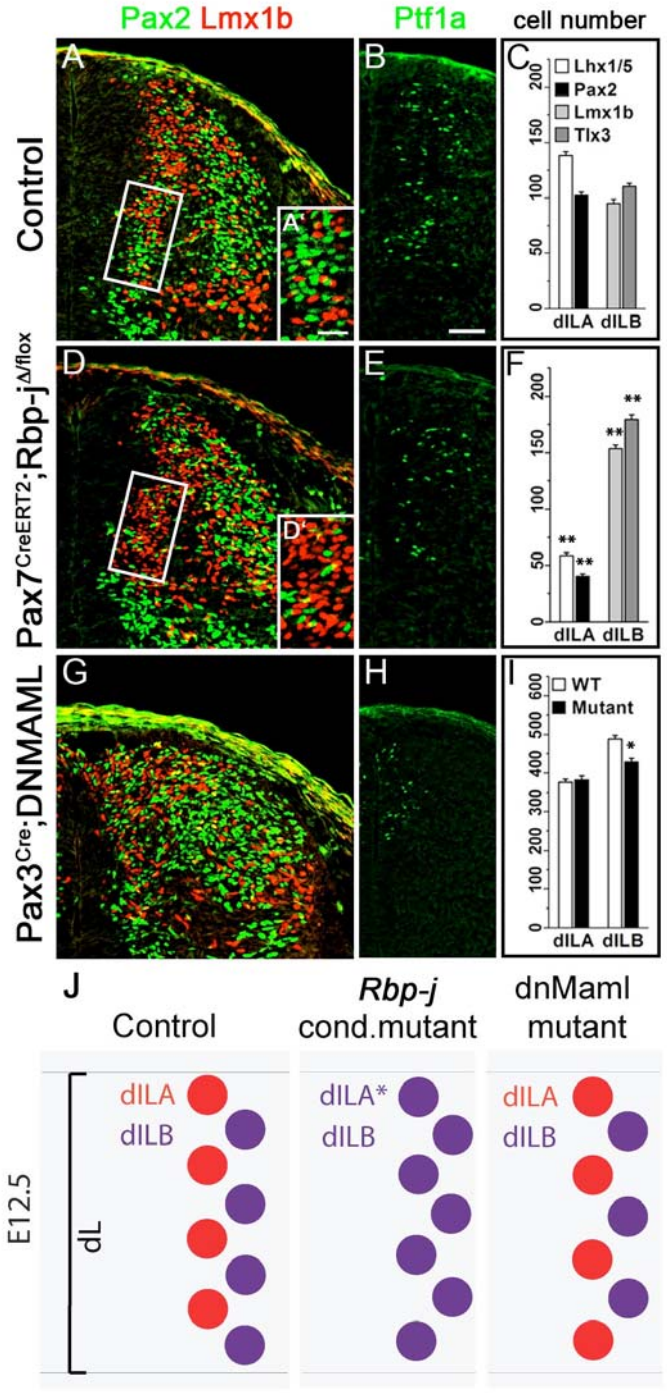

***Figure 3.5* Distinct effects of *Rbp-j* and dnMaml mutations on the determination of the fate of GABAergic neurons.** Immunohistochemistry on alar plate transverse sections of control (A,B) and *Pax7^{CreERT2};Rbp-j$^{\Delta/flox}$* mutant embryos at E12.5, two days after tamoxifen administration (D,E), and *Pax3^{Cre};DNMAML* mutant embryos (G,H). Antibodies used include Pax2 (green) and Lmx1b (red) to distinguish dILA and dILB neurons (A,D,G), and Ptf1a (green) to assess Ptf1a expression levels in mutant mice(B,E,H). The domain that was used for the quantification of dILA and dILB neurons in control (C) and *Pax7^{CreERT2};Rbp-j$^{\Delta/flox}$* mutant mice (F) is indicated by a white box and is shown at higher magnification in the insets (A',D'). This domain of newly born neurons was used since Cre recombination induced at E10.5 was efficient in this region. (I) For the comparison of *Pax3^{Cre};DNMAML* mutant and control mice, the number of dILA (Pax2+) and dILB (Tlx3+) neurons was quantified in the entire alar plate, reflecting the higher recombination efficiency of the *Pax3^{Cre}* allele. (J) Schematic summary of the phenotypes observed in *Rbp-j* and dnMaml mutant spinal cords at E12.5. Data quantified in C,F and I are from three animals each using sections from the upper limb level. Error bars represent standard error. (*) $P < 0.05$; (**) $P < 0.001$. Bar: 50 μm; insets (A',D') 20 μm.

dILB (Tlx3+) neurons, in contrast to the changes I had observed in *Rbp-j* mutant mice. Instead, a careful quantification demonstrated a small decrease in the dILB population (Figure 3.5 A,G; quantified in I). In addition, I observed morphological alterations in the dorsal spinal cord of *Pax3^{Cre};DNMAML* mutants, which reflect a general decrease in size due to the early depletion of dorsal progenitors. I also analyzed Ptf1a expression, and observed a decrease in Ptf1a protein level in *Pax3^{Cre};DNMAML* mutant compared with control mice (Figure 3.5 B,H). This alteration was not accompanied by a decrease in dILA neuron number, suggesting that Ptf1a protein levels sufficed to determine the identity of dILA neurons. In addition, I also analyzed early neuron types in the dorsal spinal cord of *Pax3^{Cre};DNMAML* mutants, and again observed no obvious change in the appearance of dI4 and dI5 neuron types (data not shown).

Thus, a major difference between the phenotypes of *Rbp-j* and dnMaml mutants exists, i.e. in *Rbp-j* mutants, dI4 and dILA neurons are not correctly specified, whereas these neurons appear unaffected by the expression of a dominant negative Mastermind-like 1 variant (summarized in Figure 3.5 J). This discrepancy between *Rbp-j* and dnMaml mutants suggests an additional role for Rbp-j, which is independent of Mastermind-like 1 and Notch signaling. This is in contrast to the effects observed on neurogenesis, where the two mutations have similar qualitative effects, and differ only in their quantitative consequences. The analysis of the conditional *Rbp-j* mutants revealed an unexpected similarity to the phenotype observed in *Ptf1a^{null}* mutants. Additional work done in the laboratory of Jane Johnson demonstrated that Rbp-j and Ptf1a interact directly. Together, my results and those obtained by Jane Johnson's laboratory indicate that Rbp-j acts in a complex with Ptf1a to determine the fate of dI4 and dILA neurons, and independently, in a second complex with Maml-1 and Notch to maintain neural progenitors and suppress neuronal differentiation (see also discussion).

3.2 . Olig3 function in the hindbrain

In the second part of my thesis, I investigated the function of the bHLH factor Olig3 in the hindbrain. Olig3 is expressed in dorsal progenitors of the hindbrain and spinal cord. My goal was to identify neuronal types generated by Olig3+ progenitors, and to assess the development of these neurons in the hindbrain of *Olig3* mutant mice. The complexity of neuron types generated in the hindbrain is great, and neuronal migration is complicated. Therefore, it is helpful to use genetic fate mapping for the investigation of hindbrain development. I generated two different knock-in mouse lines that express Cre under the control of the *Olig3* locus. The first strain expresses Cre recombinase, and the second a tamoxifen-inducible variant of Cre recombinase. Particularly the second strain was very useful to determine which neurons in the hindbrain are derivatives of Olig3+ progenitor cells.

3.2.1 . Generation of mouse strains that carry Cre sequences in the *Olig3* locus

The *Olig3*^{CrepA} and O*lig3*^{CreERT2} alleles were generated using homologous recombination in embryonic stem (ES) cells. For this, two targeting vectors were constructed in which *Olig3* coding sequences were replaced by sequences encoding Cre or a Cre-fusion protein containing the tamoxifen-responsive estrogen receptor ligand-binding domain (CreERT2) (Feil et al. 1997). The Cre sequences were fused in frame to the ATG codon of *Olig3*. In addition, a *neomycin* resistance gene (*neo*) flanked by *FRT* sites was present in the targeting vectors, to allow for selection of ES cells that had taken up the DNA. Furthermore, the vectors contained a *diphtheria toxin A* (*DTA*) cassette that enriches homologous recombination events by eliminating random integration events, in which the *DTA* cassette is retained (Figure 3.6). In order to construct these targeting vectors, I employed homologous recombination in bacteria (Lee et al. 2001) using a BAC clone containing *Olig3* isolated from a 129-mouse BAC library (Research Genetics). Both targeting vectors were electroporated into ES cells. About 480 and 290 ES cell clones containing the Cre and CreERT2 constructs, respectively, were selected by their *neomycin* resistance and screened by southern blot analysis using XbaI and HindIII restricted DNA obtained from the ES cell clones. I isolated 34 and 14 ES clones

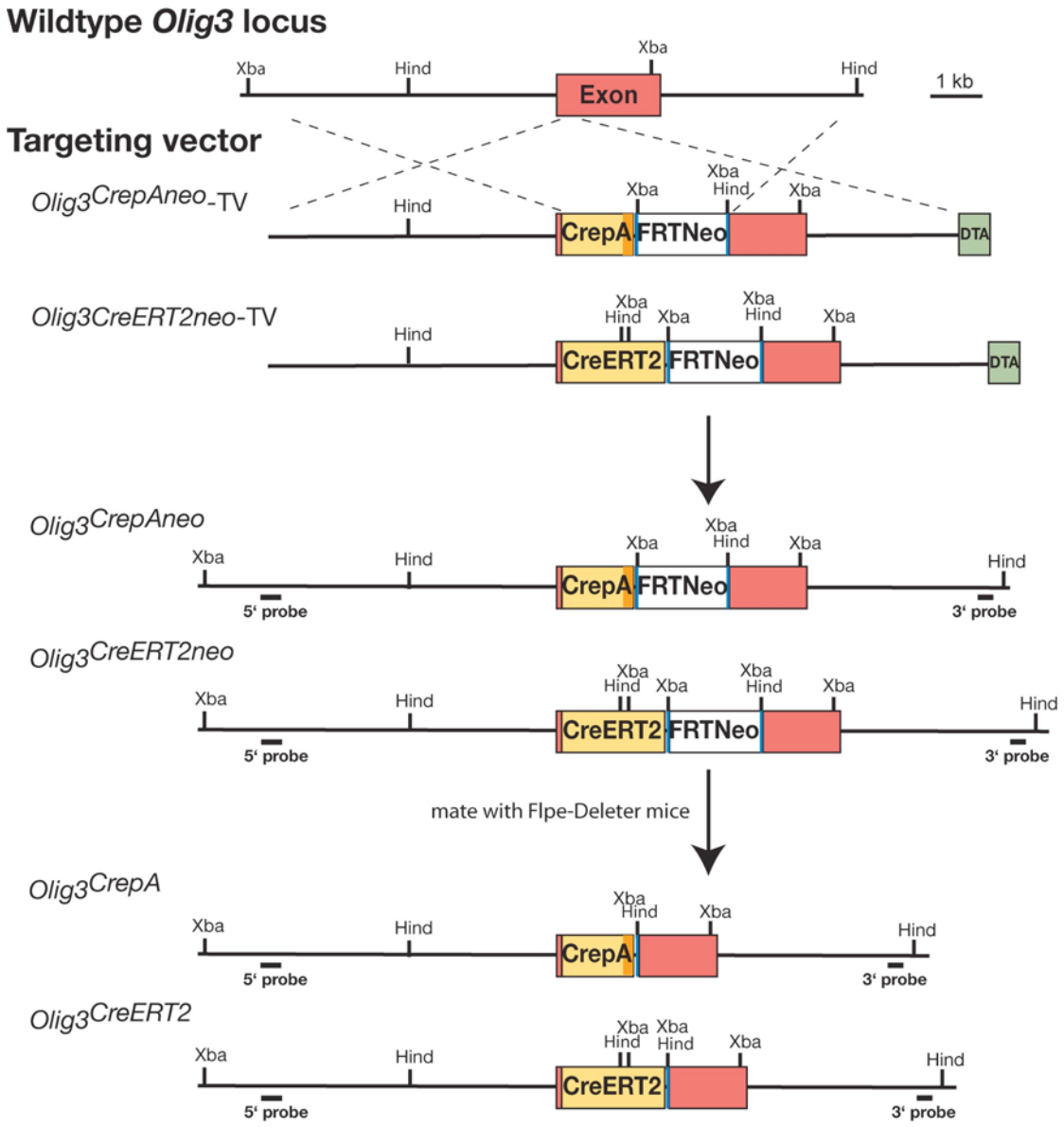

***Figure 3.6* Strategy used to generate *Olig3*^{CrepA} and *Olig3*^{CreERT2} alleles.** Schematic representation shows the wild-type *Olig3* locus, two targeting vectors (*Olig3*^{CrepAneo}-TV and *Olig3*^{CreERT2neo}-TV), and mutant *Olig3* alleles before (*Olig3*^{CrepAneo} and *Olig3*^{CreERT2neo}) and after (*Olig3*^{CrepA} and *Olig3*^{CreERT2}) removal of the *neomycin* (*neo*) cassette. The coding exon of *Olig3* (red) was interrupted by the insertion of *CrepA-FRT-neo-FRT* and *CreERT2-FRT-neo-FRT* cassettes. Indicated are CrepA and CreERT2 (yellow) and the *neo* resistance cassette (white) surrounded by *FRT* sequences (blue) (FRTNeo). In addition, a *diphtheria toxin A* (DTA, light green) cassette was included for negative selection.

that had inserted the Cre and CreERT2 vectors, respectively, by homologous recombination. The transgenic unit of the MDC injected three independent ES clones of each type into mouse blastocysts. Male chimeric mice were obtained and mated with female C57/Bl6 mice in order to obtain germ-line transmission of the mutant alleles. Thus, I established two mouse strains containing the *Olig3*^{CrepA} and O*lig3*^{CreERT2} alleles. Animals of the F1 generation were crossed with *FLPe* deleter mice to remove the *neo* cassette (Farley *et al.*, 2000). I confirmed by PCR that the *neomycin* resistance cassette was deleted in F2 animals.

The onset of expression of the murine bHLH gene *Olig3* was described to be at E9.25. In the dorsal spinal cord, Olig3 expression was described to be restricted to progenitor cells of the most dorsal part of the alar plate that generate class A (dI1-dI3) neurons (Ding *et al.*, 2005; Muller *et al.*, 2005; Takebayashi *et al.*, 2002b). I investigated recombination induced by the *Olig3*^{CrepA} allele using *ROSA26R* and *Tau*^{nlsLacZ} reporter lines. At E18.5, β-galactosidase was detected in almost all of the cells in the spinal cord of *Olig3*^{CrepA}*;Tau*^{nlsLacZ} reporter mice, for instance in neurons located in superficial layers of the dorsal spinal cord and in motor neurons (Figure 3.7 A). Additionally, β-galactosidase was observed in dorsal root ganglia. Further investigation at E14.5 confirmed the broad expression of β-galactosidase in the nervous system of *Olig3*^{CrepA}*;ROSA26R* reporter mice, i.e. in the spinal cord and in neural crest derivatives. Anterior parts of the central nervous system, i.e. most of the mid- and forebrain, did not express β-galactosidase (Figure 3.7 B). The observed reporter expression demonstrated thus possible ectopic recombination events in the *Olig3*^{CrepA} mouse strain, since the expression of β-galactosidase was broader than expected. Therefore, I performed immunohistology using anti-Cre recombinase antibodies to test for Cre protein expression. At E12.5, β-galactosidase was observed in dorsal root ganglia and the entire spinal cord, but Cre was restricted to a small population of cells that appeared to migrate from the dorsal to the ventral spinal cord (Figure 3.7 C). It is currently unclear if Cre is ectopically expressed at earlier developmental stages in *Olig3*^{CrepA} mice, leading to the broad expression of β-galactosidase, or if the endogenous *Olig3* gene is indeed expressed broadly in the posterior neural tube before E9 and becomes later more restricted. I did not follow this further, because tamoxifen-dependent recombination in *Olig3*^{CreERT2} mice was efficient, which allowed me to temporally control recombination.

For instance, I used tamoxifen to induce recombination in *Olig3*$^{CreERT2/+}$ mice at E9.5, and carefully analyzed the co-expression of Olig3 and nuclear CreERT2 proteins in the alar plate of the hindbrain 48 hours later. This demonstrated an extensive overlap in the expression of the two proteins. Few cells did not co-express CreERT2 and Olig3, which might reflect differences in the protein stability (Figure 3.8 A). Therefore, I used the *Olig3*^{CreERT2} mouse strain to further analyze neurons generated from dorsal Olig3+ progenitor cells that are observed in the hindbrain at E11.5.

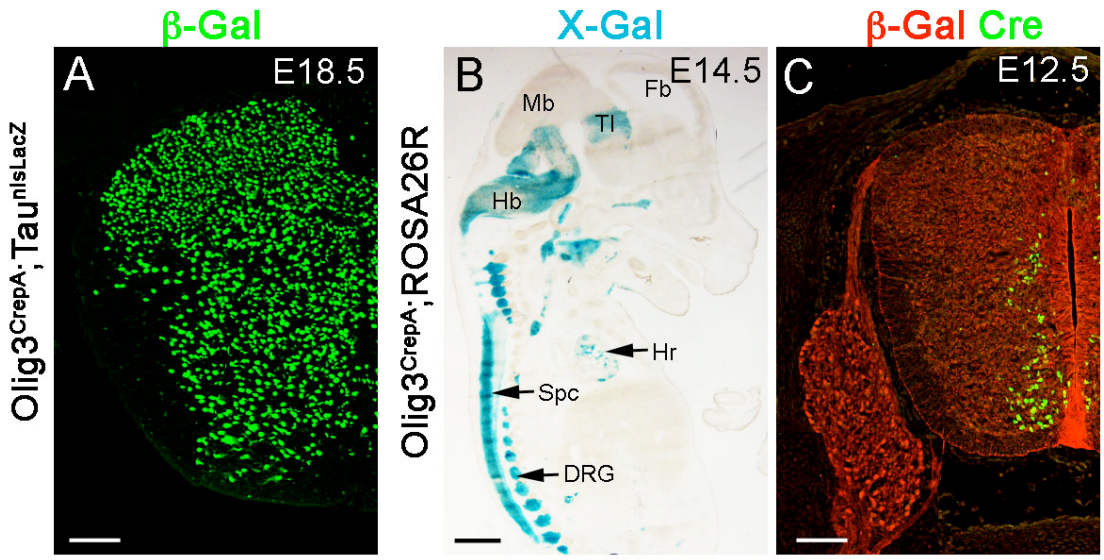

***Figure 3.7* Analysis of recombination induced by the *Olig3*^{CrepA} allele in the spinal cord and other tissues of the embryo.** (A) Immunohistochemistry of spinal cord transverse sections from E18.5 *Olig3*^{CrepA}*;Tau*^{nlsLacZ} embryos using antibodies against β-Gal shows broad β-Gal expression. (B) β-Gal expression (blue) visualized with an X-Gal staining on sagittal sections of an entire E14.5 *Olig3*^{CrepA}*;ROSA26R* embryo appears to be restricted to the nervous system and neural crest derivatives. (C) Immunohistological analysis of spinal cord transverse sections from E12.5 *Olig3*^{CrepA}*;ROSA26R* embryos using antibodies against β-Gal (red) and Cre (green). Fb, forebrain; Tl, thalamus; Mb, midbrain; Hb, hindbrain; Spc, spinal cord; Hr, heart; DRG, dorsal root ganglion. Bars: 100 μm (A, C); 1 mm (B).

3.2.2 . Olig3 expression in the alar plate of the hindbrain and characterization of neuron subtypes arising from the Olig3+ domain

To characterize Olig3+ cells in the hindbrain, I verified that four Olig3 expressing ventricular subdomains exist in rhombomere 7. Indeed, using antibodies against Math1, Ngn1, Ascl1 and Ptf1a, I was able to observe the four subdomains (Figure 3.8 D,E,F,G; summarized in I). Other characteristic features can also distinguish these four

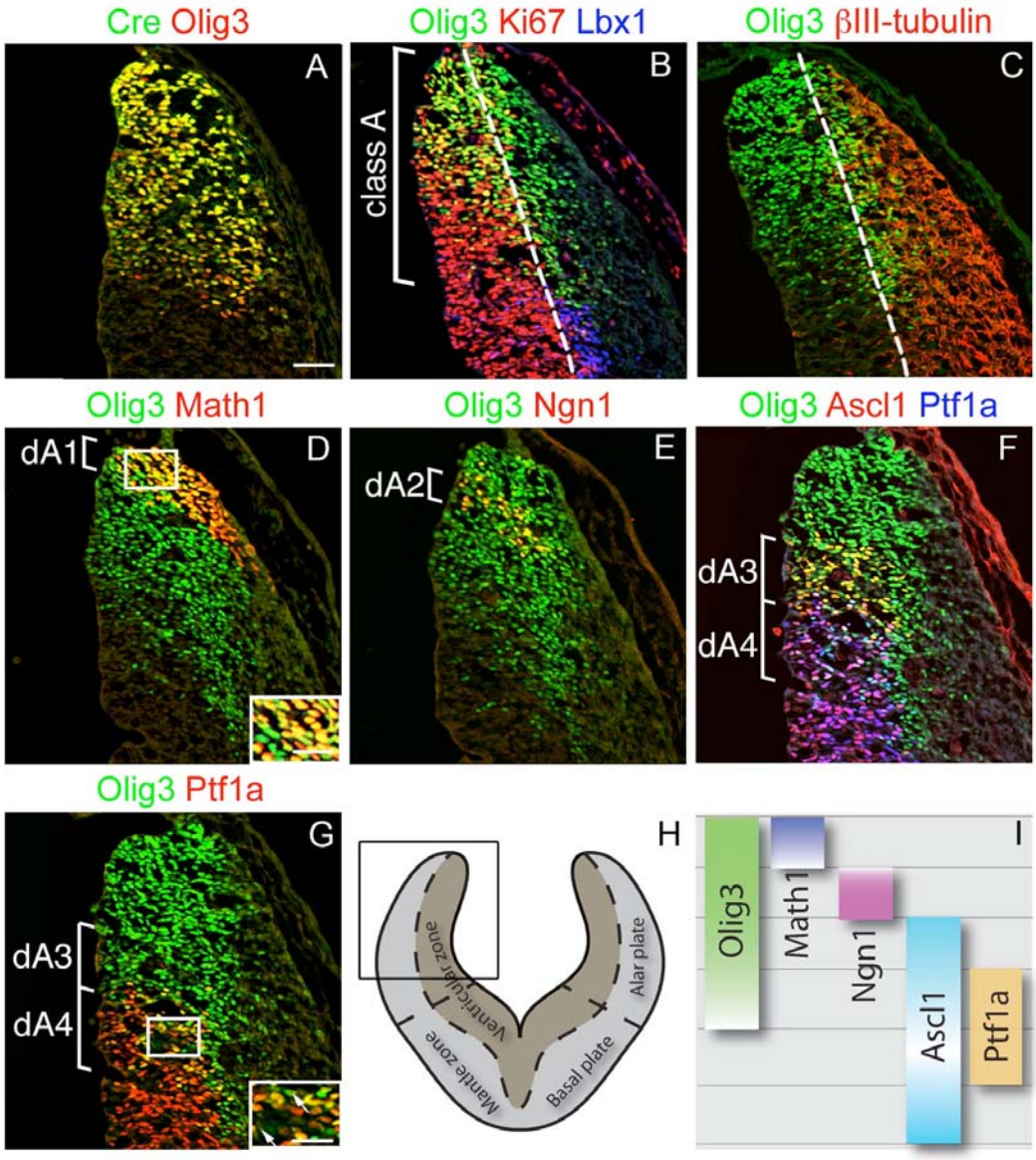

Figure 3.8 **Olig3 expression in the alar plate of the hindbrain.** Immunohistological analysis of Olig3+ cells on consecutive sections of the dorsal alar plate of rhombomere 7 at E11.5. (A-G) Olig3+ cells were observed in a broad domain of the ventricular zone. (A) Immunohistochemistry of hindbrain transverse sections in *Olig3*$^{CreERT2/+}$ mice using antibodies against Cre (green) and Olig3 (red) after administration of tamoxifen at E9.5. Immunohistological analysis of (B) Olig3 (green), Ki67 (red) and Lbx1 (blue) and (C) Olig3 (green) and βIII-tubulin (red) shows that Olig3 is expressed in progenitor cells as well as in postmitotic cells (zones' border indicated by a dashed line). Immunohistological analyses of (D) Olig3 (green) and Math1 (red), (E) Olig3 (green) and Ngn1 (red), (F) Olig3 (green), Ascl1 (red) and Ptf1a (blue), (G) Olig3 (green) and Ptf1a (red). Note that F and G show the same section; in G, the Ascl1 signal was removed, and the Ptf1a signal is shown in red. Regions indicated by white boxes (D,G) are shown in a higher magnification in the insets to clarify different patterns of Olig3 expression in distinct parts of the alar plate. Arrows in G inset indicate cells expressing different levels of Olig3. (H) Schematic representation of rhombomere 7 transverse section. The sector displayed on fluorescent pictures is indicated by a black box. (I) Distinct dorsal progenitor domains of rhombomere 7. Bars: 50 μm; insets in D, G 20 μm.

subdomains. For instance, all cells express Olig3 in the most dorsal subdomains, which are characterized by co-expression of Olig3 and Math1 and Olig3 and Ngn1 (Figure 3.8 D,E; see also inset in D for a higher magnification), whereas in more ventrally located subdomains, which are characterized by co-expression of Olig3 and Ascl1 and Olig3, Ascl1 and Ptf1a, Olig3 is mainly expressed by cells located laterally in the progenitor domain. Moreover, in this domain Olig3+ cells intermingle with Olig3- cells or cells containing low amounts of Olig3 (Figure 3.8 F,G; see also inset in G for a higher magnification). In addition, I also used Ki67, a marker for all active phases of the cell cycle (G_1, S and G_2) that therefore identifies proliferating cells, and βIII-tubulin, a marker for differentiated neurons. The majority of $Olig3^+$ cells were located in the ventricular zone, but Olig3 was also detected in a stripe of cells located in the mantle zone (Figure 3.8 B,C). This indicates that Olig3 is expressed by progenitors and postmitotic neurons. Ki67 and Olig3 were differentially co-expressed in distinct subdomains. Particularly, in the dorsal progenitor subdomains Ki67 was co-expressed with Olig3 in the majority of cells. On the contrary, Ki67+ cells rarely co-expressed Olig3 in ventrally located progenitor subdomains. (Figure 3.8 B). Thus, cells in different subdomains of the ventricular zone appear to express Olig3 in distinct phases of the cell cycle. In the dorsal subdomains, all cycling progenitors seem to express Olig3, whereas in the more ventral domains Olig3 appears to be expressed mainly in postmitotic cells that have left the cell cycle and that are leaving the progenitor domain.

Katja Reuter previously described four neuronal types that arise from the Olig3+ domain. To further analyze the origin of these neurons, I performed genetic fate mapping experiments. I used the *Olig3*^{CreERT2} allele and the *ROSA26R* reporter line that expresses β-galactosidase after Cre-mediated recombination to define these neuron types by immunohistochemistry. I first characterized rhombomere 7, the most posterior unit of the hindbrain. At E11.5, 48 hours after tamoxifen administration, the most dorsal β-galactosidase positive (β-Gal+) neuronal population detected co-expressed Lhx2/9 and corresponds thus to the dA1 subpopulation (Figure 3.9 A). Ventral of dA1 neurons, β-Gal+ dA2 and dA4 neurons were observed. The dA2 neurons expressed Lhx1/5, and the dA4 neurons co-expressed Lhx1/5 and Foxd3 (Figure 3.9 B). In addition, β-Gal+ dA3 neurons were detected that co-expressed Tlx3 (Figure 3.9 C; note that Tlx3+ neurons also express Phox2b and Lmx1b; Sieber *et al.*, 2007). Research done in other laboratories had previously characterized Math1+, Ngn1+, Ascl1+ and Ptf1a+

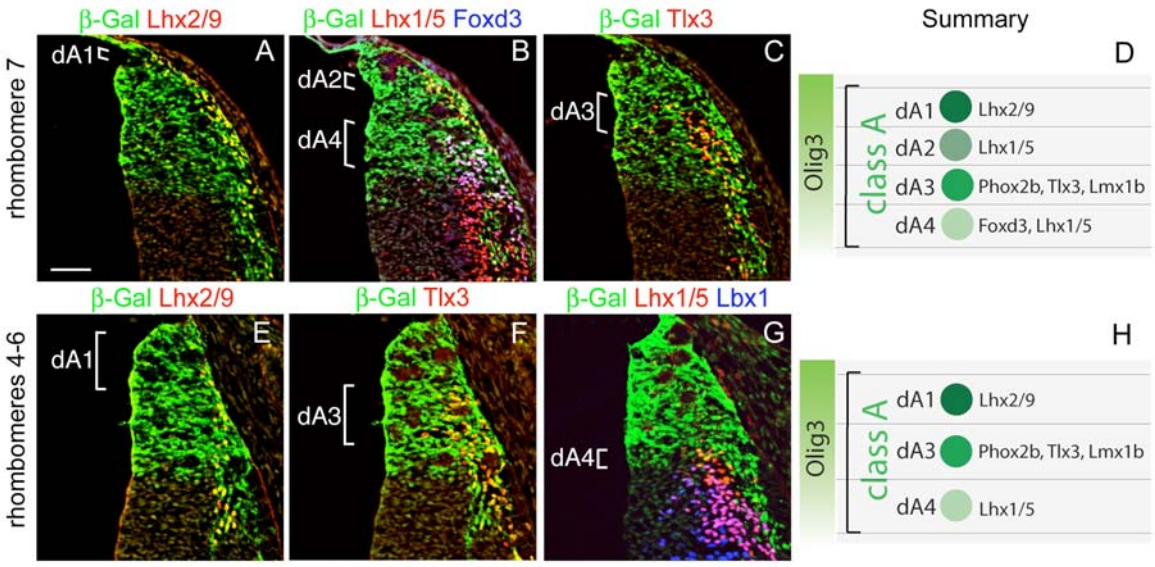

Figure 3.9 **Characterization of neuronal subtypes that arise from Olig3+ cells in the dorsal hindbrain.** Immunohistochemical analysis of neuronal types generated by Olig3+ cells using genetic lineage tracing in rhombomere 7 (A-C) and rhombomeres 4-6 (E-G). Recombination was induced in *Olig3*$^{CreERT2/+}$*;ROSA26R* mice by tamoxifen administration at E9.5; cells that expressed the *lacZ* gene were identified using anti-β-Gal antibodies. Neuronal types were defined using antibodies against Lhx2/9 (red) (A,E), Lhx1/5 (red) and Foxd3 (blue) (B), Tlx3 (red) (C,F), and Lhx1/5 (red) and Lbx1 (blue) (G). Note that E and F show an identical section that was stained for β-Gal, Lhx2/9 and Tlx3; E and F display β-Gal/Lhx2/9 and β-Gal/Tlx3 signals, respectively. Summary of class A dorsal neuron subtypes arising from the Olig3+ domain in rhombomere 7 (D) and in rhombomeres 4-6 (H) (Sieber *et al.*, 2007). Bar: 50 μm.

ventricular zone subdomains, and the neuronal types generated by these domains (Bermingham *et al.*, 2001; Qian *et al.*, 2001; Landsberg *et al.*, 2005; Machold and Fishell, 2005; Wang *et al.*, 2005; Pattyn *et al.*, 2006; Sieber *et al.*, 2007; Yamada *et al.*, 2007). In particular, they had shown that neurons arising from the Math1+ domain express Lhx2/9 and correspond thus to dA1 neurons. Neurons produced by the Ngn1+ domain express Lhx1/5 and therefore correspond to dA2neurons. Furthermore, neurons generated by the dorsal portion of the Ascl1+ domain co-express Tlx3, Phox2b and Lmx1b and therefore correspond to dA3 neurons. Finally, neurons arising from the dorsal portion of the Ptf1a+ domain co-express Lhx1/5 and Foxd3 and correspond thus to dA4 neurons. Together, my data and those published previously by others indicate that Olig3+ progenitor cells generate four dorsal neuronal subtypes in rhombomere 7, the dA1-dA4 neurons (summarized in Figure 3.9 D). Each of these neuron types appears to emerge from a distinct ventricular zone subdomain, and these four

subdomains contain cells expressing Olig3/Math1, Olig3/Ngn1, Olig3/Ascl1 and Olig3/Ascl1/Ptf1a, respectively (summarized in Figure 3.8 I).

In addition, I characterized neurons derived from Olig3+ progenitors in the more rostral parts of the hindbrain at E11.5, i.e. in rhombomeres 1-6. The most dorsal β-Gal+ neuronal population observed co-expressed Lhx2/9 (dA1, Figure 3.9 E), and it arose in all segments of the hindbrain. The fate of this neuronal population that arises from Olig3+/Math1+ progenitors was previously extensively characterized. Thus, these neurons generate mossy fiber neurons forming four major precerebellar nuclei (Bermingham *et al.*, 2001; Machold and Fishell, 2005; Wang *et al.*, 2005). I did not observe dA2 neurons in rhombomeres 1-6, and the Ngn1+ domain, which gives rise to the dA2 neuron type in rhombomere 7, is not present in rhombomeres 4-6. This observation is consistent with other reports (Landsberg *et al.*, 2005; Sieber *et al.*, 2007). Instead, ventral of dA1 neurons, β-Gal+/Tlx3+ (dA3) neurons were observed, that also co-express Phox2b and Lmx1b (Qian *et al.*, 2001; Sieber *et al.*, 2007). dA3 neurons were present in rhombomeres 4-7, but not in rhombomeres 1-3. These neurons were previously shown to generate the nucleus of the solitary tract and the area postrema (Figure 3.9 F and data not shown; cf. Pattyn *et al.*, 2000; Qian *et al.*, 2001; Dauger et al., 2003; Sieber *et al.*, 2007). An additional small β-Gal+ cell population that expressed Lhx1/5 was identified further ventrally (dA4, Figure 3.9 G). In rhombomeres 4-6, this population of dA4 neurons did not express Foxd3. In contrast, the Lhx1/5+ dA4 neurons of rhombomere 7 co-expressed Foxd3. Available evidence indicates that these neurons generate the inferior olivary nucleus (Yamada *et al.*, 2007). Distinct class A neuron subtypes emerging in rhombomeres 4-6 are summarized in Figure 3.9 H.

3.2.3 . Analysis of rhombomeres 4-7 of *Olig3* mutant mice

The first analysis of the effect of the *Olig3* mutation on the determination of the identity of neurons in rhombomere 7 was done by Katja Reuter in Carmen Birchmeier's laboratory and was published as a doctoral thesis in 2006. I will introduce some data obtained by Katja Reuter for a better understanding of my findings.

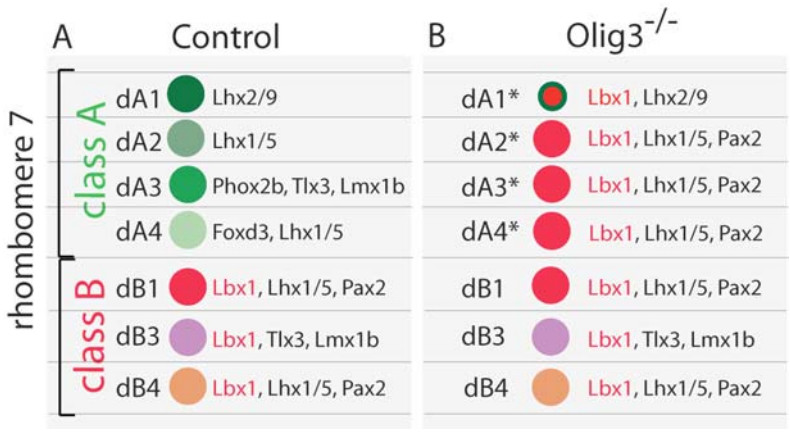

Figure 3.10 **Schematic illustration of phenotype observed in *Olig3* mutant (B) compared with control (A) mice in the alar plate of rhombomere 7 at E11.5.** Picture summarizes results presented in the doctoral thesis of Katja Reuter.

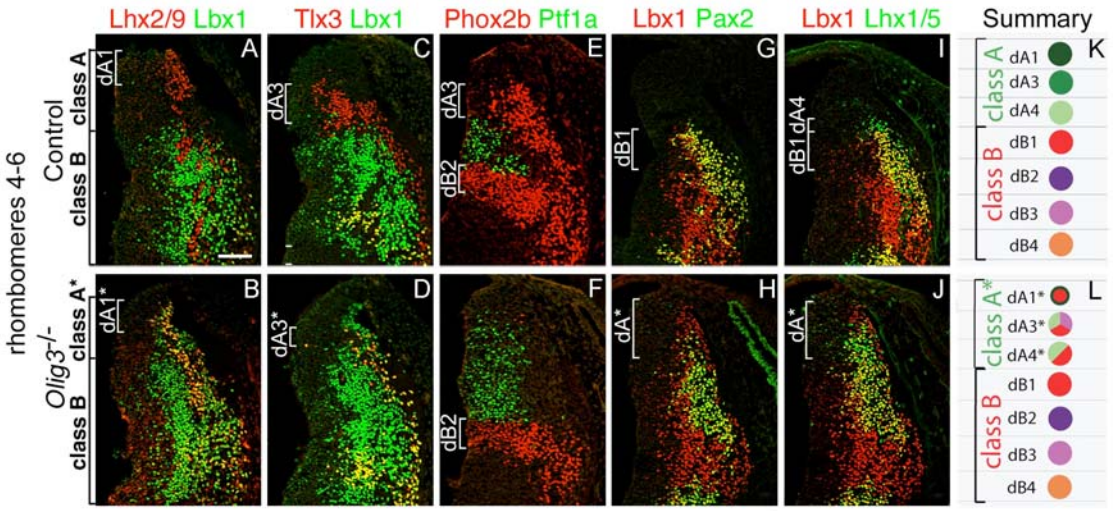

Figure 3.11 **Olig3 is required to determine the fate of class A neurons in rhombomere 4.** Immunohistological analysis of the alar plate of rhombomere 4 of control and *Olig3* mutant mice at E11.5 using antibodies against: (A,B) Lhx2/9 (red) and Lbx1 (green). In *Olig3* mutant mice, ectopic Lbx1+ neurons were present. (C,D) Tlx3 (red) and Lbx1 (green). In *Olig3* mutant mice, Tlx3+ (dA3*) neurons were generated in reduced numbers and co-expressed Lbx1. (E,F) Phox2b (red) and Ptf1a (green). Phox2b+ dA3 neurons were not present in *Olig3* mutant mice, and the expression domain of Ptf1a was expanded. (G,H) Lbx1 (red) and Pax2 (green), and (I,J) Lbx1 (red) and Lhx1/5 (green). In the dorsal alar plate of *Olig3* mutant mice, Lhx1/5+/Lbx1+, Lhx1/5+/Lbx1- and Lbx1+/Pax2+ neurons arose in an apparently intermingled manner. Note that G,I and H,J show identical sections, which were stained with antibodies against Lbx1, Pax2 and Lhx1/5; G,H and I,J display Lbx1/Pax2 and Lbx1/Lhx1/5 signals, respectively. (K,L) Summary of the neuronal types generated in the alar plate of control and *Olig3* mutant mice in rhombomere 4-6. Bar 50 μm.

In the normal development of rhombomere 7, class A neurons arise in the dorsal alar plate and Lbx1 positive class B neurons in the ventral alar plate (Figure 3.10 A; Sieber

et al., 2007). In *Olig3* mutant mice, Katja Reuter observed a pronounced dorsal expansion of Lbx1+ neurons in rhombomere 7. Most ectopic Lbx1+ neurons co-expressed Pax2 and Lhx1/5, which she denoted as dA2-4* neurons (Figure 3.10 B). In normal development, Lbx1+/Pax2+ neurons of the dorsal spinal cord and hindbrain express glutamate decarboxylase 1 (Gad1), an enzyme essential for GABA synthesis (Cheng et al., 2005), and arise exclusively in the ventral alar plate. In *Olig3* mutants, Gad1+ neurons arose ectopically in the dorsal alar plate (data not shown). The conclusion of Katja Reuter was that dA2-dA4 neurons are not correctly specified in rhombomere 7 of *Olig3* mutant mice. At their expense, neurons arose that expressed Gad1, Lbx1, Pax2, Lhx1/5, and displayed thus molecular characteristics of class B inhibitory neurons. She also identified an additional aberrant neuronal subtype close to the roof plate in *Olig3* mutants. These neurons co-expressed Lbx1 and Lhx2/9, and she denoted them as dA1* neurons (Figure 3.10 B). Additionally, she observed changes in the dorsal progenitors in rhombomere 7 of these mice, i.e. a dorsally expanded expression of Ptf1a (data not shown). Therefore, Olig3 is essential to maintain the correct expression of Ptf1a, and it is essential for the determination of the molecular identity of dA1-dA4 neurons.

I characterized the neuronal types that were born in rhombomeres 4-6 of *Olig3* mutant mice, and observed a pronounced dorsal expansion of Lbx1+ neurons also in these rhombomeres (Figure 3.11 G,H,I,J). Close to the roof plate, neurons that co-expressed Lhx2/9 and Lbx1 were identified, similarly to what was observed previously in rhombomere 7 (dA1*; Figure 3.11 A,B). Furthermore, the number of Tlx3+ neurons (dA3) in the dorsal alar plate was reduced and moreover these neurons did not express Phox2b. Thus, Tlx3+/Phox2b+ dA3 neurons were not present. Instead, Tlx3+/Lbx1+ (dA3*) neurons were observed, which appeared to intermingle with Lbx1+/Pax2+ and Lhx1/5+/Lbx1-neurons (Figure 3.11 C-F and G-J). These changes were accompanied by a dorsal expansion of Ptf1a (Figure 3.11 E,F). The phenotype observed in *Olig3* mutant mice in rhombomere 4-6 is summarized in Figure 3.11 K-L. Thus, loss of *Olig3* also results in an expanded expression of Lbx1 and Ptf1a in rhombomeres 4-7.

In rhombomeres 2-3 of *Olig3* mutant mice, I observed a reduction in the number of dA1 neurons, which did not ectopically express Lbx1 (Figure 3.12 A,D). Furthermore, I observed a dorsal expansion of Ptf1a expression (Figure 3.12 C,F). However, this

change was not accompanied by a dorsal expansion of Pax2. Moreover, no apparent ectopic Lbx1 expression was observed in rhombomeres 2-3 (Figure 3.12 B,E). Because I did not observe any major changes in the specification of neuronal types in rhombomeres 2-3, I restricted my subsequent analysis to rhombomeres 4-7 and to the derivatives of these rhombomeres.

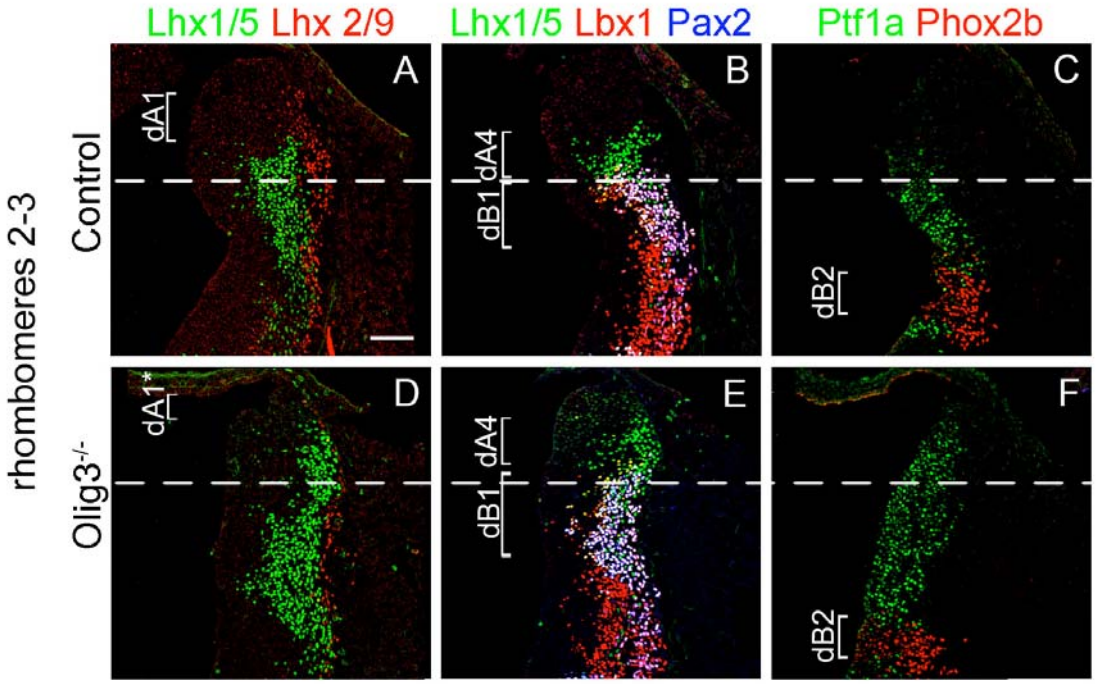

Figure 3.12 **Olig3 has a minor effect on class A neurons in rhombomeres 2-3.** Immunohistological analysis of the alar plate of rhombomeres 2-3 of control and *Olig3* mutant mice at E11.5 using antibodies against: (A,D) Lhx2/9 (red) and Lhx1/5 (green). In *Olig3* mutant mice, dA1 neurons arose in a reduced number. (B,E) Lhx1/5 (green), Lbx1 (red) and Pax2 (blue). In *Olig3* mutant mice, Lbx1 and Pax2 expression was not altered. (C,F) Ptf1a (green) and Phox2b (red). In *Olig3* mutant mice, Ptf1a expression expanded dorsally (indicated by the dashed line). Dashed lines indicate border between class A and B neurons. Bar 50 μm.

3.2.4 . Derivatives of Olig3+ cells in the hindbrain and genetic lineage tracing in homozygous *Olig3* mutant mice

The dorsal ventricular zone of the rhombencephalon generates the five main brainstem precerebellar nuclei that relay peripheral sensation and cortical input to the cerebellum. Four of these, pontine gray and reticulotegmental nuclei, lateral reticular and external cuneate nuclei, project mossy fibers to the cerebellum. In contrast, the inferior olive precerebellar nucleus (ION) projects climbing fibers to the cerebellum. In addition, the

dorsal ventricular zone generates the spinal trigeminal nucleus and the nucleus of the solitary tract that relay somatosensory and viscerosensory information, respectively (Altman and Bayer, 1980; Altman and Bayer, 1987a; Qian *et al.*, 2001; Wang *et al.*, 2005; Sieber *et al.*, 2007; Yamada *et al.*, 2007).

I used genetic fate mapping experiments, i.e. the *Olig3*^{CreERT2} allele and a *Tau*^{nlsLacZ} reporter mouse, to define brainstem nuclei that are derivatives of Olig3+ cells. I induced recombination by tamoxifen at E10.5 and visualized the recombined cells six days later by X-Gal staining. This staining relies on the use of the β-galactosidase substrate X-gal, which is converted into a blue dye by the enzyme. Whole-mount X-Gal staining was performed on dissected brain tissue. A ventral view showed blue cells in the entire inferior olivary nucleus and in the pontine gray nucleus (Figure 3.13 A). A lateral view showed that blue cells were present in the cochlear nucleus, lateral lemniscus and pontomesencephalic tegmentum (Figure 3.13 B). Therefore, Olig3+ cells generate precerebellar nuclei containing mossy fiber and climbing fiber neurons. In addition, Olig3+ cells generate neurons in the cerebellum, pons and isthmus. A more detailed analysis of Olig3 derivatives was done on sections of pons and medulla (see below).

Furthermore, I used genetic fate-mapping experiments in *Olig3* heterozygous and homozygous mutant mice (*Olig3*$^{CreERT2/+}$;*Tau*^{nlsLacZ} and *Olig3*$^{CreERT2/-}$;*Tau*^{nlsLacZ}) to assess the location of the supernumerary inhibitory Lbx1+/Pax2+ neurons, which were observed by Katja Reuter in rhombomere 7 at E11.5. I tested whether these neurons were maintained in the medulla of E18.5 embryos treated with tamoxifen at E10.5. I observed that β-Gal+/Pax2+ cells were rarely present in control animals. However in *Olig3* mutant mice, ectopic β-Gal+/Pax2+ cells were present and located in the reticular formation of the caudal medulla (Figure 3.14 A,B; see also insets in A,B for a higher magnification). Moreover, I observed on sections of the caudal medulla oblongata that the number of Pax2+ neurons was significantly increased in homozygous mutant mice versus heterozygous mice at E18.5 (for quantification see Figure 3.14 C). Thus, supernumerary Pax2+ inhibitory neurons persisted in the caudal medulla oblongata, and were still detectable in the reticular formation of *Olig3* mutant mice at E18.5.

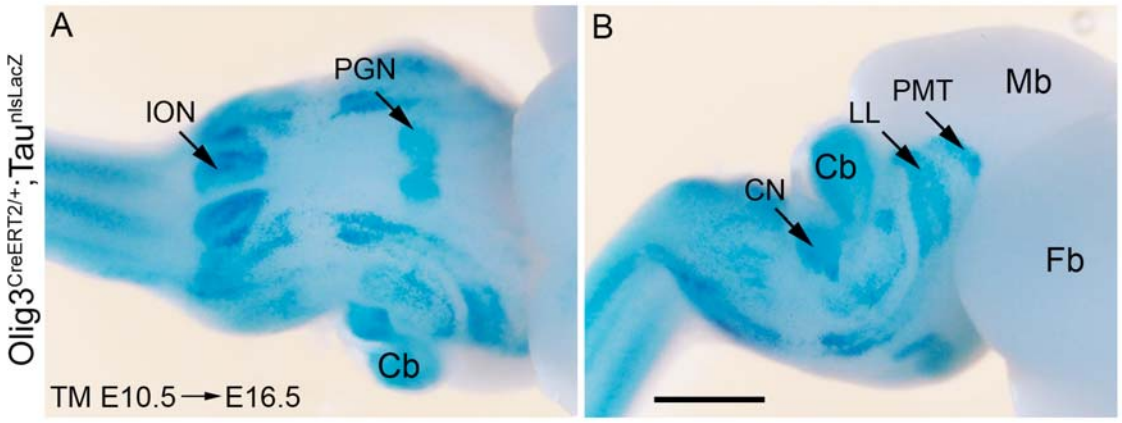

Figure 3.13 **Derivatives of Olig3+ cells in the hindbrain at E16.5.** Whole-mount X-Gal staining of dissected brain tissue from *Olig3*$^{CreERT2/+}$;*Tau*^{nlsLacZ} embryos treated with tamoxifen at E10.5. (A) Ventral view of medulla and pons. Blue cells are located in particular positions in the entire medulla, cerebellum and pons. (B) Lateral view of a E16.5 brain. ION, inferior olivary nucleus; PGN, pontine gray nucleus; Cb, cerebellum; CN, cochlear nucleus; LL, lateral lemniscus; PMT, pontomesencephalic tegmentum; Mb, midbrain; Fb, forebrain; TM, tamoxifen. Bar: 1 mm.

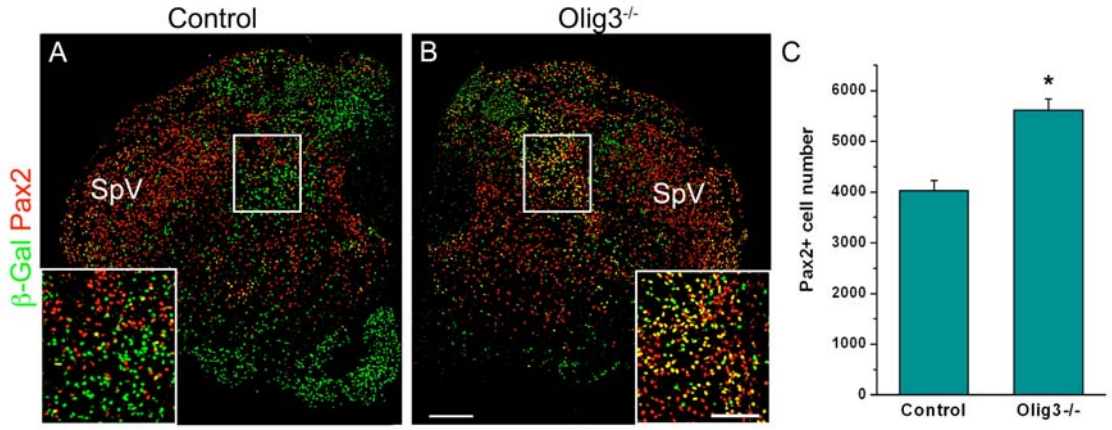

Figure 3.14 **Supernumerary inhibitory Pax2 cells in the E18.5 caudal medulla oblongata.** Immunohistological analysis of control (*Olig3*$^{CreERT2/+}$;*Tau*^{nlsLacZ}) (A) and *Olig3* mutant embryo (*Olig3*$^{CreERT2/-}$;*Tau*^{nlsLacZ}) (B) treated with tamoxifen at E10.5 using antibodies against Pax2 (red) and β-Gal (green). SpV indicates the spinal trigeminal nucleus. White boxes indicate the location of ectopic β-Gal+/Pax2+ cells in *Olig3* mutant mice compared with control mice. Insets show area within white boxes in a higher magnification. (C) The number of Pax2+ cells was quantified in the entire caudal medulla of *Olig3* mutant versus control animals. Error bars represent standard error. (*) $P < 0.05$. Bars: 200 μm in B, 100 μm in inset.

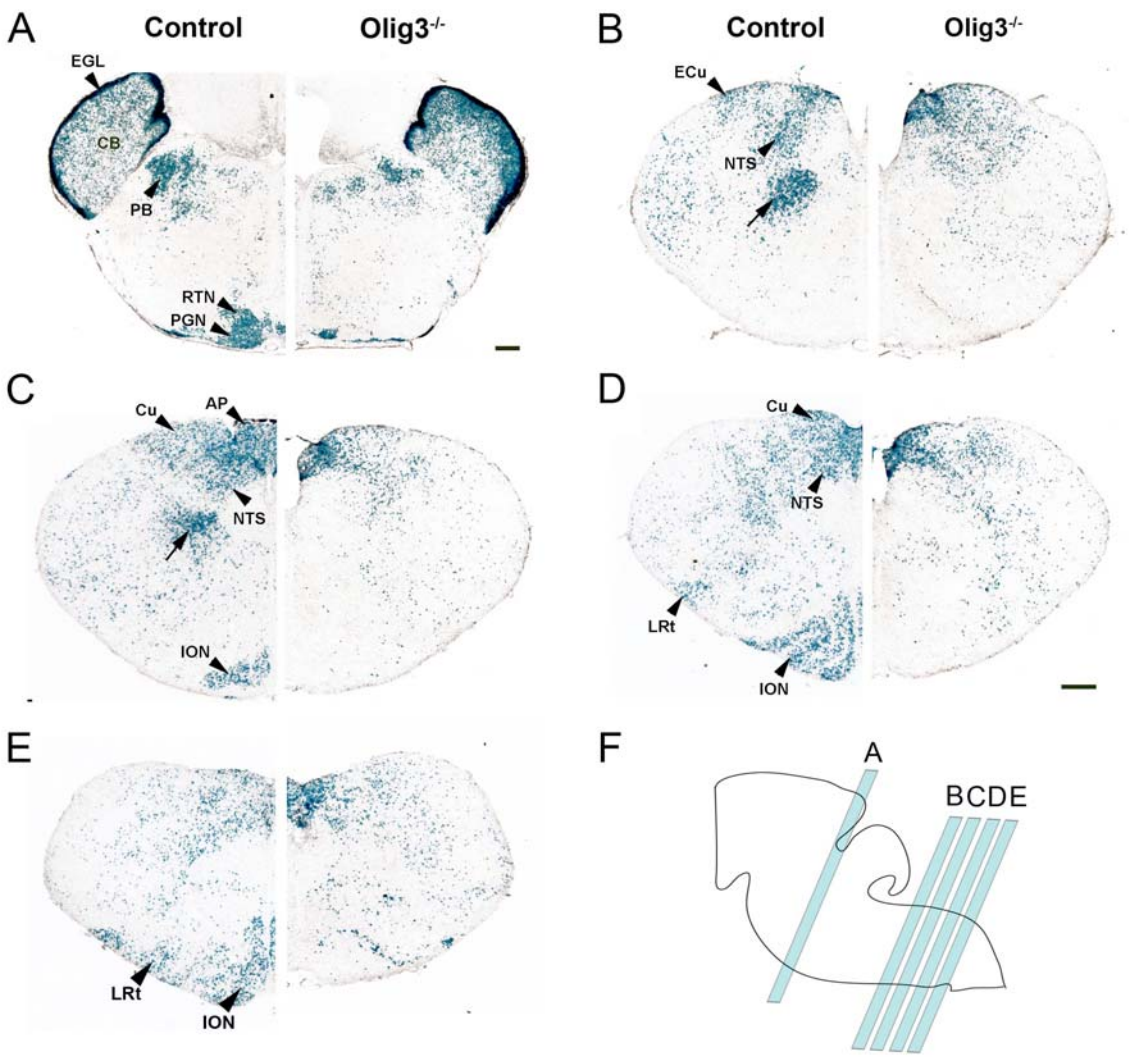

Figure 3.15 **Genetic lineage tracing in heterozygous and homozygous *Olig3* mutant mice.** (A-E) Analysis of the medulla oblongata and pons of control (*Olig3*$^{CreERT2/+}$*;ROSA26R*) and *Olig3* mutant (*Olig3*$^{CreERT2/-}$*;ROSA26R*) mice at E18.5. Recombination was induced at E10.5 by tamoxifen, and expression of the *lacZ* gene was identified by X-Gal staining on transverse sections. (F) Schematic representation of the transverse section planes presented in A-E on lateral view of midbrain, cerebellum and hindbrain. Labeled plates represent the rostral-caudal position of the presented transverse sections. Arrowheads indicate: Cu, cuneate nucleus; ECu, external cuneate nucleus, ION, inferior olivary nucleus; NTS, nucleus of the solitary tract, LRt, lateral reticular nucleus; PB, parabrachial nucleus; PGN, pontine gray nucleus; RTN, reticulotegmental nucleus; CB, cerebellum and EGL, external granule layer. Arrows indicate blue cells located in a particular position in the reticular formation of the rostral medulla oblongata. Bar: 200 μm in A and D.

Additionally, to define the consequences of the neuronal fate changes observed in *Olig3* mutant mice, I performed fate mapping experiments on a *Olig3* mutant background, using *Olig3*$^{CreERT2/+}$;*ROSA26R* and *Olig3*$^{CreERT2/-}$;*ROSA26R* animals. Again, I induced recombination at E10.5 by tamoxifen administration, and identified recombined cells and their derivatives by β-galactosidase expression using X-Gal staining on sections. In

the caudal medulla oblongata of heterozygous mutant mice at E18.5, in addition to nuclei identified in the whole-mount brain tissue, I observed blue cells in the nucleus of the solitary tract, in the lateral reticular nucleus and the cuneate nucleus (Figure 3.15 D,E). Further rostral, blue cells were present in the area postrema (Figure 3.15 C), the external cuneate nucleus (Figure 3.15 B), as well as in the reticulotegmental and parabrachial nuclei (Figure 3.15 A). Blue cells were also observed in the particular location in the reticular formation (arrows in Figure 3.15 B,C) and in the external granule cell layer of the cerebellum (Figure 3.15 A). In homozygous *Olig3* mutants, β-Gal+ cells were present in reduced numbers at the position of the lateral reticular, external cuneate, reticulotegmental, pontine gray and parabrachial nuclei (Figure 3.15 A-E). In addition, β-Gal+ cells at the position of the inferior olivary nucleus and the reticular formation were absent (Figure 3.15 C-E). Katja Reuter had already observed that the nucleus of the solitary tract and the area postrema are not formed in *Olig3* mutant mice. Indeed, in the dorsal-medial domain, where the nucleus of the solitary tract, the area postrema and the cuneate nucleus are located in normal development, the morphology was altered in *Olig3* mutant mice, and β-Gal+ cells were distributed in an aberrant manner (Figure 3.15 A-E).

Together, my data showed that Olig3+ cells generate all five precerebellar nuclei containing mossy fiber and climbing fiber neurons and moreover the nucleus of the solitary tract containing viscerosensory neurons and the area postrema. All these nuclei are dependent on Olig3 in their development.

3.2.5 . The role of Olig3 in the development of dA4 and dA3 neurons

The inferior olivary nucleus is a major precerebellar nucleus, whose importance lies in the fact that it is the only source of climbing fibers projecting to cerebellar Purkinje cells (Altman and Bayer, 1987b; Sotelo, 2004). The inferior olivary nucleus is absent in *Olig3* mutant mice. In addition, Yamada and colleagues showed in 2007 that the development of the inferior olivary nucleus depends on the Ptf1a transcription factor (Yamada *et al.*, 2007). Ptf1a and Olig3 are co-expressed in a small progenitor domain in rhombomere 7 that gives rise to Lhx1/5+/Foxd3+ neurons (dA4), which migrate tangentially to the site where the inferior olivary nucleus forms in normal development.

I addressed the question if Olig3 and Ptf1a cooperate to specify dA4 neurons, using overexpression experiments in the chick. The hindbrains of chick embryos were electroporated *in ovo* at Hamburger Hamilton stage 16 with an expression construct that produces mouse Olig3, and the embryos were analyzed 48 h later. On the electroporated side, I observed a pronounced decrease in the numbers of Lbx1+ and Pax2+ neurons (Figure 3.16 A,B; Lbx1 quantification in D). This was accompanied by a suppression of Ptf1a (Figure 3.16 C). Thus, Olig3 overexpression can suppress Lbx1 and Ptf1a, which result in a reduced generation of Pax2+ neurons. In addition, I observed that Foxd3+ neurons were generated in reduced numbers (Figure 3.16 F). I also overexpressed a Ptf1a expression construct, which had little effect on the generation of Foxd3+ (dA4) neurons (Figure 3.16 E). However, when I co-electroporated Olig3 and Ptf1a expression constructs, I induced Foxd3 expression (Figure 3.16 G). The ectopic Foxd3+ neurons were not only observed in the dorsal hindbrain, but they also appeared ventrally. I conclude that Olig3 and Ptf1a can cooperate, and that they together can control the determination of the Foxd3+ (dA4) neuronal fate.

The results shown above demonstrated that Olig3 plays a crucial role in the development of the inferior olivary nucleus by cooperation with Ptf1a. However, the overexpression experiments did not address the question if Olig3 serves as an instructive factor that together with Ptf1a determines the fate of dA4 climbing fiber neurons. Alternatively, Olig3 might just suppress another factor that interferes with the production of dA4 neurons during normal development. A likely candidate for such a factor that needs to be suppressed is Lbx1: Lbx1 is ectopically expressed in *Olig3* mutant mice, and Lbx1 overexpression in the spinal cord was known to interfere with the determination of class A dorsal neurons. To investigate this, I generated *Olig3/Lbx1* double mutant mice and analyzed whether deficits present in *Olig3* mutants were rescued by the absence of *Lbx1*. Foxd3+ dA4 neurons were not formed in *Olig3* mutants, and they were generated in *Lbx1* mutants (Figure 3.17 A,B,D). Interestingly, their generation was rescued in *Olig3/Lbx1* double mutant embryos (Figure 3.17 C). I conclude that Olig3 has a permissive role in the determination of the dA4 fate, and that the sole function of Olig3 in this process is the suppression of Lbx1.

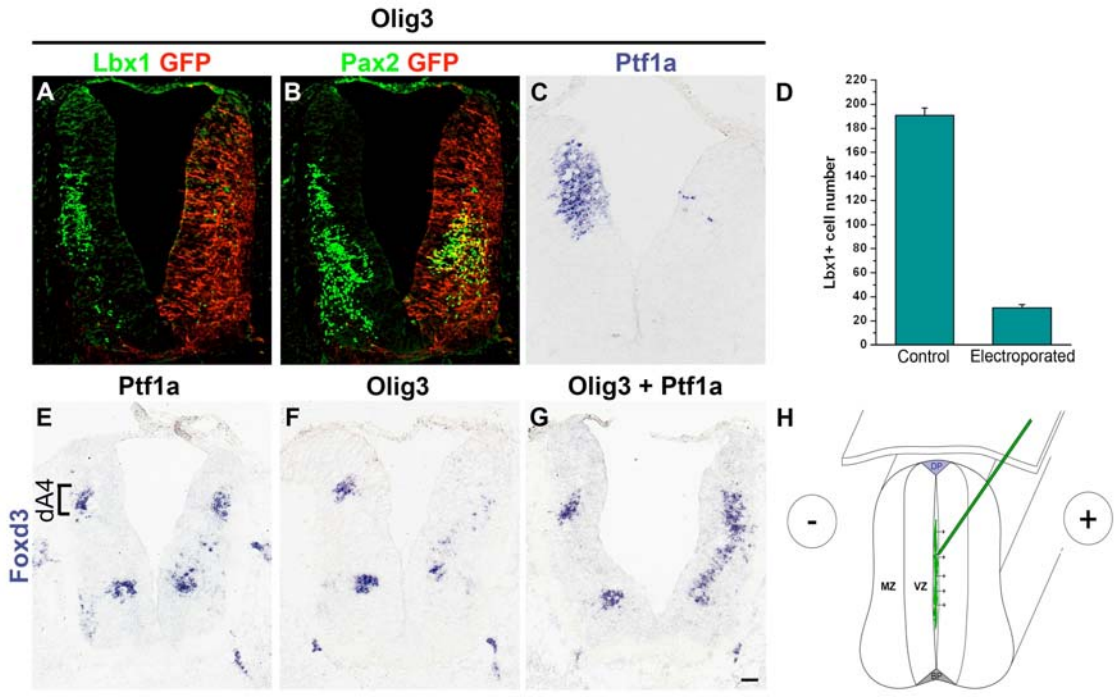

Figure 3.16 **Cooperation of Olig3 and Ptf1a in the determination of Foxd3+ dA4 fate.** Chick hindbrains electroporated with mouse Olig3 (A-C, F), Ptf1a (E), Olig3 and Ptf1a (G). Effects were assessed by immunohistochemistry using antibodies against Lbx1 (green) (A), Pax2 (green) (B), or by *in situ* hybridization using probes specific for Ptf1a (C) and Foxd3 (E-G). In addition, a GFP vector was co-electroporated to identify electroporated cells. Always the right side of rhombomere 7 was electroporated (indicated by GFP expression in A and B). Note that A and B show an identical section stained with antibodies against Lbx1, Pax2 and GFP; A and B display the Lbx1/GFP and Pax2/GFP signals, respectively. (D) Quantification of cells that expressed Lbx1 in the dorsal part of rhombomere 7. (H) Schematic illustration of the chick *in ovo* electroporation method. Bar: 50 µm.

I also compared the generation of Phox2b+/Tlx3+ dA3 neurons in *Olig3*, *Lbx1* and *Olig3/Lbx1* double mutant mice. In *Olig*3 mutants, the dA3 neuronal population was not formed (Figure 3.17 E,F), however it was generated in *Lbx1* mutants (data not shown). The appearance of Phox2b+/Tlx3+ dA3 neurons was not rescued in *Olig3/Lbx1* mutants. At the expense of Phox2b+/Tlx3+ dA3 neurons, ectopic Foxd3+ neurons appeared in the double mutants at the position were dA3 neurons arose in normal development (Figure 3.17 E,G). Therefore, for the determination of the dA3 neuronal fate, Olig3 does more than simply suppress Lbx1.

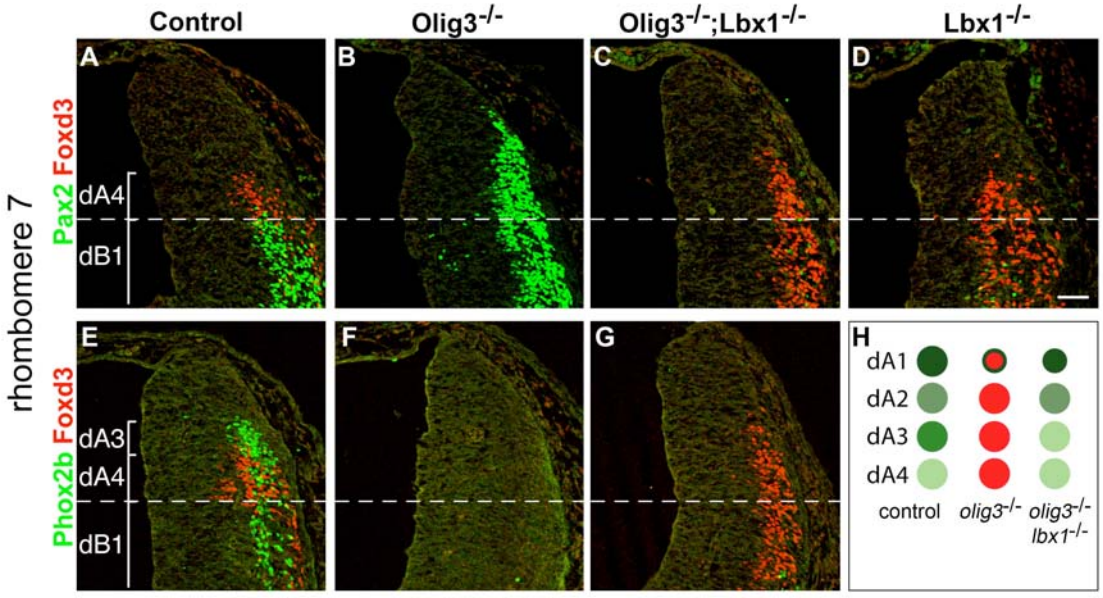

***Figure 3.17* Permissive function of Olig3 in the determination of the Foxd3+ dA4 fate.** Immunohistochemical analysis of the dorsal alar plate in (A,E) control, (B,F) *Olig3* mutant, (C,G) *Olig3/Lbx1* double mutant and (D) *Lbx1* mutant mice, using antibodies against Foxd3 (red) and Pax2 (green) (A-D) and Foxd3 (red) and Phox2b (green) (E-G). Dashed lines indicate the border between class A and B neurons. (H) Summary of neuronal types observed in control, *Olig3*, and *Olig3/Lbx1* mutant mice. Bar: 50 µm.

To address the role of Olig3 in the specification of dA3 neurons, I generated *Olig3/Ptf1a* double mutant mice. Ptf1a is a factor known to suppress Tlx3 expression, when overexpressed in chick spinal cords (Mizuguchi *et al.*, 2006; Wildner *et al.*, 2006). Therefore, this raised the question whether the role of Olig3 in the specification of dA3 neurons is just the suppression of Ptf1a. Olig3 is able to suppress Ptf1a in rhombomere 7 in chick overexpression experiments shown above (Figure 3.16 C). Moreover, overexpression of Ptf1a in rhombomere 7 suppresses Tlx3 and Phox2b expression (data not shown). In rhombomere 7 of *Olig*3 mutants, the dA3 neuronal population was not formed (Figure 3.18 A,C). In opposite, dA3 neurons were generated in *Ptf1a* mutants (Figure 3.18 A,D). Astonishingly, Tlx3 expression was rescued in the *Olig3/Ptf1a* double mutants but not the expression of Phox2b, which is a more specific marker for dA3 neurons. Thus, there were Phox2b-/Tlx3+ neurons denoted as dA3* generated in these double mutants instead of Phox2b+/Tlx3+ dA3 neurons in control mice (Figure 3.18 A,B). The situation was similar in rhombomeres 4-6. In *Olig3* mutant mice, dA3 neurons were generated in reduced numbers and they were only expressing Tlx3 (Figure 3.18 E,G). However, in *Ptf1a* mutant mice dA3 neurons were generated

and they expressed both Tlx3 and Phox2b (Figure 3.18 E,H). In *Olig3/Ptf1a* double mutants, the number of Tlx3+ neurons at the position of dA3 neurons was similar to control animals but Phox2b was still absent (Figure 3.18 E,F). Thus, in rhombomeres 4-7, the role of Olig3 in the specification of dA3 neurons seems to be dual. First, Olig3 serves as a permissive factor to allow the expression of Tlx3 in dA3 neurons by suppressing Ptf1a. Second, Olig3 is essential for the induction of Phox2b in dA3 neurons.

In conclusion, my data show that Olig3 acts in the specification of climbing fiber neurons of the inferior olivary nucleus (dA4 neurons) by suppressing Lbx1 expression. Moreover, the role of Olig3 in the specification of dA3 neurons is dual: (i) it suppresses Lbx1 as well as Ptf1a and (ii) it might have an instructive role in the induction of Phox2b expression.

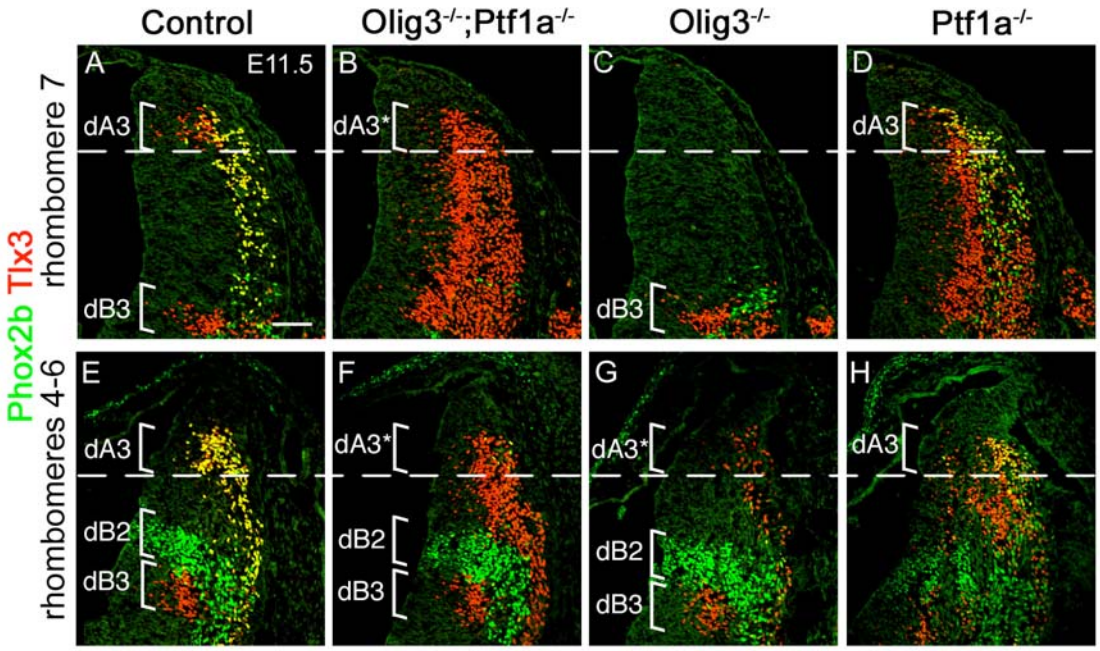

Figure 3.18 **Dual role of Olig3 in the specification of dA3 neurons.** Immunohistochemical analysis of the dorsal alar plate of (A-D) rhombomere 7 and (E-H) rhombomeres 4-6 in (A,E) control, (B,F) *Olig3/Ptf1a* double mutant (C,G) *Olig3* mutant and (D,H) *Ptf1a* mutant mice, using antibodies against Tlx3 (red) and Phox2b (green). Dashed lines indicate the border between dA3 and dA4 neurons. Bar: 50 µm.

4 . Discussion

I characterized the functions of two transcription factors, Rbp-j and Olig3, using mice that carry mutations in the genes encoding the two factors. Both, Rbp-j and Olig3, play essential roles in neuronal fate determination. I will discuss my findings on these two factors separately.

4.1 . Rbp-j functions in the dorsal spinal cord

In the development of the dorsal spinal cord, two phases of neurogenesis are observed. During the early phase, distinct neuronal cell types are generated in stripes, reflecting the classical patterning mechanisms used for neuronal fate determination in the spinal cord. A different picture is observed during the late phase of neurogenesis, when a broad and apparently homogenous progenitor domain produces two different types of neurons, dILA and dILB, which arise in a salt-and-pepper pattern. dILA and dILB neurons assume distinct neurotransmitter phenotypes during terminal differentiation, GABAergic (inhibitory) and glutamatergic (excitatory), respectively (Muller *et al.*, 2002). Previously, Hendrik Wildner showed that these two neuron types could be generated from the same progenitor cell by asymmetric cell division. In particular, dILA neurons are exclusively produced by asymmetric divisions (Wildner *et al.*, 2006). It is not known, which molecular mechanism allows the two daughter cells to assume distinct fates. In light of studies performed in *Drosophila,* Notch signaling seemed to be a good candidate that might regulate this process. Thus, a first goal of my thesis was to assess the function of Notch signaling in the development of dorsal neuron types.

The Rbp-j transcription factor is a major transcriptional mediator of Notch signaling. After the activation of the Notch pathway, Rbp-j, NICD and Maml-1 form a transcriptional complex, which activates the transcription of Notch target genes (Nam *et al.*, 2006). I used two different genetic approaches to address the functions of Notch: (i) Rbp-j conditional mutations, which were introduced using two different Cre lines, $Pax3^{Cre}$ and $Pax7^{CreERT2}$; this was expected to eliminate all transcriptional responses to Notch signaling; (ii) overexpression of a dominant negative variant of Maml-1

(dnMaml), which was expected to interfere with the recruitment of co-activators to the Notch-activated Rbp-j (i.e. the NICD/Rbp-j) complex; this was expected to reduce but not to eliminate completely the Notch-dependent transcriptional responses.

4.1.1 . Two distinct roles of Rbp-j in the dorsal spinal cord

In vertebrates, the best-known function of the DNA binding factor Rbp-j is the mediation of the transcriptional response of Notch signals. Rbp-j-dependent Notch signaling activates the expression of Hes1 and Hes5, two repressor-type bHLH factors, which suppress neuronal differentiation and maintain cells in a progenitor state (Kageyama *et al.*, 2008). Indeed, I observed major effects on neurogenesis and a depletion of the progenitor pool in all the mutants that I analyzed. In particular, *Pax3^{Cre};Rbp-j$^{flox/flox}$* mutant mice displayed precocious neuronal differentiation and a depletion of the progenitor pool prior to the beginning of the late phase of neurogenesis. Overexpression of dnMaml resulted also in a reduced number of progenitors in the dorsal spinal cord. Thus, one very important role of Rbp-j is to act in the complex with NICD and Maml-1 as a transcriptional activator of genes, which regulate the balance between progenitor cell renewal and differentiation.

However, in addition to the role in neurogenesis, I also observed changes in the specification of dorsal neuron types. In *Pax3^{Cre};Rbp-j$^{flox/flox}$* and *Pax7^{CreERT2};Rbp-j$^{\Delta/flox}$* mutant mice, dI4 and dILA neurons were not formed in the early and late neurogenic waves, respectively. Both of these neuron types give rise to inhibitory (GABAergic) neurons in the spinal cord. At their expense, glutamatergic dI5 and dILB neurons arose in *Rbp-j* mutant mice. In contrast, mice that express dnMaml displayed no obvious changes in the determination of GABAergic neuronal fates. Thus, the two mutations gave apparently different phenotypes, which I cannot explain if I assume that these reflect Notch functions.

The contradictory results obtained with *Rbp-j* and dnMaml mutant mice were reconciled by the work done independently and in parallel in Raymond MacDonald's and Jane Johnson's laboratories. They investigated the role of the PTF1 complex in pancreas and in the dorsal spinal cord. These studies revealed that PTF1 is a trimeric complex containing the bHLH transcription factor Ptf1a/p48, E-proteins such as Tcf12, and

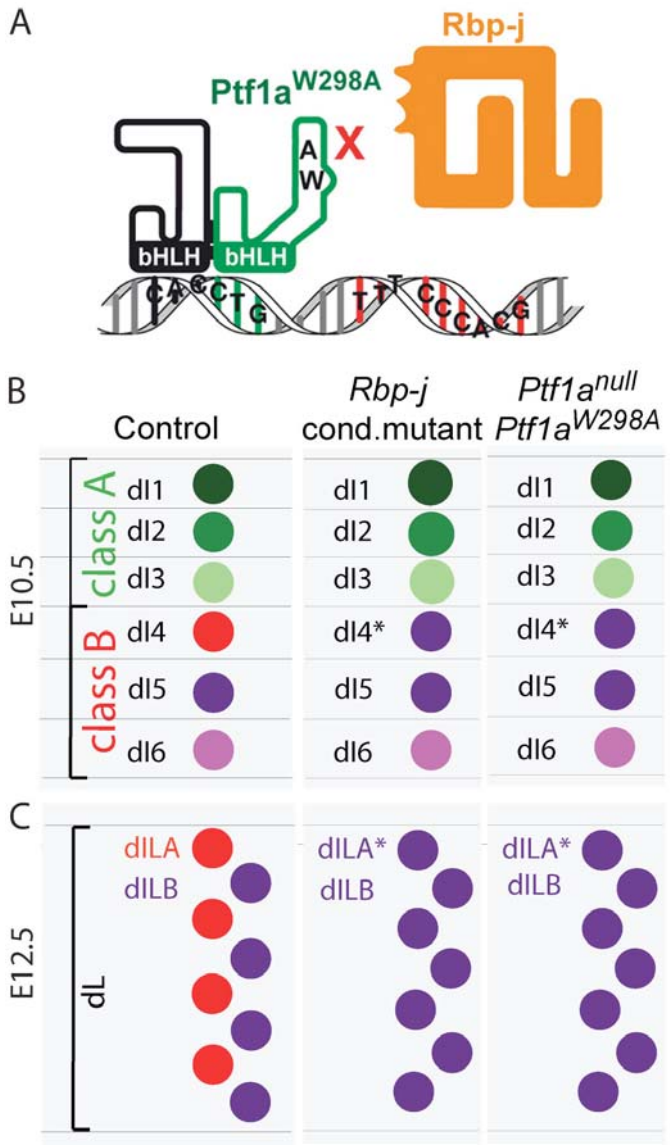

Figure 4.1 **The Ptf1a-Rbp-j complex is essential for the specification of dI4 and dILA neurons.** (A) Schematic representation of a single amino acid exchange in the Ptf1a protein resulting in the inability of Ptf1a to bind Rbp-j. (B,C) Comparison of phenotypes observed in conditional *Rbp-j*, *Ptf1a* null and *Ptf1a*^{W298A} mutant mice in the dorsal spinal cord during the early (B) and the late (C) neurogenic waves. *Rbp-j* mutation mimics phenotypes observed in *Ptf1a* null and *Ptf1a*^{W298A} mutant mice showing that Rbp-j functions within the PTF1 complex to specify GABAergic fate. (A) Adopted from (Hori *et al.*, 2008).

Rbp-j or Rbp-l. This complex binds a compound DNA sequence that includes the E-box and a TC-box, the latter representing a consensus Rbp-j binding site (Beres *et al.*, 2006). Previous studies showed that mutation of *Ptf1a/p48* causes the loss of GABAergic neurons in the dorsal spinal cord. Ptf1a/p48 is expressed in a strictly defined domain in the dorsal spinal cord and hindbrain. Cells expressing this protein give rise to dI4 and dILA neurons (Glasgow *et al.*, 2005). The phenotype observed in either *Pax3*^{Cre}*;Rbp-j*$^{flox/flox}$ or *Pax7*^{CreERT2}*;Rbp-j*$^{\Delta/flox}$ mutant mice mimics the one observed in *Ptf1a* null mutant mice. This suggests that in the dorsal spinal cord a Ptf1a-Rbp-j complex might be essential for the specification of GABAergic neurons. In Jane Johnson's and Raymond MacDonald's laboratories, *Ptf1a*^{W298A} mutant mice were generated and

analyzed. The *Ptf1a*^{W298A} allele encodes a Ptf1a variant with a single amino acid exchange that precludes binding of Rbp-j to Ptf1a (Figure 4.1 A). In these mutant mice, dI4 and dILA neurons were not generated. Thus, a transcription complex containing Ptf1a and Rbp-j is responsible *in vivo* for determining the fate of inhibitory neurons. Moreover, in *Ptf1a* null, *Ptf1a*^{W298A} and conditional *Rbp-j* mutants, the absence of dI4 and dILA neurons was accompanied by an increase in the dI5 and dILB populations (Figure 4.1 B,C). Available evidence indicates that in the early phase of neurogenesis Ptf1a/p48 acts mainly as a suppressor and allows the generation of inhibitory neurons by suppressing the excitatory fate (Hori *et al.*, 2008).

Human mutations in PTF1A support the conclusion that the functional complex requires PTF1A-RBP-J protein-protein interactions. These mutations result in a C-terminal truncated PTF1A and cause pancreatic agenesis and cerebellar hypoplasia (Sellick *et al.*, 2004). The mutant variant lacks the sequence, which is essential for Rbp-j binding in the mouse. The truncated human PTF1A can still form heterodimers with an E-protein, but no longer heterotrimers with Rbp-j or Rbp-l (Beres *et al.*, 2006).

In conclusion, the comparison of the phenotypes obtained in the dorsal spinal cord by: (i) conditional mutation of *Rbp-j*, (ii) inhibition of Notch signaling through dnMaml expression, and (iii) mutation of *Ptf1a/p48* demonstrated that the dramatic effect on the specification of GABAergic neurons reflects a Notch-independent role of Rbp-j in a complex with Ptf1a. Thus, Rbp-j plays two distinct roles in the dorsal spinal cord: it functions in the maintenance of neuronal progenitors as a component of the Notch pathway, i.e. in the complex with NICD and Maml-1, as well as in the neuronal specification in the complex with Ptf1a (Figure 4.2).

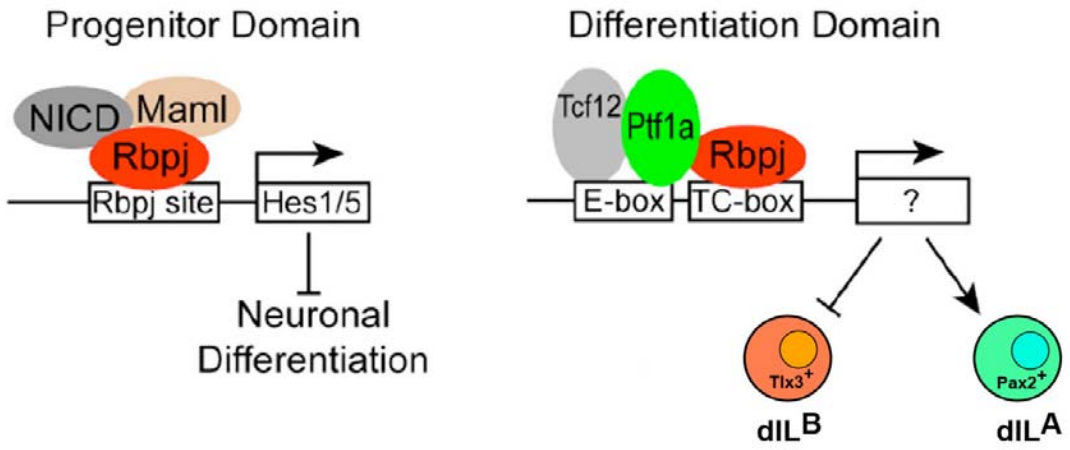

Figure 4.2 **Distinct functions of the two independent Rbp-j containing transcription complexes.** Diagram depicting the two Rbp-j containing complexes. Rbp-j with the Notch intracellular domain (NICD) and Maml-1 enhance expression of Hes1 and Hes5, which in turn inhibit neuronal differentiation and maintain the progenitor domain. The PTF1 transcription factor complex determines neuronal identity by inducing GABAergic specific genes (Pax2) and suppressing glutamatergic specific genes (Tlx3). Adopted from (Hori *et al.*, 2008).

The function of Rbp-j in the PTF1 complex is unusual and does not preclude that Notch signaling can affect asymmetric cell divisions. Indeed in the ventral spinal cord, two populations of V2 neurons, V2a and V2b, are generated from a genetically identical progenitor domain apparently by asymmetric cell division, which appears to be controlled by Notch. In *Presenilin1* mutant mice, where activation of Notch signaling is reduced, the number of V2a neurons was increased and this was accompanied by complete absence of V2b neurons. This study also demonstrated, using chick *in ovo* electroporation, that the Notch ligand Dll4 but not Dll1 was required for the promotion of the V2b cell fate. Additionally, overexpression of Notch intracellular domain and dominant negative variant of Mastermind-like 1 provided evidence that activated Notch acts cell-autonomously to specify V2b neurons and for that the function of Mastermind-like 1 is required. Thus, this study showed clearly that Notch signaling is important for the fate choice between V2a and V2b neurons (Peng *et al.*, 2007).

In parallel to my work, another group analyzed the function of Notch in the dorsal spinal cord. This work relied on the use of *Presenilin1* and hypomorph *Dll1* mutant mice, and described minor changes, i.e. a reduced number of dILB neurons at E12.5. The authors therefore proposed as a model that activation of the Notch pathway promotes the dILB fate (Mizuguchi *et al.*, 2006). This is in strong contrast to my

observation that Rbp-j promotes the dILA fate. It is possible that the small change observed by this group reflects the function of Notch in progenitor maintenance. It should be remembered that the proportion of dILA to dILB neurons changes slightly as neurogenesis proceeds, i.e. at E11.5 the ratio of dILA/dILB is 1.3, at E12.5 the ratio is 0.7, and at E13.5 the ratio is 0.9 (Wildner *et al.*, 2006). Small changes in the proportion of dILA/dILB neurons generated could therefore also reflect differences in the stage of neurogenesis, like the proportions of progenitor divisions that generate again progenitor cells, that are expected to be affected in *Presenilin1* and hypomorph *Dll1* mutant mice.

4.1.2 . Evolution of the Notch-independent Rbp-j function

The structure of Rbp-j is highly conserved. The amino acid sequences of fly and mouse Rbp-j proteins are in 75% identical. In the central 248 residues, which include the DNA binding domain, the identity is even higher and reaches 93%. This level of structural conservation is unusual for transcription factors, and has only been found in Rbp-j and in homeodomain proteins (Honjo, 1996). Not only the structure of Rbp-j is highly conserved, but also the DNA binding specificity is identical in vertebrates and invertebrates, suggesting that Rbp-j plays a very fundamental role in living organisms. Indeed, Rbp-j functions within the Notch pathway and controls many developmental processes, as evident from work done in *Caenorhabditis elegans*, *Drosophila melanogaster*, mice and humans.

However, Rbp-j is not only found in animals, but homologous proteins are also present in fungal species. This puts the origin of the Rbp-j family even further back in evolution, to a beginning that is currently not understood. Interestingly, the Notch receptor, its ligands and co-activators do not exist in fungi. This suggests that the ancestral function of Rbp-j is a Notch-independent regulation of transcription (Prevorovsky *et al.*, 2007). Thus, the function of Rbp-j in a complex with Ptf1a discussed in this thesis might reflect such an ancient role. Interestingly, a trimeric PTF1 complex does not only exist in mammals; an orthologous complex has also been found in flies. *Drosophila melanogaster* has a Ptf1a ortholog (Fer1) that can form a complex with *Drosophila* E-proteins and dRbp-j. Remarkably, the conservation is so great that mixed complexes of *Drosophila* and mammalian subunits are functional. Interestingly,

the Ptf1a ortholog (Fer1) expression is restricted to the fly nervous system (Masui *et al.*, 2007). Thus, the function of the PTF1 complex in the nervous system development might date back in evolution further than the vertebrate/invertebrate branch point.

There are five mouse Rbp-j-related genes, whose sequences are identical or highly homologous to that of *Rbp-j*. One encodes the functional *Rbp-j* gene and contains 11 exons scattered over 50 kb. Three of the five genes are apparently pseudogenes of the processed type, because they contain the entire coding sequence on one exon and scattered stop codons in the sequences (Honjo, 1996). The fifth gene is not a pseudogene and encodes an Rbp-j-related protein, Rbp-l. This protein exhibits 48% overall identity to Rbp-j and binds to a DNA sequence that is almost identical to that of Rbp-j. The striking feature of the Rbp-l protein is its inability to associate with any of known Notch intracellular domains (Minoguchi *et al.*, 1997). Thus, during evolution of metazoans, the *Rbp-j* gene was probably duplicated. Orthologs of *Rbp-l* are found only in vertebrates, for instance in *Danio rerio* and *Gallus gallus*. Therefore, the duplication likely occurred in an ancestor common to all vertebrates, and gave rise to the *Rbp-l* and *Rbp-j* genes, which subsequently diverged quickly. Apparently, during further evolution, the *Rbp-l* gene product lost its ability to bind Notch. Interestingly, the ability to interact with Ptf1a was conserved, and both Rbp-j and Rbp-l are functional components of the PTF1 complex in mice. In the pancreas, PTF1 complexes that contain Rbp-j or Rbp-l can be observed. Rbp-j is an essential component of the PTF1 complex in the early development of pancreas, and is later gradually replaced by Rbp-l. Rbp-j uses the same interaction domain for binding to NICD and Ptf1a, and NICD and Ptf1a compete with each other for Rbp-j binding (Beres *et al.*, 2006; Masui *et al.*, 2007). Therefore, the developmental transition in the PTF1 complex, in which Rbp-j is exchanged by Rbp-l, may serve to separate the PTF1 function from Notch signaling. During the development of the dorsal spinal cord only Rbp-j is present. Thus, a competition between NICD and Ptf1a for Rbp-j binding could also be possible in the dorsal spinal cord, i.e. an antagonism between NICD-Rbp-j and Ptf1a-Rbp-j complexes could exist, which might have functional implications.

4.2 . The Olig3 function in the dorsal hindbrain

In the second part of my thesis I analyzed the role of the bHLH factor Olig3 in the development of the dorsal hindbrain. Olig3 is a member of the bHLH family of transcription factors. Some members of this family possess proneural activity and participate in the determination of neuronal fates. Olig3 is expressed in the dorsal ventricular zone of the alar plate of the hindbrain. Olig3+ progenitors give rise to class A neurons of the dorsal hindbrain. To analyze the derivatives of Olig3+ cells, I used genetic lineage tracing and demonstrated that Olig3+ cells give rise to noradrenergic neurons of the nucleus of the solitary tract and to neurons of precerebellar nuclei. As a consequence of *Olig3* mutation, the nucleus of the solitary tract did not form, and precerebellar nuclei, such as the inferior olivary nucleus, were absent or reduced in size.

4.2.1 . Derivatives of the Olig3+ progenitor domain

Olig3 is expressed in the ventricular zone of the dorsal alar plate of the hindbrain. In order to follow the fate of the Olig3+ cells, I generated two knock-in Cre lines in which Cre is expressed under the control of the *Olig3* locus: $Olig3^{CrepA}$ and $Olig3^{CreERT2}$. Astonishingly, the β-galactosidase expression domain observed in reporter mice, in which recombination was induced by $Olig3^{CrepA}$, was broader than expected. Thus, Olig3 might have a broader expression during early development than it was previously realized, or the mutant allele allows ectopic Cre expression. Because of this “ectopic” recombination induced by $Olig3^{CrepA}$, I used only the $Olig3^{CreERT2}$ allele for further studies. In addition, this allele provided the possibility to control recombination temporally. This is a second example where I successfully used tamoxifen-inducible variants of Cre.

Using $Olig3^{CreERT2}$ for genetic fate mapping, I showed that Olig3+ cells generate four and three neuronal subtypes in rhombomere 7 and rhombomeres 4-6, respectively. Neurons that arise from Olig3+ cells are denoted as class A neurons, i.e. dA1-4 neurons in rhombomere 7, and dA1, dA3 and dA4 neurons in rhombomeres 4-6. My data together with other previously published studies establish now firmly the origin and fate of many of these neurons. dA1 neurons are produced in all rhombomeres and give rise

to mossy fiber neurons in some precerebellar nuclei like external cuneate, lateral reticular, pontine gray and reticulotegmental nuclei. In addition, they are destined to become neurons of the cerebellum, in particular external granule layer neurons and deep cerebellar nuclei (Bermingham *et al.*, 2001; Li *et al.*, 2004; Landsberg *et al.*, 2005; Machold and Fishell, 2005; Wang *et al.*, 2005). The second population arising further ventrally is denoted as the dA2 neuronal subtype and is only produced in rhombomere 7. The fate of this population is poorly understood, mainly because of the absence of good markers that would make it possible to follow them during migration in subsequent development. Lhx1/5, the only factors dA2 neurons are known to express, are also present in many other neuronal types in the hindbrain. Indirect evidence indicates that dA2 neurons generate the cuneate nucleus. The dA3 neurons arise in rhombomeres 4-7 and give rise to the viscerosensory neurons of the nucleus of the solitary tract and to neurons of the area postrema (Qian *et al.*, 2001; Dauger *et al.*, 2003; Pattyn *et al.*, 2006). The fourth class A population, dA4 neurons, is characterized by the expression of Foxd3 in rhombomere 7. The dA4 neurons, born in rhombomere 7, give rise to climbing fiber neurons of the inferior olivary nucleus (Yamada *et al.*, 2007). dA4 neurons are also generated in rhombomeres 4-6, but these do not express Foxd3, and their fate remains unclear.

4.2.2 . The function of Olig3, Ptf1a and Lbx1 in the determination of dorsal neuron types

In the dorsal spinal cord and hindbrain, Ptf1a is expressed in a ventricular zone that gives rise to Lbx1+/Pax2+ inhibitory and dA4 climbing fiber excitatory neurons of the inferior olivary nucleus. Ptf1a is essential to determine the fate of both neuronal types (Yamada *et al.*, 2007). The precursor domain of the Foxd3+ dA4 neurons also expresses, in addition to Ptf1a, Olig3. Because Olig3 and Ptf1a are both essential for these neurons, I investigated a possible interaction between the two proteins and co-electroporated both Ptf1a and Olig3 expression vectors in the chick hindbrain. Indeed, this led to an induction of Foxd3, a molecular characteristic of dA4 climbing fiber neurons. Ectopic Foxd3+ neurons were not observed close to the floor and roof plate, indicating that Ptf1a and Olig3 act in a context-dependent manner. Thus, Ptf1a and Olig3 are both important for fate determination of climbing fiber neurons, and they

appear to cooperate in this process. However, when I electroporated Olig3 only, I observed a suppression of Ptf1a, which is in apparent contradiction to a cooperative function of the two factors *in vivo*. Detailed analysis of the Olig3+/Ptf1a+ progenitor domain revealed that Olig3 is expressed in Ki67-negative cells located laterally to the ventricular zone that appears to generate dA4 neurons. This indicated that Olig3 was transiently expressed in dA4 progenitors that exited the cell cycle and differentiated. Ptf1a was more broadly expressed in this domain, and only few cells co-expressed Ptf1a and Olig3. Thus, onset of Ptf1a and Olig3 expression appears to occur in distinct phases of the cell cycle, and results in a transient co-expression of these two factors in normal development. Distinct time courses of Ptf1a and Olig3 expression could reconcile the loss and gain-of-function data.

A further neuronal population that was absent in *Olig3* mutant mice were dA3 neurons, which generate the viscerosensory neurons of the nucleus of the solitary tract and the area postrema. At the expense of dA4 and dA3 neurons, ectopic Lbx1 neurons appeared in *Olig3* mutants. On the other hand, overexpression of Olig3 in chick neural tubes caused a downregulation of Lbx1 expression. Therefore, an important and maybe the only function of Olig3 in the specification of class A neurons is the suppression of Lbx1. If this were the case, the altered fate determination of dA3 and dA4 neurons in *Olig3* mutant mice should be reverted by the additional mutation of *Lbx1*. Analysis of *Olig3/Lbx1* double mutant mice demonstrated that this was indeed the case for dA4, but not dA3 neurons. Thus, Olig3 and Ptf1a together induce the dA4 fate, but the primary role of Olig3 in this process is the suppression of Lbx1. However, in the specification of the dA3 neuronal fate, Olig3 does probably more than merely suppressing Lbx1.

To further analyze the interaction between Olig3 and Ptf1a, I generated *Olig3/Ptf1a* double mutants. In these mutants, an unusual dA3 neuron type, to which I refer as dA3*, was generated. The dA3* neurons expressed Tlx3 but not Phox2b, indicating that Tlx3 but not Phox2b expression was rescued in the *Olig3/Ptf1a* double mutants. Thus, Olig3 has additionally an instructive role in the specification of dA3 neurons, i.e. it provides information that allows induction of Phox2b expression. This role might be fulfilled by cooperation with another factor, for instance Ascl1, which is expressed in the progenitor domain generating dA3 neurons. Results obtained in the dorsal spinal cord could support such a notion, since a cooperative function of Ascl1 and Olig3 in the

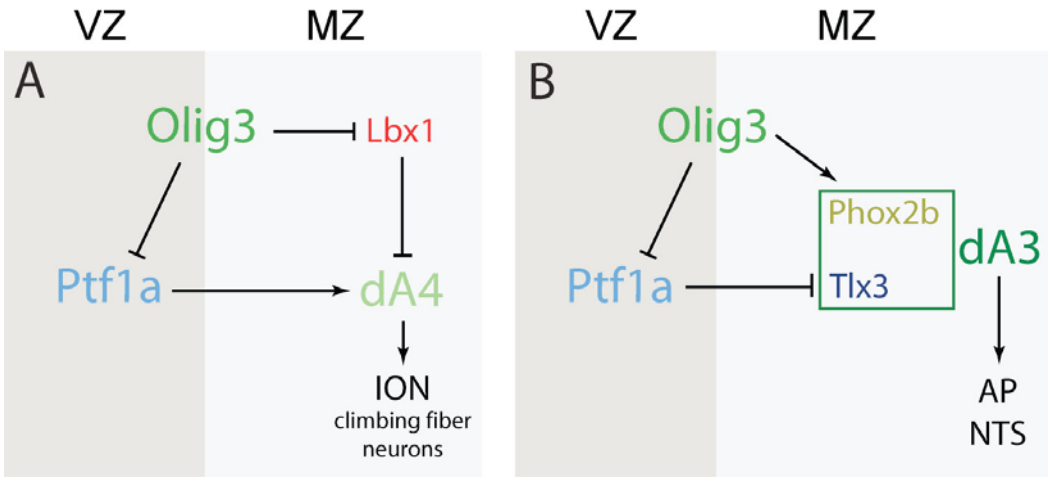

***Figure 4.3* Model of Olig3 functions in fate determination of dA3 and dA4 neurons.** (A) Olig3 and Ptf1a cooperate to induce the dA4 fate and Olig3 exerts its function primarily by suppressing Lbx1; dA4 neurons give rise to climbing fiber neurons of the inferior olivary nucleus (ION); it should be noted that in normal development Olig3 and Ptf1a are only transiently co-expressed in cells that locate to the border of the ventricular zone (VZ) and mantle zone (MZ). (B) Olig3 suppresses Ptf1a and this allows the induction of Tlx3 expression in the dA3 neurons; Olig3 plays an instructive role in the induction of Phox2b expression in the dA3 fate. dA3 neurons give rise to neurons of the area postrema (AP) and to the nucleus of the solitary tract (NTS).

determination of the dI3 neuronal fate was indeed observed previously (Muller *et al.*, 2005). It would be interesting to test if this cooperation is also present in the hindbrain.

In conclusion, my data show that Olig3 acts in the specification of climbing fiber neurons of the inferior olivary nucleus (dA4 neurons) by suppressing Lbx1 expression (Figure 4.3 A). Moreover, the role of Olig3 in the specification of dA3 neurons is dual: (i) it suppresses Lbx1 as well as Ptf1a and (ii) it might have an instructive role in the induction of Phox2b expression (Figure 4.3 B).

4.2.3 . A similar role of Olig3 in the dorsal spinal cord and hindbrain

It is interesting to see that neurons with similar molecular characteristics are generated in columns that span the spinal cord and reach into the hindbrain. This indicates that similarities exist in the mechanisms that determine neuronal fates in the two units. In particular, Olig3 marks the dorsal ventricular zone in both units, and a dorsal expansion of Lbx1 expression was observed in the spinal cord and hindbrain of *Olig3* mutant

mice. Furthermore, in the spinal cord and hindbrain of the chick, ectopic expression of Olig3 suppresses the emergence of Lbx1+ neurons. Thus, several aspects of Olig3 function are conserved in the spinal cord and hindbrain. However, many differences exist between the hindbrain and the spinal cord. For instance, in the hindbrain the complexity of neuronal types generated is higher than the one observed in the spinal cord. Olig3 is essential for the specification of four neuronal subtypes in rhombomere 7 but for the specification of three neuronal subtypes in the spinal cord. Moreover, hindbrain and spinal cord neurons often have distinct functions, and subtle differences in the expression of molecular markers are observed. For instance, the Olig3 and Ptf1a interaction is essential for the specification of dA4 hindbrain neurons. This interaction is unique for the hindbrain and a progenitor domain that co-expresses Ptf1a and Olig3 does not exist in the spinal cord. Moreover, Foxd3+ dA4 neurons exist only in rhombomere 7. The differences between neuron types generated in the spinal cord and hindbrain, and even the differences observed between the rhombomeres could be caused by the distinct expression of *Hox* genes in these units of the nervous system.

4.2.4 . Major function of Olig3 in the specification of neuronal types

Olig genes encode a subclass of neuronal bHLH transcription factors. In the mouse, there are three *Olig* genes and two of them, *Olig1* and *Olig2*, are specifically expressed in the progenitor domain of the ventral spinal cord that generates motor neurons and oligodendrocytes. Extensive studies showed that prior to generation of oligodendrocytes, the domain of Olig2 expression corresponds to the progenitor domain that generates motor neurons. Gain-of-function experiments suggest that Olig2 initiates motor neuron differentiation and cell cycle arrest, in part by promoting expression of proneural factors such as Ngn2 (Zhou and Anderson, 2002). Thus, Olig2 possesses proneural properties and additionally plays a key role in specifying the subtype identity. In opposite to Olig1 and Olig2 factors, Olig3 is expressed in a distinct region of the spinal cord and has different functions. Studies done on *Olig3* mutant mice in the dorsal spinal cord showed that the major function of Olig3 is the specification of class A neurons and that the mouse Olig3 factor does not exhibit a strong proneural function like other bHLH factors. Similar results were obtained from the analysis of Olig3 functions in the dorsal hindbrain presented here, i.e. the major effect of the *Olig3*

mutation was an aberrant specification of class A neurons. However, microarray analysis of *Olig3* mutant mice in the spinal cord revealed changes in expression levels of some factors implicated in cell cycle control and neural differentiation such as Zic1 transcription factor (unpublished data of my thesis work). Loss- and gain-of-function mutations showed that Zic1 inhibits neuronal differentiation and instead increases numbers of neural precursors in the dorsal spinal cord (Aruga *et al.*, 2002). It is possible that Olig3 suppresses the expression of genes like *Zic1*, which in turn regulate the expression of proneural factors such as Math1 and Ngn2. However, available evidence indicates that the major function of Olig3 is to control the correct determination of class A neuronal fates in the dorsal spinal cord and hindbrain.

5. Summary

Correct function of neural networks depends on a balance of inhibitory and excitatory activity. The balance is initially generated through the determination of inhibitory and excitatory neuronal fates controlled by transcription factors.

A first goal in my thesis was to define if Notch, which controls asymmetric divisions in other systems, plays a role in the determination of inhibitory and excitatory fates in the dorsal spinal cord. To address this, I employed genetic analysis in mice and used two transgenic mouse models. In the first, a dominant-negative variant of Mastermind-like1 (dnMaml) was expressed in an inducible manner, which inhibits the transcriptional response to Notch signaling. In the second, I employed conditional mutagenesis of *Rbp-j*, the major transcriptional mediator of the Notch pathway. In *Rbp-j* and dnMaml mutant mice, I observed a depletion of the progenitor domain in the dorsal spinal cord, consistent with the known function of Notch signaling in the maintenance of neuronal progenitors. I also found that the GABAergic neurons were not formed in *Rbp-j* mutant mice, but this effect was not observable in the dnMaml mutants. Independent studies in Jane Johnson's laboratory described a similar function for the bHLH factor Ptf1a, which is a component of the PTF1 transcriptional complex. My results together with those of Jane Johnson indicate that Rbp-j functions independently of Notch in this PTF1 complex.

A second goal was the analysis of the bHLH transcription factor Olig3 that is expressed in the ventricular zone of the dorsal alar plate of the hindbrain. For this, I generated two new mouse strains, *Olig3*^{Cre} and *Olig3*^{CreERT2}, and used these for genetic fate mapping. I found that the Olig3+ progenitor domain gives rise to several neuronal types in the dorsal alar plate of the hindbrain, which contribute to the nucleus of the solitary tract and to precerebellar nuclei. In *Olig3* mutant mice, the nucleus of the solitary tract did not form, and precerebellar nuclei were absent or smaller. My further work that relies on overexpression experiments in the chick hindbrain showed that Olig3 and Ptf1a together induce the fate of climbing fiber neurons of the inferior olivary nucleus. However, analysis of *Olig3/Lbx1* double mutant mice demonstrated that Olig3 exerts its role solely by suppressing Lbx1 in specification of climbing fiber neurons. In contrast,

analysis of *Olig3/Ptf1a* double mutant mice revealed that Olig3 has an instructive role in the determination of noradrenergic neurons of the nucleus of the solitary tract.

Zusammenfassung

Die korrekte Funktion neuronaler Netzwerke beruht auf einem Gleichgewicht zwischen hemmenden und aktivierenden Impulsen. Dieses Gleichgewicht wird *ab initio* durch Transkriptionsfaktoren hergestellt, die den inhibitorischen bzw. exzitatorischen Charakter neuronaler Zellen festlegen.

Als erstes Ziel meiner Promotionsarbeit habe ich im Modellorganismus Maus untersucht, ob der Notch-Rezeptor, der in anderen Systemen asymmetrische Zellteilung steuert, diese Funktion auch bei der Determinierung hemmender und aktivierender Neurone im dorsalen Rückenmark ausübt. In der ersten von zwei verwendeten transgenen Mauslinien wurde eine dominant-negative Variante von Mastermind-like1 (dnMaml) induzierbar exprimiert, um so die Notch-abhängige transkriptionelle Aktivierung zu hemmen. In der zweiten Mauslinie wurde *Rbp-j*, der wichtigste Transkriptionsfaktor im Notch-Signalweg, konditionell mutiert. In beiden Mauslinien fand ich, in Übereinstimmung mit der beschriebenen Rolle von Notch bei der Erhaltung von Vorläuferzellen, eine Minderung der Vorläuferdomäne im dorsalen Rückenmark. GABAerge Neurone fehlten in den *Rbp-j*-, nicht jedoch in den dnMaml-Mäusen. Unabhängige Untersuchungen aus dem Labor von Jane Johnson zeigten eine ähnliche Funktion für den bHLH Transkriptionsfaktor Ptf1a, einen Bestandteil des PTF1 Transkriptionsfaktorkomplexes. Zusammengenommen deuten diese Ergebnisse darauf hin, daß Rbp-j eine Notch-unabhängige Funktion im PTF1-Komplex ausübt.

Ein zweites Ziel meiner Dissertation war die Analyse des bHLH Transkriptionsfaktors Olig3, der in der Ventrikulärzone der dorsalen Alarplatte des Rhombenzephalon exprimiert wird. Ich habe dafür zwei neue Mauslinien etabliert, $Olig3^{Cre}$ und $Olig3^{CreERT2}$, die ich zur genetischen Zellschicksalsanalyse eingesetzt habe. Ich fand, daß die Olig3+ Vorläuferdomäne verschiedene Neuronentypen in der dorsalen Alarplatte des Rhombenzephalon hervorbringt, die zum Nucleus solitarius und zu präzerebellaren Kernen beitragen. In *Olig3* mutanten Mäusen wurde der Nucleus

solitarius nicht gebildet, die präzerebellaren Kerne waren reduziert oder fehlten. Weiterführende Arbeiten im Hühnchen zeigten, daß Olig3 und Ptf1a zusammen die Kletterfasern des Nucleus olivarius inferior induzieren. Die Analyse dieser Fasern in *Olig3/Lbx1* Maus-Doppelmutanten ergab, daß Olig3 hier auschließlich über die Unterdrückung von Lbx1 wirkt. In *Olig3/Ptf1a* Doppelmutanten hat Olig3 hingegen eine aktive Rolle in der Determinierung noradrenerger Neurone des Tractus solitarius.

6 . Bibliography

Altman, J. and Bayer, S. A. (1980). Development of the brain stem in the rat. I. Thymidine-radiographic study of the time of origin of neurons of the lower medulla. *J Comp Neurol* **194**, 1-35.

Altman, J. and Bayer, S. A. (1987a). Development of the precerebellar nuclei in the rat: I. The precerebellar neuroepithelium of the rhombencephalon. *J Comp Neurol* **257**, 477-89.

Altman, J. and Bayer, S. A. (1987b). Development of the precerebellar nuclei in the rat: II. The intramural olivary migratory stream and the neurogenetic organization of the inferior olive. *J Comp Neurol* **257**, 490-512.

Alvarez-Medina, R., Cayuso, J., Okubo, T., Takada, S. and Marti, E. (2008). Wnt canonical pathway restricts graded Shh/Gli patterning activity through the regulation of Gli3 expression. *Development* **135**, 237-47.

Arnett, H. A., Fancy, S. P., Alberta, J. A., Zhao, C., Plant, S. R., Kaing, S., Raine, C. S., Rowitch, D. H., Franklin, R. J. and Stiles, C. D. (2004). bHLH transcription factor Olig1 is required to repair demyelinated lesions in the CNS. *Science* **306**, 2111-5.

Aruga, J., Tohmonda, T., Homma, S. and Mikoshiba, K. (2002). Zic1 promotes the expansion of dorsal neural progenitors in spinal cord by inhibiting neuronal differentiation. *Dev Biol* **244**, 329-41.

Beres, T. M., Masui, T., Swift, G. H., Shi, L., Henke, R. M. and MacDonald, R. J. (2006). PTF1 is an organ-specific and Notch-independent basic helix-loop-helix complex containing the mammalian Suppressor of Hairless (RBP-J) or its paralogue, RBP-L. *Mol Cell Biol* **26**, 117-30.

Bermingham, N. A., Hassan, B. A., Wang, V. Y., Fernandez, M., Banfi, S., Bellen, H. J., Fritzsch, B. and Zoghbi, H. Y. (2001). Proprioceptor pathway development is dependent on Math1. *Neuron* **30**, 411-22.

Birnboim, H. C. and Doly, J. (1979). A rapid alkaline extraction procedure for screening recombinant plasmid DNA. *Nucleic Acids Res* **7**, 1513-23.

Bradley, A. and Robertson, E. (1986). Embryo-derived stem cells: a tool for elucidating the developmental genetics of the mouse. *Curr Top Dev Biol* **20**, 357-71.

Bröhl, D., Strehle, M., Wende, H., Hori, K., Bormuth, I., Nave, K. A., Muller, T. and Birchmeier, C. (2008). A transcriptional network coordinately determines transmitter and peptidergic fate in the dorsal spinal cord. *Dev Biol* **322**, 381-93.

Byun, J., Verardo, M. R., Sumengen, B., Lewis, G. P., Manjunath, B. S. and Fisher, S. K. (2006). Automated tool for the detection of cell nuclei in digital microscopic images: application to retinal images. *Mol Vis* **12**, 949-60.

Cayouette, M. and Raff, M. (2002). Asymmetric segregation of Numb: a mechanism for neural specification from Drosophila to mammals. *Nat Neurosci* **5**, 1265-9.

Cheng, L., Arata, A., Mizuguchi, R., Qian, Y., Karunaratne, A., Gray, P. A., Arata, S., Shirasawa, S., Bouchard, M., Luo, P., Chen, C. L., Busslinger, M., Goulding, M., Onimaru, H. and Ma, Q. (2004). Tlx3 and Tlx1 are post-mitotic selector genes determining glutamatergic over GABAergic cell fates. *Nat Neurosci* **7**, 510-7.

Chenn, A. and McConnell, S. K. (1995). Cleavage orientation and the asymmetric inheritance of Notch1 immunoreactivity in mammalian neurogenesis. *Cell* **82**, 631-41.

Chesnutt, C., Burrus, L. W., Brown, A. M. and Niswander, L. (2004). Coordinate regulation of neural tube patterning and proliferation by TGFbeta and WNT activity. *Dev Biol* **274**, 334-47.

Chizhikov, V. V. and Millen, K. J. (2004). Control of roof plate development and signaling by Lmx1b in the caudal vertebrate CNS. *J Neurosci* **24**, 5694-703.

Chizhikov, V. V. and Millen, K. J. (2005). Roof plate-dependent patterning of the vertebrate dorsal central nervous system. *Dev Biol* **277**, 287-95.

Dauger, S., Pattyn, A., Lofaso, F., Gaultier, C., Goridis, C., Gallego, J. and Brunet, J. F. (2003). Phox2b controls the development of peripheral chemoreceptors and afferent visceral pathways. *Development* **130**, 6635-42.

de la Pompa, J. L., Wakeham, A., Correia, K. M., Samper, E., Brown, S., Aguilera, R. J., Nakano, T., Honjo, T., Mak, T. W., Rossant, J. and Conlon, R. A. (1997). Conservation of the Notch signalling pathway in mammalian neurogenesis. *Development* **124**, 1139-48.

Dessaud, E., McMahon, A. P. and Briscoe, J. (2008). Pattern formation in the vertebrate neural tube: a sonic hedgehog morphogen-regulated transcriptional network. *Development* **135**, 2489-503.

Ding, L., Takebayashi, H., Watanabe, K., Ohtsuki, T., Tanaka, K. F., Nabeshima, Y., Chisaka, O., Ikenaka, K. and Ono, K. (2005). Short-term lineage analysis of dorsally derived Olig3 cells in the developing spinal cord. *Dev Dyn* **234**, 622-32.

Dullin, J. P., Locker, M., Robach, M., Henningfeld, K. A., Parain, K., Afelik, S., Pieler, T. and Perron, M. (2007). Ptf1a triggers GABAergic neuronal cell fates in the retina. *BMC Dev Biol* **7**, 110.

Engleka, K. A., Gitler, A. D., Zhang, M., Zhou, D. D., High, F. A. and Epstein, J. A. (2005). Insertion of Cre into the Pax3 locus creates a new allele of Splotch and identifies unexpected Pax3 derivatives. *Dev Biol* **280**, 396-406.

Farley, F. W., Soriano, P., Steffen, L. S. and Dymecki, S. M. (2000). Widespread recombinase expression using FLPeR (flipper) mice. *Genesis* **28**, 106-10.

Glasgow, S. M., Henke, R. M., Macdonald, R. J., Wright, C. V. and Johnson, J. E. (2005). Ptf1a determines GABAergic over glutamatergic neuronal cell fate in the spinal cord dorsal horn. *Development* **132**, 5461-9.

Gowan, K., Helms, A. W., Hunsaker, T. L., Collisson, T., Ebert, P. J., Odom, R. and Johnson, J. E. (2001). Crossinhibitory activities of Ngn1 and Math1 allow specification of distinct dorsal interneurons. *Neuron* **31**, 219-32.

Gross, M. K., Dottori, M. and Goulding, M. (2002). Lbx1 specifies somatosensory association interneurons in the dorsal spinal cord. *Neuron* **34**, 535-49.

Hamburger and Hamilton (1951). A series of normal stages in the development of the chick embryo. *Journal of Morphology* **88**, 49.

Helms, A. W. and Johnson, J. E. (1998). Progenitors of dorsal commissural interneurons are defined by MATH1 expression. *Development* **125**, 919-28.

Helms, A. W. and Johnson, J. E. (2003). Specification of dorsal spinal cord interneurons. *Curr Opin Neurobiol* **13**, 42-9.

Hippenmeyer, S., Vrieseling, E., Sigrist, M., Portmann, T., Laengle, C., Ladle, D. R. and Arber, S. (2005). A developmental switch in the response of DRG neurons to ETS transcription factor signaling. *PLoS Biol* **3**, e159.

Honjo, T. (1996). The shortest path from the surface to the nucleus: RBP-J kappa/Su(H) transcription factor. *Genes Cells* **1**, 1-9.

Hooper, M., Hardy, K., Handyside, A., Hunter, S. and Monk, M. (1987). HPRT-deficient (Lesch-Nyhan) mouse embryos derived from germline colonization by cultured cells. *Nature* **326**, 292-5.

Hori, K., Cholewa-Waclaw, J., Nakada, Y., Glasgow, S. M., Masui, T., Henke, R. M., Wildner, H., Martarelli, B., Beres, T. M., Epstein, J. A., Magnuson, M. A., Macdonald, R. J., Birchmeier, C. and Johnson, J. E. (2008). A nonclassical bHLH Rbpj transcription factor complex is required for specification of GABAergic neurons independent of Notch signaling. *Genes Dev* **22**, 166-78.

Hoshino, M., Nakamura, S., Mori, K., Kawauchi, T., Terao, M., Nishimura, Y. V., Fukuda, A., Fuse, T., Matsuo, N., Sone, M., Watanabe, M., Bito, H., Terashima, T., Wright, C. V., Kawaguchi, Y., Nakao, K. and Nabeshima, Y. (2005). Ptf1a, a bHLH

transcriptional gene, defines GABAergic neuronal fates in cerebellum. *Neuron* **47**, 201-13.

Huang, M., Huang, T., Xiang, Y., Xie, Z., Chen, Y., Yan, R., Xu, J. and Cheng, L. (2008). Ptf1a, Lbx1 and Pax2 coordinate glycinergic and peptidergic transmitter phenotypes in dorsal spinal inhibitory neurons. *Dev Biol* **322**, 394-405.

Innis, Gelfand, Sninsky. (1989). PCR Protocols: A Guide To Methods And Applications. **Academic Press, San Diego, CA 92101-4495, USA**, pp. 482.

Inoue, H., Nojima, H. and Okayama, H. (1990). High efficiency transformation of Escherichia coli with plasmids. *Gene* **96**, 23-8.

Jerpseth, J. (1992). XL1-Blue MRF' E. coli cells: McrA-, McrCB-, McrF-, Mrr-, HsdR- derivative of XL1-Blue cells. *Strategies* **6**, 81.

Joyner, A. L. (2002). Establishment of anterior-poterior and dorsal-ventral pattern in the early central nervous system. **in Mouse Development, Academic Press, San Diego, California 92101-4495, USA**, 107-126.

Kadesch, T. (2000). Notch signaling: a dance of proteins changing partners. *Exp Cell Res* **260**, 1-8.

Kageyama, R., Ohtsuka, T., Hatakeyama, J. and Ohsawa, R. (2005). Roles of bHLH genes in neural stem cell differentiation. *Exp Cell Res* **306**, 343-8.

Kageyama, R., Ohtsuka, T., Shimojo, H. and Imayoshi, I. (2008). Dynamic Notch signaling in neural progenitor cells and a revised view of lateral inhibition. *Nat Neurosci* **11**, 1247-51.

Kiecker, C. and Niehrs, C. (2001). A morphogen gradient of Wnt/beta-catenin signalling regulates anteroposterior neural patterning in Xenopus. *Development* **128**, 4189-201.

Kovall, R. A. (2007). Structures of CSL, Notch and Mastermind proteins: piecing together an active transcription complex. *Curr Opin Struct Biol* **17**, 117-27.

Kuhn, R., Rajewsky, K. and Muller, W. (1991). Generation and analysis of interleukin-4 deficient mice. *Science* **254**, 707-10.

Lamb, T. M. and Harland, R. M. (1995). Fibroblast growth factor is a direct neural inducer, which combined with noggin generates anterior-posterior neural pattern. *Development* **121**, 3627-36.

Landsberg, R. L., Awatramani, R. B., Hunter, N. L., Farago, A. F., DiPietrantonio, H. J., Rodriguez, C. I. and Dymecki, S. M. (2005). Hindbrain rhombic lip is comprised of discrete progenitor cell populations allocated by Pax6. *Neuron* **48**, 933-47.

Lee, E. C., Yu, D., Martinez de Velasco, J., Tessarollo, L., Swing, D. A., Court, D. L., Jenkins, N. A. and Copeland, N. G. (2001). A highly efficient Escherichia coli-based chromosome engineering system adapted for recombinogenic targeting and subcloning of BAC DNA. *Genomics* **73**, 56-65.

Lee, K. J., Dietrich, P. and Jessell, T. M. (2000). Genetic ablation reveals that the roof plate is essential for dorsal interneuron specification. *Nature* **403**, 734-40.

Li, S., Qiu, F., Xu, A., Price, S. M. and Xiang, M. (2004). Barhl1 regulates migration and survival of cerebellar granule cells by controlling expression of the neurotrophin-3 gene. *J Neurosci* **24**, 3104-14.

Liem, K. F., Jr., Tremml, G. and Jessell, T. M. (1997). A role for the roof plate and its resident TGFbeta-related proteins in neuronal patterning in the dorsal spinal cord. *Cell* **91**, 127-38.

Liu, B., Liu, Z., Chen, T., Li, H., Qiang, B., Yuan, J., Peng, X. and Qiu, M. (2007). Selective expression of Bhlhb5 in subsets of early-born interneurons and late-born association neurons in the spinal cord. *Dev Dyn* **236**, 829-35.

Liu, J. P., Laufer, E. and Jessell, T. M. (2001). Assigning the positional identity of spinal motor neurons: rostrocaudal patterning of Hox-c expression by FGFs, Gdf11, and retinoids. *Neuron* **32**, 997-1012.

Lobe, C. G., Koop, K. E., Kreppner, W., Lomeli, H., Gertsenstein, M. and Nagy, A. (1999). Z/AP, a double reporter for cre-mediated recombination. *Dev Biol* **208**, 281-92.

Louvi, A. and Artavanis-Tsakonas, S. (2006). Notch signalling in vertebrate neural development. *Nat Rev Neurosci* **7**, 93-102.

Lu, Q. R., Sun, T., Zhu, Z., Ma, N., Garcia, M., Stiles, C. D. and Rowitch, D. H. (2002). Common developmental requirement for Olig function indicates a motor neuron/oligodendrocyte connection. *Cell* **109**, 75-86.

Lupo, G., Harris, W. A. and Lewis, K. E. (2006). Mechanisms of ventral patterning in the vertebrate nervous system. *Nat Rev Neurosci* **7**, 103-14.

Machold, R. and Fishell, G. (2005). Math1 is expressed in temporally discrete pools of cerebellar rhombic-lip neural progenitors. *Neuron* **48**, 17-24.

Maden, M. (2006). Retinoids and spinal cord development. *J Neurobiol* **66**, 726-38.

Masui, T., Long, Q., Beres, T. M., Magnuson, M. A. and MacDonald, R. J. (2007). Early pancreatic development requires the vertebrate Suppressor of Hairless (RBPJ) in the PTF1 bHLH complex. *Genes Dev* **21**, 2629-43.

Millen, K. J., Millonig, J. H. and Hatten, M. E. (2004). Roof plate and dorsal spinal cord dl1 interneuron development in the dreher mutant mouse. *Dev Biol* **270**, 382-92.

Millonig, J. H., Millen, K. J. and Hatten, M. E. (2000). The mouse Dreher gene Lmx1a controls formation of the roof plate in the vertebrate CNS. *Nature* **403**, 764-9.

Minoguchi, S., Taniguchi, Y., Kato, H., Okazaki, T., Strobl, L. J., Zimber-Strobl, U., Bornkamm, G. W. and Honjo, T. (1997). RBP-L, a transcription factor related to RBP-Jkappa. *Mol Cell Biol* **17**, 2679-87.

Mizuguchi, R., Kriks, S., Cordes, R., Gossler, A., Ma, Q. and Goulding, M. (2006). Ascl1 and Gsh1/2 control inhibitory and excitatory cell fate in spinal sensory interneurons. *Nat Neurosci* **9**, 770-8.

Mizuguchi, R., Sugimori, M., Takebayashi, H., Kosako, H., Nagao, M., Yoshida, S., Nabeshima, Y., Shimamura, K. and Nakafuku, M. (2001). Combinatorial roles of olig2 and neurogenin2 in the coordinated induction of pan-neuronal and subtype-specific properties of motoneurons. *Neuron* **31**, 757-71.

Muhr, J., Graziano, E., Wilson, S., Jessell, T. M. and Edlund, T. (1999). Convergent inductive signals specify midbrain, hindbrain, and spinal cord identity in gastrula stage chick embryos. *Neuron* **23**, 689-702.

Muller, T., Anlag, K., Wildner, H., Britsch, S., Treier, M. and Birchmeier, C. (2005). The bHLH factor Olig3 coordinates the specification of dorsal neurons in the spinal cord. *Genes Dev* **19**, 733-43.

Muller, T., Brohmann, H., Pierani, A., Heppenstall, P. A., Lewin, G. R., Jessell, T. M. and Birchmeier, C. (2002). The homeodomain factor lbx1 distinguishes two major programs of neuronal differentiation in the dorsal spinal cord. *Neuron* **34**, 551-62.

Muroyama, Y., Fujihara, M., Ikeya, M., Kondoh, H. and Takada, S. (2002). Wnt signaling plays an essential role in neuronal specification of the dorsal spinal cord. *Genes Dev* **16**, 548-53.

Muskavitch, M. A. (1994). Delta-notch signaling and Drosophila cell fate choice. *Dev Biol* **166**, 415-30.

Nakhai, H., Sel, S., Favor, J., Mendoza-Torres, L., Paulsen, F., Duncker, G. I. and Schmid, R. M. (2007). Ptf1a is essential for the differentiation of GABAergic and glycinergic amacrine cells and horizontal cells in the mouse retina. *Development* **134**, 1151-60.

Nam, Y., Sliz, P., Song, L., Aster, J. C. and Blacklow, S. C. (2006). Structural basis for cooperativity in recruitment of MAML coactivators to Notch transcription complexes. *Cell* **124**, 973-83.

Nieuwkoop, P. (1952). Activation and organisation of the central nervous systemin amphibians . III Syntesis of a new working working hypothesis. *J Exp Zool* **120**, 83-108.

Nordstrom, U., Jessell, T. M. and Edlund, T. (2002). Progressive induction of caudal neural character by graded Wnt signaling. *Nat Neurosci* **5**, 525-32.

Novitch, B. G., Chen, A. I. and Jessell, T. M. (2001). Coordinate regulation of motor neuron subtype identity and pan-neuronal properties by the bHLH repressor Olig2. *Neuron* **31**, 773-89.

Pagliardini, S., Ren, J., Gray, P. A., Vandunk, C., Gross, M., Goulding, M. and Greer, J. J. (2008). Central respiratory rhythmogenesis is abnormal in lbx1- deficient mice. *J Neurosci* **28**, 11030-41.

Pattyn, A., Goridis, C. and Brunet, J. F. (2000). Specification of the central noradrenergic phenotype by the homeobox gene Phox2b. *Mol Cell Neurosci* **15**, 235-43.

Pattyn, A., Guillemot, F. and Brunet, J. F. (2006). Delays in neuronal differentiation in Mash1/Ascl1 mutants. *Dev Biol* **295**, 67-75.

Peng, C. Y., Yajima, H., Burns, C. E., Zon, L. I., Sisodia, S. S., Pfaff, S. L. and Sharma, K. (2007). Notch and MAML signaling drives Scl-dependent interneuron diversity in the spinal cord. *Neuron* **53**, 813-27.

Prevorovsky, M., Puta, F. and Folk, P. (2007). Fungal CSL transcription factors. *BMC Genomics* **8**, 233.

Qian, Y., Fritzsch, B., Shirasawa, S., Chen, C. L., Choi, Y. and Ma, Q. (2001). Formation of brainstem (nor)adrenergic centers and first-order relay visceral sensory neurons is dependent on homeodomain protein Rnx/Tlx3. *Genes Dev* **15**, 2533-45.

Qian, Y., Shirasawa, S., Chen, C. L., Cheng, L. and Ma, Q. (2002). Proper development of relay somatic sensory neurons and D2/D4 interneurons requires homeobox genes Rnx/Tlx-3 and Tlx-1. *Genes Dev* **16**, 1220-33.

Rhyu, M. S., Jan, L. Y. and Jan, Y. N. (1994). Asymmetric distribution of numb protein during division of the sensory organ precursor cell confers distinct fates to daughter cells. *Cell* **76**, 477-91.

Sadler, T. W. (2005). Embryology of neural tube development. *Am J Med Genet C Semin Med Genet* **135C**, 2-8.

Saiki, R. K., Scharf, S., Faloona, F., Mullis, K. B., Horn, G. T., Erlich, H. A. and Arnheim, N. (1985). Enzymatic amplification of beta-globin genomic sequences and restriction site analysis for diagnosis of sickle cell anemia. *Science* **230**, 1350-4.

Sambrook, R. (2001). Molecular Cloning: A Laboratory Manual. **Cold Spring Harbor Laboratory Press, Cold Spring Harbor, New York 11803-2500, USA**.

Sanger, F., Nicklen, S. and Coulson, A. R. (1977). DNA sequencing with chain-terminating inhibitors. *Proc Natl Acad Sci U S A* **74**, 5463-7.

Schwenk, F., Baron, U. and Rajewsky, K. (1995). A cre-transgenic mouse strain for the ubiquitous deletion of loxP-flanked gene segments including deletion in germ cells. *Nucleic Acids Res* **23**, 5080-1.

Sellick, G. S., Barker, K. T., Stolte-Dijkstra, I., Fleischmann, C., Coleman, R. J., Garrett, C., Gloyn, A. L., Edghill, E. L., Hattersley, A. T., Wellauer, P. K., Goodwin, G. and Houlston, R. S. (2004). Mutations in PTF1A cause pancreatic and cerebellar agenesis. *Nat Genet* **36**, 1301-5.

Sieber, M. A., Storm, R., Martinez-de-la-Torre, M., Muller, T., Wende, H., Reuter, K., Vasyutina, E. and Birchmeier, C. (2007). Lbx1 acts as a selector gene in the fate determination of somatosensory and viscerosensory relay neurons in the hindbrain. *J Neurosci* **27**, 4902-9.

Sorge, J. A. (1988). Bacteriophage lambda cloning vectors. *Biotechnology* **10**, 43-60.

Soriano, P. (1999). Generalized lacZ expression with the ROSA26 Cre reporter strain. *Nat Genet* **21**, 70-1.

Sotelo, C. (2004). Cellular and genetic regulation of the development of the cerebellar system. *Prog Neurobiol* **72**, 295-339.

Southern, E. M. (1975). Detection of specific sequences among DNA fragments separated by gel electrophoresis. *J Mol Biol* **98**, 503-17.

Tabor, S. and Richardson, C. C. (1987). DNA sequence analysis with a modified bacteriophage T7 DNA polymerase. *Proc Natl Acad Sci U S A* **84**, 4767-71.

Takebayashi, H., Nabeshima, Y., Yoshida, S., Chisaka, O., Ikenaka, K. and Nabeshima, Y. (2002a). The basic helix-loop-helix factor olig2 is essential for the development of motoneuron and oligodendrocyte lineages. *Curr Biol* **12**, 1157-63.

Takebayashi, H., Ohtsuki, T., Uchida, T., Kawamoto, S., Okubo, K., Ikenaka, K., Takeichi, M., Chisaka, O. and Nabeshima, Y. (2002b). Non-overlapping expression of Olig3 and Olig2 in the embryonic neural tube. *Mech Dev* **113**, 169-74.

Takebayashi, H., Yoshida, S., Sugimori, M., Kosako, H., Kominami, R., Nakafuku, M. and Nabeshima, Y. (2000). Dynamic expression of basic helix-loop-helix Olig family members: implication of Olig2 in neuron and oligodendrocyte differentiation and identification of a new member, Olig3. *Mech Dev* **99**, 143-8.

Tamura, K., Taniguchi, Y., Minoguchi, S., Sakai, T., Tun, T., Furukawa, T. and Honjo, T. (1995). Physical interaction between a novel domain of the receptor Notch and the transcription factor RBP-J kappa/Su(H). *Curr Biol* **5**, 1416-23.

Tani, S., Kurooka, H., Aoki, T., Hashimoto, N. and Honjo, T. (2001). The N- and C-terminal regions of RBP-J interact with the ankyrin repeats of Notch1 RAMIC to activate transcription. *Nucleic Acids Res* **29**, 1373-80.

Tanigaki, K., Han, H., Yamamoto, N., Tashiro, K., Ikegawa, M., Kuroda, K., Suzuki, A., Nakano, T. and Honjo, T. (2002). Notch-RBP-J signaling is involved in cell fate determination of marginal zone B cells. *Nat Immunol* **3**, 443-50.

Timmer, J. R., Wang, C. and Niswander, L. (2002). BMP signaling patterns the dorsal and intermediate neural tube via regulation of homeobox and helix-loop-helix transcription factors. *Development* **129**, 2459-72.

Tu, L., Fang, T. C., Artis, D., Shestova, O., Pross, S. E., Maillard, I. and Pear, W. S. (2005). Notch signaling is an important regulator of type 2 immunity. *J Exp Med* **202**, 1037-42.

Wang, V. Y., Rose, M. F. and Zoghbi, H. Y. (2005). Math1 expression redefines the rhombic lip derivatives and reveals novel lineages within the brainstem and cerebellum. *Neuron* **48**, 31-43.

Wildner, H., Muller, T., Cho, S. H., Brohl, D., Cepko, C. L., Guillemot, F. and Birchmeier, C. (2006). dILA neurons in the dorsal spinal cord are the product of terminal and non-terminal asymmetric progenitor cell divisions, and require Mash1 for their development. *Development* **133**, 2105-13.

Wine-Lee, L., Ahn, K. J., Richardson, R. D., Mishina, Y., Lyons, K. M. and Crenshaw, E. B., 3rd. (2004). Signaling through BMP type 1 receptors is required for development of interneuron cell types in the dorsal spinal cord. *Development* **131**, 5393-403.

Xu, Y., Lopes, C., Qian, Y., Liu, Y., Cheng, L., Goulding, M., Turner, E. E., Lima, D. and Ma, Q. (2008). Tlx1 and Tlx3 coordinate specification of dorsal horn pain-modulatory peptidergic neurons. *J Neurosci* **28**, 4037-46.

Yamada, M., Terao, M., Terashima, T., Fujiyama, T., Kawaguchi, Y., Nabeshima, Y. and Hoshino, M. (2007). Origin of climbing fiber neurons and their developmental dependence on Ptf1a. *J Neurosci* **27**, 10924-34.

Yu, D., Ellis, H. M., Lee, E. C., Jenkins, N. A., Copeland, N. G. and Court, D. L. (2000). An efficient recombination system for chromosome engineering in Escherichia coli. *Proc Natl Acad Sci U S A* **97**, 5978-83.

Yu, W., McDonnell, K., Taketo, M. M. and Bai, C. B. (2008). Wnt signaling determines ventral spinal cord cell fates in a time-dependent manner. *Development* **135**, 3687-96.

Zechner, D., Muller, T., Wende, H., Walther, I., Taketo, M. M., Crenshaw, E. B., 3rd, Treier, M., Birchmeier, W. and Birchmeier, C. (2007). Bmp and Wnt/beta-catenin signals control expression of the transcription factor Olig3 and the specification of spinal cord neurons. *Dev Biol* **303**, 181-90.

Zhou, Q. and Anderson, D. J. (2002). The bHLH transcription factors OLIG2 and OLIG1 couple neuronal and glial subtype specification. *Cell* **109**, 61-73.

Zhou, Q., Choi, G. and Anderson, D. J. (2001). The bHLH transcription factor Olig2 promotes oligodendrocyte differentiation in collaboration with Nkx2.2. *Neuron* **31**, 791-807.

Declaration

Ich versichere, daß ich die von mir vorgelegte Dissertation selbständig angefertigt, die benutzten Quellen und Hilfsmittel vollständig angegeben und die Stellen der Arbeit einschließlich Tabellen, Karten und Abbildungen, die anderen Werken im Wortlaut oder dem Sinn nach entnommen sind, in jedem Einzelfall als Entlehnung kenntlich gemacht habe; daß diese Dissertation noch keiner anderen Fakultät oder Universität zur Prüfung vorgelegen hat; daß sie noch nicht veröffentlicht worden ist sowie, daß ich eine solche Veröffentlichung vor Abschluß des Promotionsverfahrens nicht vornehmen werde. Die Bestimmungen dieser Promotionsordnung sind mir bekannt. Die von mir vorgelegte Dissertation ist von Prof. Dr. Carmen Birchmeier und von Prof. Dr. Fritz Rathjen betreut worden.

Justyna Cholewa-Waclaw